ENGINEERING
APPLICATIONS

SOCIAL | TECHNOLOGY | ENGINEERING | MATHEMATICS

Engineering Applications (ENAP) is a multidisciplinary journal and covers all fields of basic science and engineering. The Journal is involved in both experimental and theoretical studies on the subject area of basic science and engineering. The Journal is a multidisciplinary journal and covers all fields of basic science and engineering. It is the main purpose of the Journal that to convey the latest development on science and technology towards the related scientists and to the readers. The Journal is also involved in both experimental and theoretical studies on the subject area of basic science and engineering. ADEJ is a fully free journal, which does not take any article processing charge from authors.

Engineering Applications (ENAP) *is a multidisciplinary journal and covers all fields of basic science and engineering*

- Aerospace Engineering
- Environmental Engineering
- Civil Engineering
- Geomatics Engineering
- Mechanical Engineering
- Geology Science and Engineering
- Mining Engineering
- Chemical Engineering
- Metallurgical and Materials Engineering
- Electrical and Electronics Engineering
- Mathematical Applications in Engineering
- Computer Engineering
- Food Engineering

CONTENTS

Volume 1 Issue 1

ARTICLES

Pressurized gating system design and optimization in steel castings

Mustafa Murat Zor *[1] , **Alper Yoloğlu** [1] , **Serdar Kesim** [1] , **Ferhat Tülüce** [1]

¹ÇİMSATAŞ Çukurova Construction Machinery IND. TRADE. A.S. Mersin, Türkiye, foundry@cimsatas.com

Abstract

The aim of this study is to establish a correlation between the proven version of the pressurized gating system for steel castings and the cost-effective version of the pressurized gating system in industrial conditions. In the study, a computer-aided design solid modeling program was used in the design of the pressurized gating system for steel castings and the ratio of the pressurized gating system was selected as 1: 3: 1. Flow simulation of the gating-designed casting part was made in computer-aided design metal casting simulation. In the study, calculations used in the design of the pressurized gating system were made based on the weight of the part and effective casting height. The study clearly shows that the well-designed pressurized gating system has revealed that it plays a significant role in preventing non-metallic casting defects in steel castings, such as sand, gas, and slag. In addition, the '' Spin Trap '' that is recommended to be used in gating systems in ferrous based castings in the literature, was used for the first time in the ÇİMSATAŞ foundry in the steel castings at the end of the runner in the pressurized gating system and the appropriate result was obtained. Computer-aided flow and solidification simulation was used in the design of the gating system containing Spin Trap.

1. Introduction

In steel castings, all the cavities created in the sand mold are called the gating system for the liquid metal to fill the mold cavity without any problems. As important as the effective use of feeders in a cast part is, the correct design of the gating system is just as important. The basic components of the gating system in the casting processes; casting chamber (casting countersink), vertical runner, horizontal runner, and ingate consists of four parts. Although the main task of the gating system is to direct the molten metal and fill the mold with molten metal, a well-designed gating system plays an important role in preventing various casting defects (non-metallic inclusions such as sand, gas, and slag) that may occur on and inside the casting part [1-3]. Likewise, a poorly designed runner system can cause errors in the last part that may require repair, or cause the part to be scrapped. Well-designed gating system; should be able to fill the mold at the appropriate time, direct the liquid metal to the desired and/or targeted location, allow air and gases to escape from the mold, prevent non-metallic inclusions from entering the mold, not cause the mold to deteriorate with erosion, not cause gas suction due to turbulence, and should be of minimum weight [3-9].

2. Pressurized Gating System

The tightest cross-sectional area of the pressurized gating systems used in steel casting processes is the ingate. Horizontal runner, vertical runner, and casting chamber are designed according to the ingate cross-sectional area. In the pressurized gating system, the total cross-sectional area decreases towards the mold cavity, and back pressure formation is prevented by the pressure of the liquid metal in the runner. In the pressurized gating system,

the gas absorption is significantly reduced because the horizontal runner remains constantly filled throughout the casting period. In addition, the use of a pressurized gating system in steel castings ensures uniform filling in the ingates and minimum runner weight for high runner efficiency. For the pressurized gating system to be designed successfully, the molding system conditions, the total weight of the part (total part weight including the gating and feeders), the position of the part in the mold, it is necessary to determine the cope side and drag side heights of the part. Typical ratios used in pressure gating system design are 1:3:2 and 1:3:1 [3-6].

3. Spin Trap System

It is known that the pressurized gating system in steel castings can significantly prevent the penetration of non-metallic inclusions such as sand, gas, and slag, which are formed during the pouring of the liquid metal into the part. However, in some cases, there are situations where the pressure gating system fails to prevent these inclusions from entering the part. There are many versions of various slag capture systems in the literature for steel castings. In recent years, the use of a Spin Trap chamber at the end of pressurized gating systems for steel castings has been recommended by many authors in the literature. The Spin Trap system is defined in the literature as a version of the slag trap system used for the development of the gating system in the casting processes. The main purpose of the Spin Trap system is; to obtain a cleaner casting part by grabbing non-metallic inclusions such as sand, gas, and slag that the gating system cannot prevent from entering the part, and to optimize the gating system [6-15].

4. Material and Method

In this study, it is aimed to develop a pressurized gating system for steel castings by using a computer-aided solid modeling program. The pressurized gating system design of the fork part is based on the total weight of the part (total weight including gating and feeders). The part was molded in the green sand molding system and cast in the ÇİMSATAŞ foundry. In the study, the material of the part was determined according to the TS EN 10293 standard (material of the casting part is G17CrMo9-10 + QT). Due to the high carbon equivalent of this material and the visuality of the part, it is aimed to minimize non-metallic inclusions such as sand, gas, and slag that may occur on the surface of the part during casting. The total weight of the part is 145 kg and the effective casting height is 33.2 cm. The pressurized gating system design of the part was made in the computer-aided solid modeling program and the flow simulation of the part was made in the computer-aided metal casting and solidification program.

In the study, the cope side height of the casting part was determined as 330 mm and the drag side height of the casting part was determined as 37 mm. The filling time of the part was determined with the help of the equation given in Equation 1. The coefficient of 'k', which varies according to the total weight of the part in this equation, was found by using the graph given in Figure 1.

$$t = k\sqrt{W} \tag{1}$$

Here; t: filling time (sec), k: filling time coefficient, W: represents total weight of the casting part (Ib-Ib: pounds,1 Ib. = 0.452 kg).
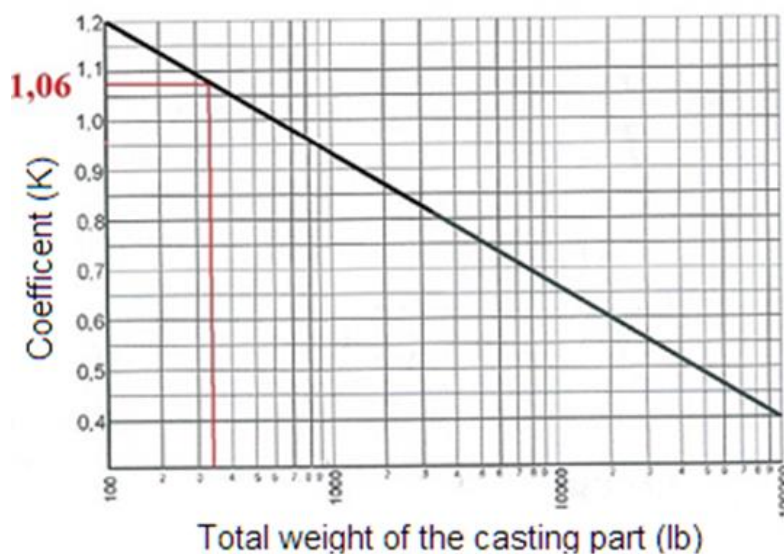

Figure 1. The coefficient 'k' corresponds to the total weight of the part

The weight in kilograms corresponding to 1 lb. is 0.452 kg. According to this;

145 kg / 0.452 kg/lb. = 320.8 lb.

The coefficient 'k' is 1.06, corresponding to 320.8 lb. in Figure 1. Accordingly, the filling time of the part;

$1.06\sqrt{320.8}$ = 19 sec.

In the study, after the filling time of the part was calculated, the effective casting height during the casting of the part was determined. In the calculation of the effective pouring height, the schematic representation in Figure 2 was used and the equation given in Equation 2 The effective casting height of the part was found with the help of;

$$h = H - (P^2 / 2c) \tag{2}$$

Here; h: effective pouring height (cm), H: distance between the sprue inlet and the ladle (cm), P: the cope side height of the part (cm), c: the depth in the lower degree region of the part (cm).
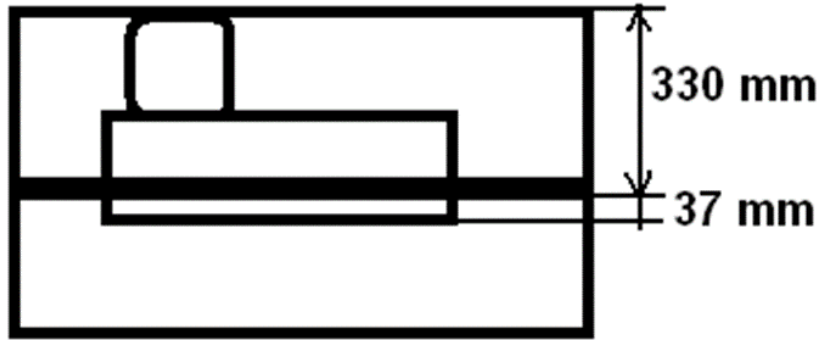
Figure 2. Schematic representation of the top and bottom heights of the part to be molded

The 'H' dimension is the distance between the ladle and the sprue hole. Based on the experiences of the ÇİMSATAŞ foundry, calculations are made by taking the 'H' dimension as a reference in the gating system designs, 25 cm above the cope side height in the resin molding system, and 20 cm above the cope side height in the green sand molding system.

H = 33+ 20 = 53 cm.

Effective casting height of the part;

h = 53 - (33² / 2 x (33 + 3.7)) = 38.2 cm.

In the study, after the effective casting height of the part is calculated, the metal flow rate is given in the equation given in Equation 3. with the help of and calculated using the graph in Figure 3.

$$v = C\sqrt{2gH} \tag{3}$$

Here; v: metal flow rate (cm/sec), C: flow coefficient, H: effective casting height of the part (cm), g: gravity acceleration (981 cm/s²).
From the graph in Figure 3, the metal flow coefficient corresponding to the total weight of the casting part was determined as 0.706.

$0.706\sqrt{2x981x38.2}$ = 193.3 cm/sec.

The volume, filling time and metal flow rate of the casting part was calculated to determine the ingate cross-sectional area, which is the most important step in the pressurized gating system design of the casting part. The ingate cross-sectional area of the casting part is given in equation 4 with the help of determination.

$$A = V/t \text{ x } v \tag{4}$$

Here; A: ingate cross-sectional area (cm²), V: part volume (cm²), v: metal flow rate (cm/sec).

In order to calculate the ingate cross-sectional area of the part, the part volume must be calculated. Part volume;

$$145000 \text{ gr} / 7.2 \text{ gr/cm}^3 = 20138.8 \text{ cm}^3.$$

Ingate cross-sectional area;

$$20138.8 / (19 \times 193.3) = 5.48 \text{ cm}^2.$$

In the study, the gating system ratio was chosen as 1:3:1 in the design of the pressurized gating system. However, since the ingate of the casting part has an angle of 90° concerning the gating system, the ingate cross-sectional area has been multiplied by a factor of 1.8 and calculated according to the casting practice of ÇİMSATAŞ foundry. According to ÇİMSATAŞ casting practice, the ingate cross-sectional area of the casting part;

$$5.48 \times 1.8 = 9.86 \text{ cm}^2.$$
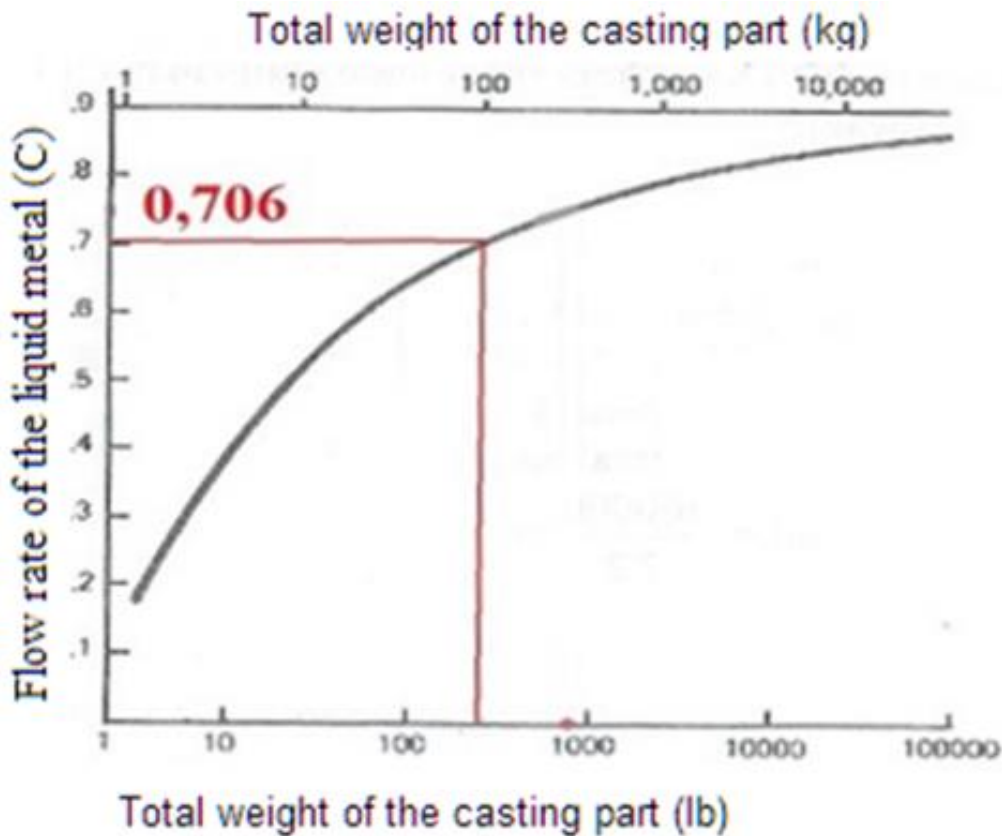
Figure 3. Metal flow coefficient corresponding to the total weight of the casting part

Table 1. Pressurized gating system ratio and dimensions

Gating system ratio	vertical runner	horizontal runner	Ingate
1:3:1	1	3	1
	9.86 cm²	29.58 cm²	9.86 cm²

The visual of the pressurized gating system, which was designed in the computer-aided solid modeling program using the data in Table 1, is shown in Figure 4.

Metal flow and filling simulation of the casting part, for which the pressurized gating system is designed; with lip pouring ladle and pouring temperature 1600°C made by choice. The nominal chemical composition of the casting part was selected as shown in Table 2 and the metal flow and filling simulation was performed.

Table 2. Nominal chemical composition of the casting part

Contents	% C	% Mn	% S	%P	% Si	% Ni	%Cr	% Mo
min	0.13	0.5	0	0	0.4	0	2nd	0.9
Max	0.2	0.9	0.02	0.02	0.6	0.3	2,5	1,2
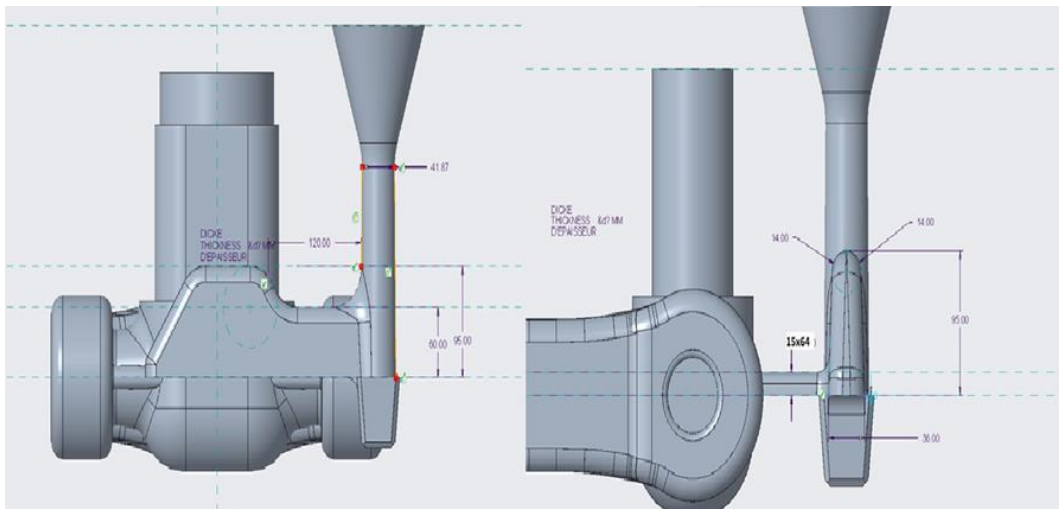
Figure 4. Schematic representation of the designed pressurized gating system
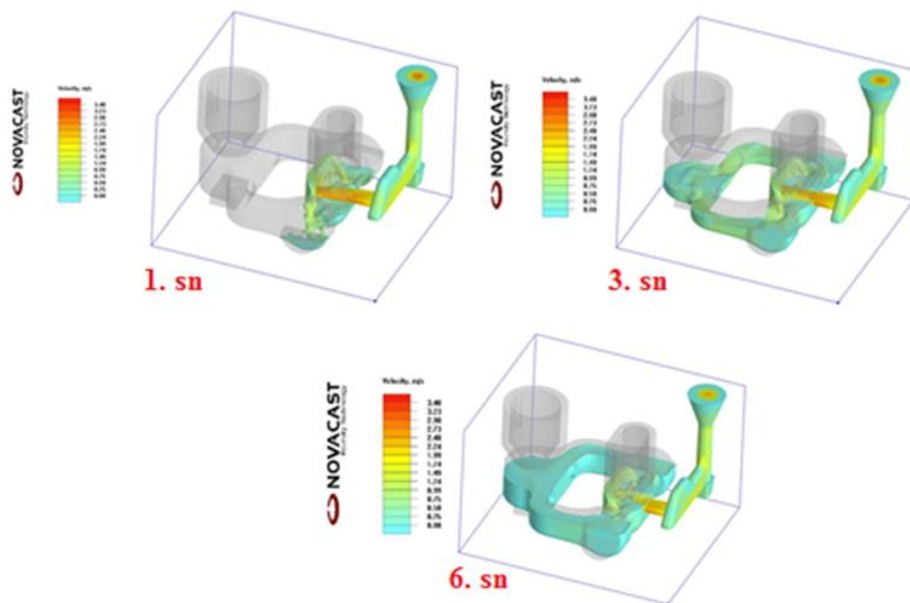
Figure 5. Image of the metal flow and filling simulation of the casting part at 1, 3, and 6 seconds
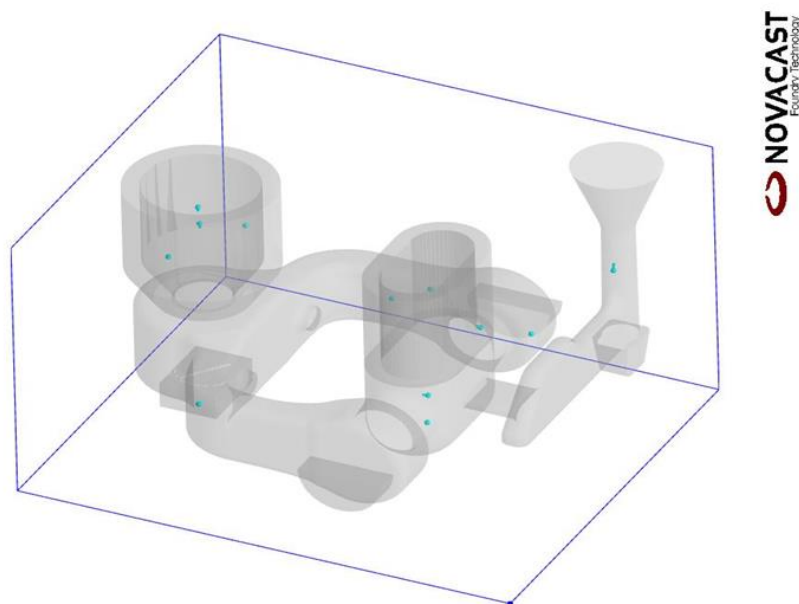
Figure 6. Image of the slag simulation of the casting part

After simulating metal flow and slag on the part, 12 parts were molded in the green sand molding system in the ÇİMSATAŞ foundry and the castings were carried out with a lip pouring ladle at 1586 °C.

Figure 7. Image of casting parts with a pressurized gating system

By using the metal flow and filling simulation data of the part for which the pressurized gating system was designed, the Spin Trap chamber was placed at the end of the gating system without changing the dimensions of the part gating system, and the part was simulated again under the same conditions as shown in Figure 8-9.
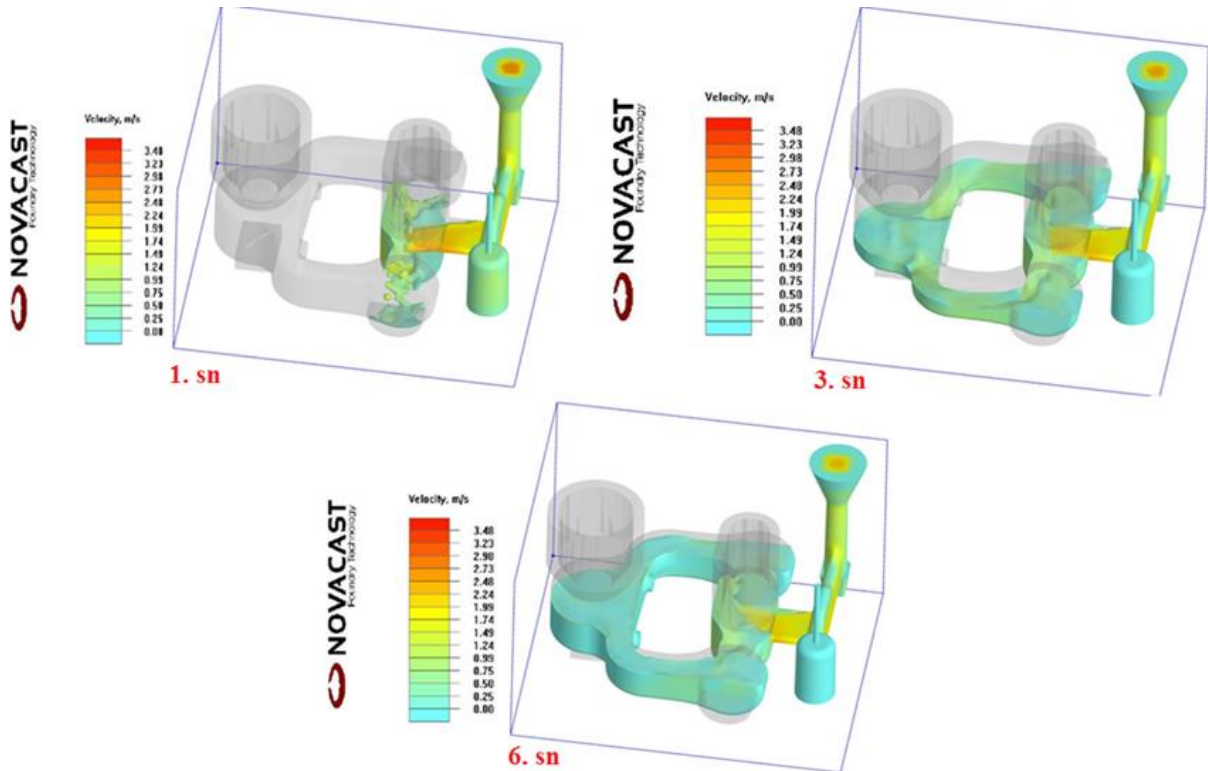
Figure 8. Image of the metal flow and filling simulation of the casting part at 1, 3, and 6 seconds
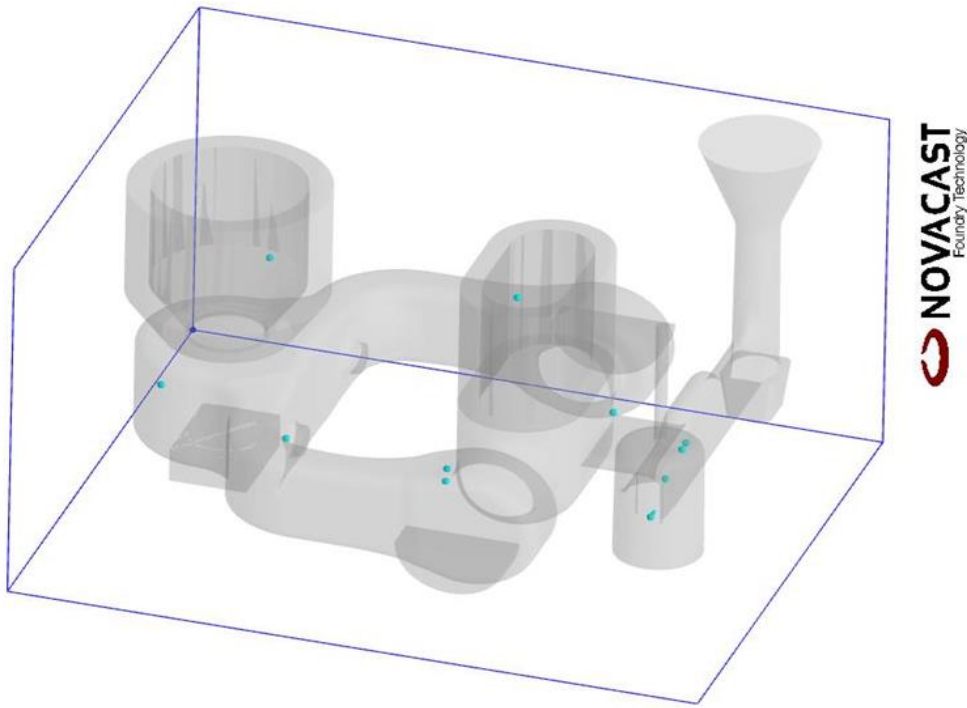
Figure 9. Image of the slag simulation of the casting part

According to the simulation results data, the Spin Trap chamber was assembled at the end of the pressurized gating system on the part model, as shown in Figure 10.

Figure 10. Image of the Spin Trap chamber assembled on the pressurized gating system in the part model

After the Spin Trap chamber was assembled on the part model, 12 parts were molded in the green sand molding system in the ÇİMSATAŞ foundry and the castings were carried out with a lip pouring ladle at 1586°C. The sand molds of the parts with Spin Trap chambers where the castings were made were shake-out and the parts were cleaned. In the next operation, the Spin Trap chamber from the gating systems of the parts was cut with a torch. The Spin Trap chambers that were cut with a torch were firstly examined by eye. The Spin Trap chambers, which were cut with a torch, were first visually inspected. Then, the Spin Trap chambers were examined by performing the destructive inspection.

Figure 11. Image of the casting parts with the Spin Trap chamber

5. Findings

In this article, casting parts were designed according to the simulation results with different pressurized gating system versions. The findings were obtained from the simulation and casting results of the parts.

- It is found that the simulation results highly represent the actual casting results.
- Although the pressurized gating system for steel castings minimizes the penetration of non-metallic inclusions into the part, it has been concluded that in some specific cases there may be situations where these inclusions cannot prevent their penetration into the part.
- The filling times of the casting parts without the Spin Trap chamber were in the range of 17-18 seconds, and the filling times of the parts poured with the Spin Trap chamber were in the range of 19-20 seconds. It has been observed that the spin trap chamber increases the total weight of the part by 4 kg and the filling time of the part by 2 seconds.
- In Figure 5; It has been observed that the velocity of the liquid metal is in the range of 2.24 – 2.48 m/s at the ingate, and in the simulation of the part with the Spin Trap chamber in figure 8, this velocity value remains in the same range.
- In Figure 6; Although the data that the part gating system could not catch slag was obtained, the presence of non-metallic inclusions that can be seen in the gating systems of the cast parts in figure 7 was detected.
- In Figure 9; It has been observed that the Spin Trap chamber significantly captures non-metallic inclusions in the first moments of part filling, and the pressure gating system increases the capturing capacity of these inclusions in the first moments of casting. The results obtained in Figure 12 revealed that the part simulation significantly confirmed the actual situation.
- In Figure 13; Destructive inspection was performed on the Spin Trap chambers and the presence of non-metallic inclusions was detected in the cut pieces.

6. Results

Although the pressurized gating system for steel castings minimizes the penetration of non-metallic inclusions into the part, it is concluded that it cannot prevent the non-metallic inclusions escaping from the ladle during casting to entering the part at the desired level.

With the design of the Spin Trap chamber pressure gating system in the ÇİMSATAŞ foundry, the surface quality of the cast steel parts has improved positively. The improvement in the casting part surfaces which get obtained by using a spin trap was reduced the rework needed (such as cosmetic welding, grinding, etc.).

The results of the study show that the Spin Trap chamber, which has been widely used in non-ferrous castings in recent years, has also given positive results in the steel casting process.
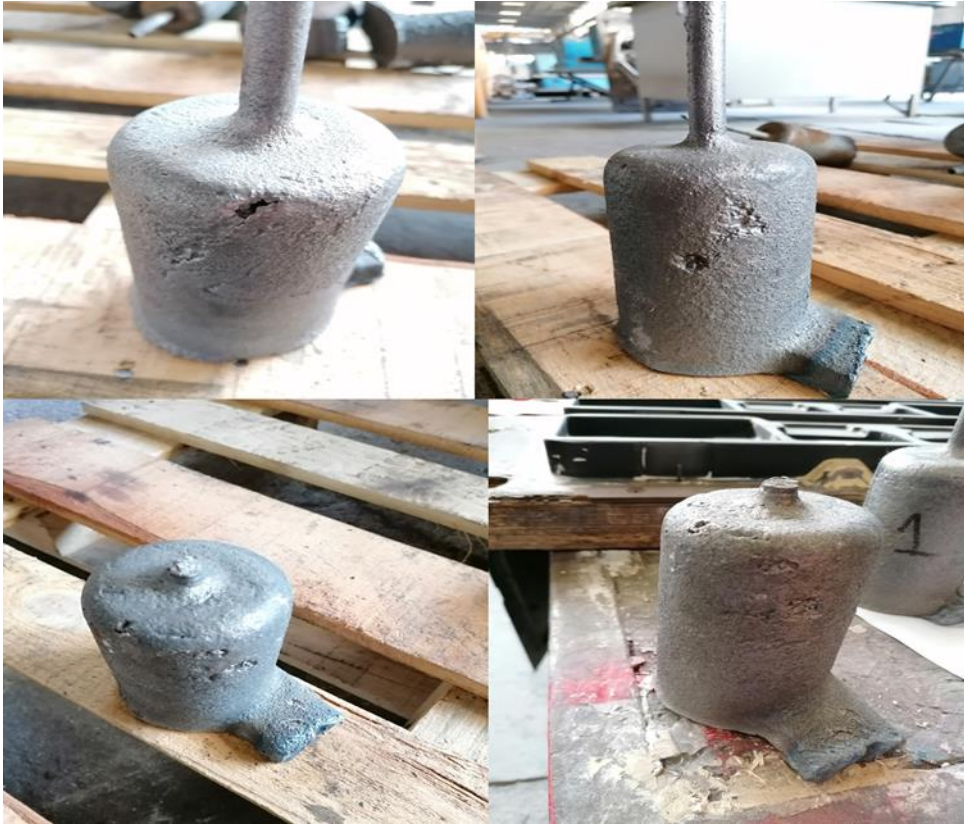
Figure 12. Images of inclusions captured in the Spin Trap chamber
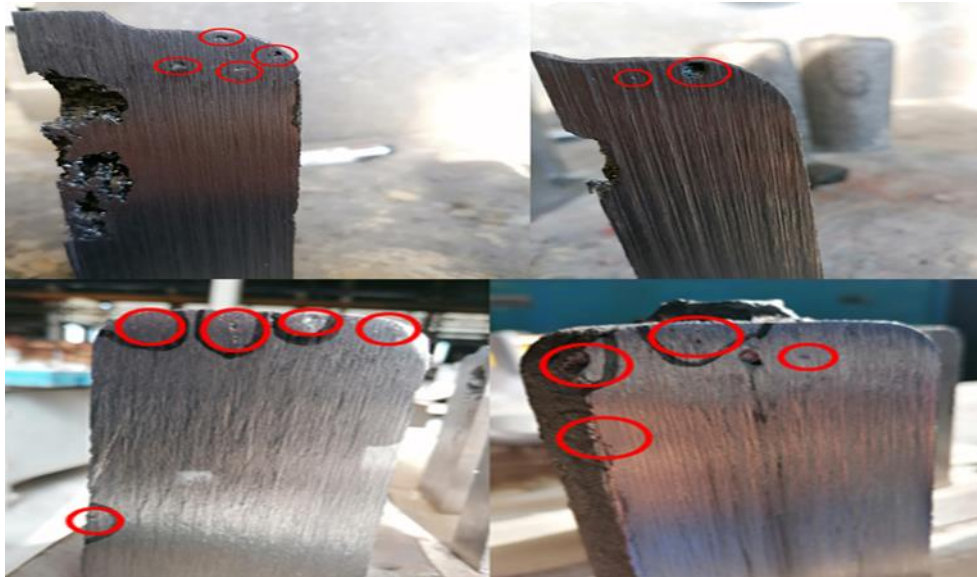
Figure 13. Images of non-metallic inclusions trapped inside Spin Trap chambers

Acknowledgements

Author contributions

Mustafa Murat Zor: Conceptualization, Methodology, Software **Alper Yoloğlu:** Data curation, Writing-Original draft preparation, **Serdar Kesim:** Visualization, Investigation, Writing-Reviewing and Editing. **Ferhat Tülüce:** Software, Validation.

Conflicts of interest

The authors declare no conflicts of interest.

References

1. Campell, J. (2015). Complete Casting Handbook. 2nd ed., Butterworth-Heinemann, Oxford.
2. Campell, J. (2004). Casting Practice The 10 Rule of Castings. 1st ed., Butterworth-Heinemann, Oxford.
3. Karsay, S. I. (1976). Ductile Iron Production. 1st ed., Quebec Iron and Titanium Corporation, Canada.
4. Dojka, R., Jezierski, J., & Campell, J. (2018). Optimized Gating System for Steel Castings. Journal of Materials Engineering and Performance, 27(10), 5152-5163.
5. Jezierski, J., Dojka, R. & Jenerka, K. (2017). Optimizing Gating System for Steel Castings. 5th International Conference on Modern Manufacturing Technologies in Industrial Engineering, 14-17.
6. Jezierski, J., Dojka, R., Kubiak, Zurek, K. & Ltd, T. (2016). Experimental Approach for Optimization of Gating System in Castings. Metal 2016: 25th Anniversary International Conference on Metallurgy and Materials, 104-109
7. Hsu, F., Jolly, M. & Campell, J. (2006). Vortex-Gate Design for Gravity Casting. International Journal of Casting Metal Research, 19(1), 5736-5750
8. Ducic, N., Slavkovic, R., Milicevic, I., Cojbasic, Z., Manasijevic, S. & Radisa, R. (2017). Optimization of the Gating System for Sand Casting Using Genetic Algorithm. International Journal of Metal casting Research, 11(2), 225-265
9. Ogawa, K., Kanou, S., & Kashihara, S. (2006). Fewer Sand Inclusion Defects by CAE. Komatsu Technical Report, 52(158), p 1-7
10. David, P., Massone, J., Boeri, R., & Sikora, J. (2006). Gating System Design to Cast Thin Wall Ductile Iron Plates. International Journal of Metal Casting Research, 19(2), 98-109
11. Melendez, A. J., Carlson, K. D., Beckermann, C. (2010). Modelling of Deoxidation Formation in Steel Casting. International Journal of Casting Metal Research, 23(5), 278-288
12. Campell, J. (2012). Stop Pouring, Start Casting. International Journal of Metal Casting Research, 6(3), 7-18
13. Hsu, F., Jolly, M., & Campell, J. (2009). A Multiple-Gate Runner System for Gravity Casting. Journal of Material Processing Technology, 209(17), p 5736-5750
14. Renukananda, K., & Ravi, B. (2016). Multi-Gate System in Casting Process: Comparative Study of Liquid Metal and Water Flow. Materials and Manufacturing Process, 31(8), 1091-1101
15. Moderasi, A., Safihani, A., Noohi, A., Hamiznezhad, N., & Maki, S. (2017). Gating System Design and Simulation of Gray Iron Casting to Eliminate Oxide Layers Caused by Turbulence. International Journal of Metal Casting Research, 11(2), 328-339
16. Zor, M. M., Yoloğlu, A., & Kesim, S. (2022). Pressurized gating system design and optimization in steel castings. *Advanced Engineering Days (AED)*, *2*, 40-43.

LA-ICP-MS trace element analysis of magnetite from Gökçedoğan Cu-Zn deposit (Kargı-Çorum) in Central Pontides, Turkey

Cihan Yalçın [*1], **Nurullah Hanilçi** [2], **Mustafa Kumral** [3], **Mustafa Kaya** [3]

[1]Ministry of Industry and Technology, General Directorate of Industrial Zones, Ankara, Türkiye, cihan.yalcin@sanayi.gov.tr
[2]İstanbul University-Cerrahpaşa, Geological Engineering, İstanbul, Türkiye, nhanilci@gmail.com
[3]İstanbul Technical University, Geological Engineering, İstanbul, Türkiye, kumral@itu.edu.tr; kayamusta@itu.edu.tr

Abstract

Magnetite is a common mineral in paragenesis in many mineral deposits, and it is recognized that it covers the conditions of the environment in which it is formed due to its physico-chemical properties. For this reason, chemical compositions of magnetites are used in researches on the origin and formation of ore deposits. Gökçedoğan Cu-Zn massive sulfide deposit (VMS) in the Central Pontides is a syngenetic stratiform deposit observed in metamorphic rocks. The ore paragenesis contains pyrite, chalcopyrite, sphalerite, magnetite, hematite, covellite, malachite, and goethite respectively. Because of its physicochemical properties, in-situ laser-ablation inductively coupled plasma mass-spectrometry (LA-ICP-MS) analysis of magnetite in the ore zone was performed and a new perspective was promoted to the deposit. From analysis Fe is between 72.06-73.39% and O is between 20.78-21.15% respectively. V content is approximately higher than the other trace elements. Analyzes were checked out in both Cu/(Si+Ca)-Al(Zn+Ca) and Cu/Ca-Al(Si+Zn+Ca) diagrams and it was decided that they exhibit similar distributions to VMS deposits in the world. In the spider diagram drew up, it has been showed that Gökçedoğan VMS deposit is close to Besshi Type Windy Craggy deposit with its high Si values.

1. Introduction

Magnetite is one of the most common oxide minerals observed in igneous, sedimentary and metamorphic rocks, and it is a mineral that can consist of important signatures in many ore deposits [1-2]. Due to its crystallographic structure, magnetite has an inverted spinel structure where a number of trace elements can replace Fe^{2+} or Fe^{3+} [3]. Because of its crystallographic structure, magnetite gives important physico-chemical traces of different geological environments [4-7]. It also hides important clues as it preserves the magnetite composition, which has a stable structure due to its physicochemical properties [8]. This mineral is found in paragenesis in many mineral deposits [7, 9]. The physico-chemical conditions in the formation of these mineral deposits still control the composition of the iron oxide minerals. For this reason, magnetites have important data about the formation of the mineral deposit in its paragenesis [10-13]. The geochemical content of magnetite [14], which is generally observed in VMS-type deposits, is used both in the classification and exploration of mineral deposits by in-situ laser-ablation inductively coupled plasma mass-spectrometry (LA-ICP-MS) method [15].

Volcanogenic massive sulfide (VMS) deposits are significant origins for Cu, Zn and Pb, which are formed in many tectonic environments [16]. Volcanogenic massive sulfide (VMS) deposits are separated into 3 major types as Kuroko, Besshi and Cyprus Type [17]. Fox [18] described that pelitic mafic lithologies are relevant for Besshi Type deposits. It is recognized that there are areas similar to the Besshi type deposit, the typical example of which

is in Japan, in various districts around the world. The world's largest Besshi type deposit is the Windy Craggy in northwestern of British Columbia [19]. Magnetite is one of the common minerals in the paragenesis of VMS deposits [20-23] and gets information about the alteration processes, fluid compositions and physicochemical conditions of mineralization [24].

Significant Volcanogenic Massive Sulfide deposits (VMS) are formed along the Pontide orogenic belt, which is one of the main tectonic belts in Turkey. Kuroko or Black Sea type deposits were classified in the Eastern Pontides [25-27] and Cyprus [28] and Besshi type deposits [29-30] in the Central Pontides.

There are rock groups consisting of specific tectonic slices [31] in the Gökçedoğan (Kargı-Çorum) district (Central Pontide). In this district, which is in the subduction-accretionary complex as a tectonic location, units existing to the Kunduz metamorphics mostly crop out [31]. In these metamorphics, Besshi Type Cu-Zn mineralization is observed in parallel with the schistosity within the metabasite and quartzschist alternations [29]. Mainly chalcopyrite, sphalerite, pyrite, magnetite, hematite, covellite, malachite and goethite minerals are observed in ore paragenesis [32]. In this paper, we mention new data gathered from trace element geochemistry of magnetite using LA-ICP-MS.

2. Material and Method

In recent years, trace element analyzes of oxide or sulfide minerals have been performed by in-situ laser-ablation inductively coupled plasma mass-spectrometry (LA-ICP-MS) method to point out the genesis of many mineral deposits. With this method, a new perspective has been gained to the mineral deposits [33-36]. Thus, in this study, trace element analysis results of magnetite in the Gökçedoğan Cu-Zn mineralization in the Central Pontides were evaluated.

Electron probe microanalysis studies (EPMA) of magnetite detected in ore paragenesis were carried out in CAMECA SX100 device at ITU ATUM Research and Application Center. Diagrams were set up with the gained data.

2.1. Geological Background

In the Central Pontides, lithostratigraphic units of various origin are observed together along the 'suture zones' formed by the closure of the Paleotethys and Neotethys oceans [37-39]. Pre-Jurassic HP/LT metamorphic rock groups and ophiolitic rocks cropping out in extensive areas south of the Central Pontides are the products of a subduction-accretionary complex built up by the closure of the Paleotethys and Neotethys oceans [40-43]. The study area, is located in the Central Pontides, include Middle Jurassic and Cretaceous Accretionary Complex are also named as Central Pontide Supercomplex (Figure 1).
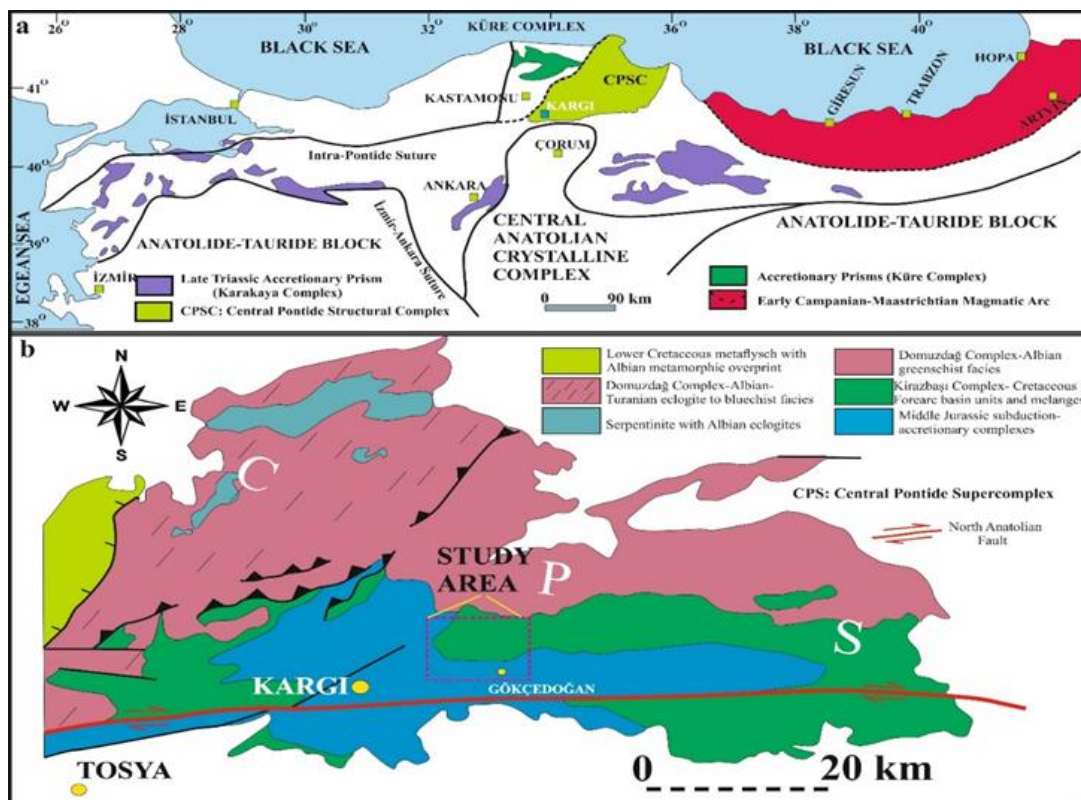
Figure 1. a) Position of the study area between Turkey's structural zones (modified from Günay et al., [30]), b) Position of the study area in the Central Pontide Supercomplex (modified from Aygül et al., [42])

There are rock groups in the Paleozoic-Quaternary age range in this district. The basement of the region consists of the Kunduz metamorphites, which are exhibited of metabasite, gneiss and schists respectively. This unit is overlain by carbonate rocks of Paleozoic-Mesozoic periods with a tectonic contact. In addition, the ophiolitic melange overlies the Kunduz metamorphics in wide areas with thrust faults. With the presence of specific lithostratigraphic sequences, Gölköy, Pelitözü and Ophiolitic mélange tectonic slices have been described in the region [31].

2.2. Mineralization

The stratiform Cu-Zn mineralizations in the study area crop out in the west of Kömürlükdere and Şahin Dere within the Kunduz Metamorphics (Figure 2). Gökçedoğan Cu-Zn mineralization was formed in metabasites belonging to Kunduz metamorphics. Mineralizations are observed in altering levels of metabasite and quartzschist parallel to the schistosity. Along the ore zone, not only chloritization and limonitization are common, but graphitization is also observed at some sequences. In addition, gypsum levels were still observed in the area where Şahin Dere mineralization is located [29]. Mainly actinolite, chlorite, epidote, opaque minerals and quartz are observed in the metabasite with nematoblastic texture (Figure 3).
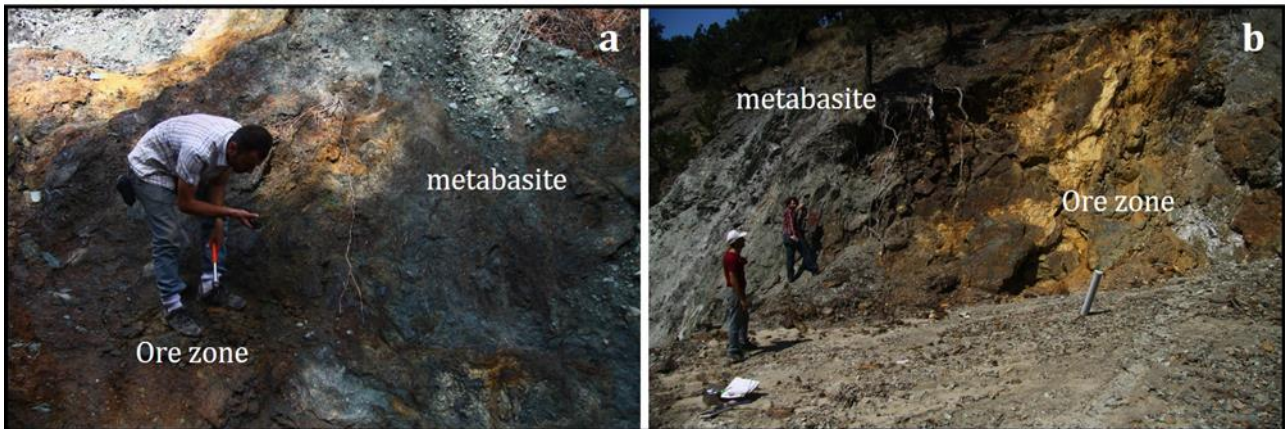
Figure 2. General view of metabasite hosted Cu-Zn mineralization in Gökçedoğan (a. Şahindere, b. Kömürlükdere)
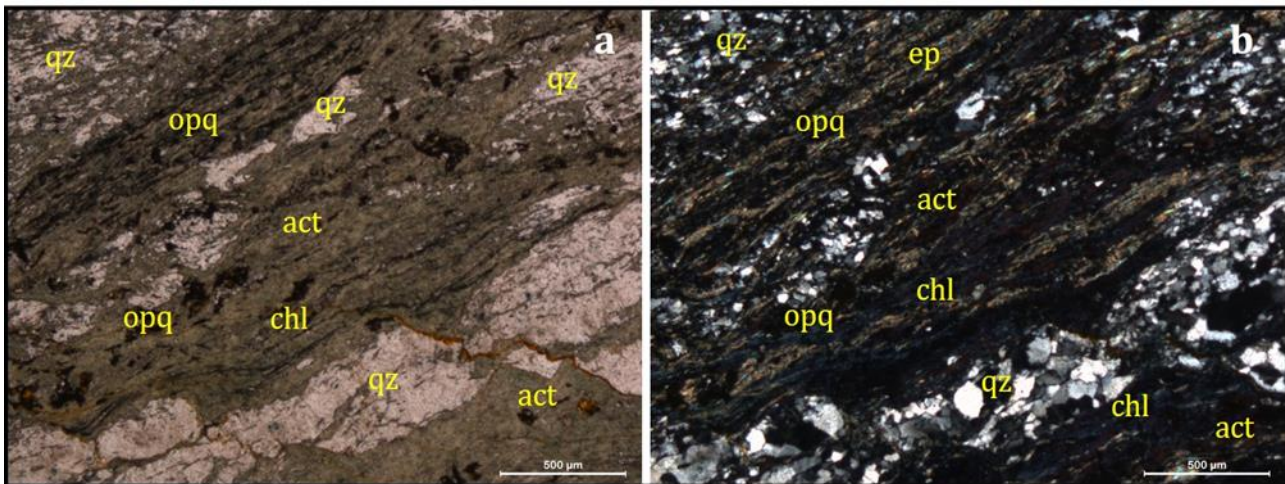
Figure 3. Polarizing microscope images of metabasite, Abbreviations: (act) actinolite, (chl) chlorite, (ep) epidote, (qz) quartz, (opq) opaque mineral

In the ore petrography, it was seen that sphalerites replaced chalcopyrite and pyrite, and pseudocubic magnetites were transformed into hematite [29]. For mineral chemistry, magnetites, which were arranged parallel to the foliation and underwent deformation, were used (Figure 4). In these specimens, magnetites are aligned in one direction owing to the deformation effect (Figure 4a). Although the surface of subhedral and anhedral magnetites is clear and well preserved in general, it has been decided that they are transformed into hematite in places (Figure 4b). On the other hand, hematites are finer grained and generally irregular than magnetites (Figure 4).

Geochemical analyzes of the specimens collected from this district were carried out. Corresponding to the results of the analysis, it was declared that Cu and Zn values in the Kömürlükdere and Göçükdibi ore zones

enriched up to 5 times compared to the clark value [44]. Fe_2O_3 results are also rather high due to banded pyrite, magnetite, hematite and goethite minerals generally observed in the ore zone.
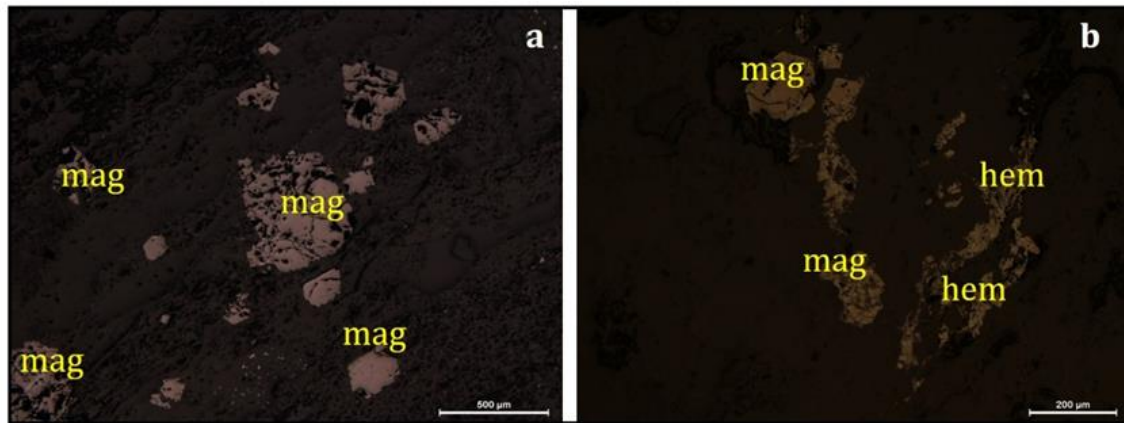
Figure 4. Microscope images of the polished sections. Abbreviations: (mag) magnetite, (hem) hematite

3. Results

Mineral chemistry analysis of magnetites in mineral paragenesis was performed to get signatures of the formation of Gökçedoğan Cu-Zn VMS deposit. Since the concentrations of some trace elements in magnetite were below the detection limits, the results of the analysis of only 15 trace elements were obtained. LA-ICP-MS analysis results of magnetite mineral are given in Table 1.

Most trace element abundances in magnetites are less than 0.1 ppm (Table 1). In the samples whose trace element compositions are exceedingly variable, Fe is between 72.06-73.39% and O is between 20.78-21.15% respectively. V is approximately higher than the other elements.

Various diagrams were prepared according to the analysis results obtained. In these diagrams, magnetite analysis results of hydrothermal, skarn, VMS and porphyry deposits are compared.

Gökçedoğan mineralization shows a similar distribution with VMS type deposits on both Al/(Zn+Ca) vs. Cu/(Si+Ca) and Al/(Si+Ca+Zn) vs. Cu/Ca diagrams (Figure 5a, 5b). In the spider diagram, Gökçedoğan mineralization has high Si, identical to the character of the VMS type deposits, and exhibits a distribution similar to the Windy Craggy deposit, which is the largest Besshi Type Deposit (Figure 5c).

Table 1. LA-ICPMS results for trace elements (%) in magnetite from the Gökçedoğan Cu-Zn deposit

%wt	KGD-317	KGD-317	KGD-317	KGD-317	KGD-317
Mg	0,01	0,01	0,01	0,01	0,01
Al	0,02	0,02	0,08	0,01	0,02
Ti	0,02	0,01	0,01	0,01	0,01
V	0,11	0,12	0,06	0,07	0,11
Mn	0,03	0,08	0,02	0,03	0,05
Ni	0,01	0,01	0,03	0,01	0,01
Zn	0,06	0,11	0,28	0,35	0,05
Sn	0,02	0,01	0,02	0,02	0,02
Cr	0,01	0,1	0,1	0,01	0,04
Fe	72,69	73,39	72,07	72,06	72,66
O	20,93	21,15	20,86	20,78	20,92
Cu	0,032	0,045	0,025	0,03	0,03
K	0,002	0,001	0,001	0,002	0,001
Ca	0,055	0,003	0,042	0,031	0,01
Si	0,008	0,6	0,05	0,055	0,013
Total	94,007	95,659	93,658	93,478	93,954

4. Discussion

There is a lack of LA-ICP-MS data for magnetite from VMS deposits in Pontides. For this reason, it is significant to analyze and compare magnetite in VMS deposits according to trace element compositions. In this context, some researchers have previously obtained results with this method.

Singoyi et al. [12] measured the trace element composition of magnetite from VMS deposits in Australia and stated that the Sn/Ga and Al/Co diagram could yield significant results, Nadoll et al. [45] analyzed and evaluated trace elements in magnetite obtained from hydrothermal ore deposits and their host rocks using LA-ICP-MS methods. The same authors still investigated porphyry and skarn Cu deposits in the USA according to the amount of trace elements in magnetites [46]. Makvandi et al. [47] defined three types of magnetite in VMS environments and revealed the geological conditions according to magnetite compositions. These conditions are composition of fluids, temperature, mineralogy, conditions of metamorphism and sources of oxygen and sulfur respectively. In this study, however, the magnetite composition shows that the Gökçedoğan VMS deposit has a character similar to the VMS deposits. In addition, it has been revealed that the Windy Craggy deposit, which is the world's largest Besshi Type VMS deposit, has similarities with magnetite compositions.
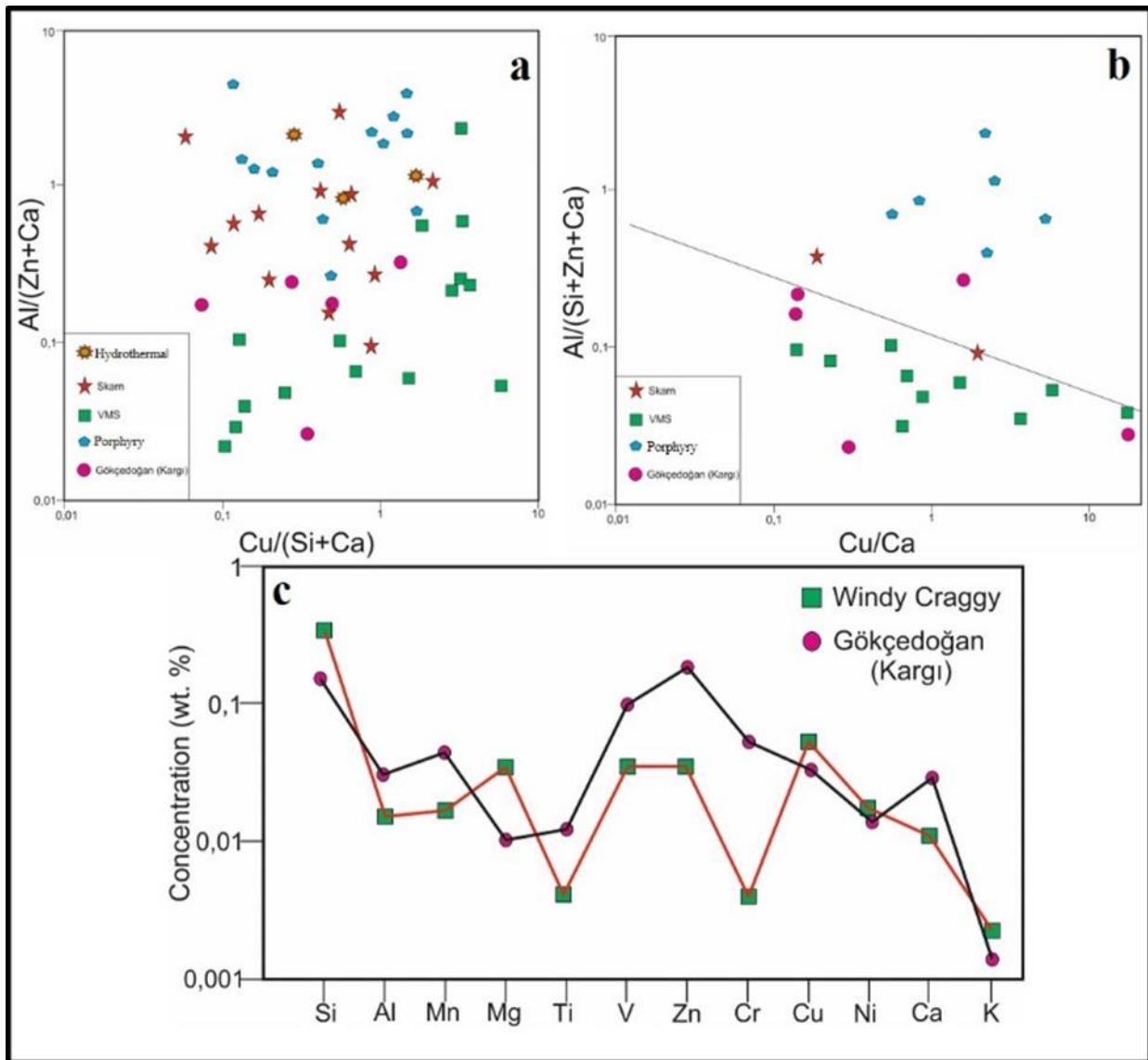
Figure 5. a) Al/(Zn+Ca) vs. Cu/(Si+Ca) diagram, b) Al/(Si+Ca+Zn) vs. Cu/Ca diagram, c) Spider diagram for Besshi Type deposits [48].

5. Conclusion

Gökçedoğan VMS deposit is associated with metabsites in the Central Pontides. The mineralization in the accretionary complex is stratiform type and syngenetic. There are important VMS deposits observed along the Pontide belt, and Cyprus Type and Besshi Type deposits are observed in the Central Pontides. For this reason, it is

important for the metallogenesis of the region to present new approaches with the chemical composition of magnetites in paragenesis in VMS deposits.

Trace element analysis of magnetite in the paragenesis of Gökçedoğan VMS deposit observed in the Central Pontides was carried out. As a result of this study, it was decided that Gökçedoğan Cu-Zn deposit exhibits similar geochemical characteristics with Windy Craggy Besshi Type deposit.

Rapid and efficient results can be obtained by chemical analysis of magnetites in mineral exploration. The results of trace elements of the mineral can be obtained in the analyzes made with the LA-ICP-MS method. As a result of this study, the origin approach of the Gökçedoğan VMS deposit, which is the Besshi type deposit, according to the magnetite composition has been revealed. The number of analyzes should be increased by making measurements from different types of magnetite. Thus, the formation conditions in similar deposits will be comparable.

Acknowledgement

Funding

Author contributions

Cihan Yalçın: Writing-Reviewing and Editing, Geology, Methodology, Geochemistry. **Nurullah Hanilçi:** Ore Geology, Editing, Geochemistry. **Mustafa Kumral:** Ore Petrography, **Mustafa Kaya:** Petrography, EPMA.

Conflicts of interest

The authors declare no conflicts of interest.

References

1. Ramdohr, P. (1980). The ore minerals and their intergrowths. Pergamon, New York.
2. Scheka, S. A., Platkov, A. V., Vezhosek, A. A., Levashov, G. B., & Oktyabrsky, R. A. (1980). The trace element paragenesis of magnetite. Nauka, Moscow, p 147.
3. Nadoll, P., Angerer, T., Mauk, J. L., French, D., & Walshe, J. (2014). The chemistry of hydrothermal magnetite: a review. Ore Geology Reviews., 61, 1–32. https://doi.org/ 10.1016/j.oregeorev.2013.12.013.
4. Lindsley, D. H. (1976). The crystal chemistry and structure of oxideminerals as exemplified by the Fe-Ti oxides. In: Rumble III, D (ed) Oxide Minerals. Reviews in Mineralogy: Mineralogical Society of America, pp 1–60.
5. Wechsler, B. A., Lindsley, D. H., & Prewitt, C. T. (1984). Crystal structure and cation distribution in titanomagnetites (Fe3-xTixO4). Am Mineral, 69, 754–770.
6. Bowles, J. F. W., Howie, R. A., Vaughan, D. J., & Zussman, J. (2011). Rock-forming minerals- non-silicates: oxides, hydroxides and sulphides, Second edn. Geological Society, London.
7. Dupuis, C., & Beaudoin, G. (2011). Discriminant diagrams for iron oxide trace element fingerprinting of mineral deposit types. Miner Depos, 46, 319–335.
8. Dare, S. A., Barnes, S. J., Beaudoin, G., M´eric, J., Boutroy, E., & Potvin-Doucet, C. (2014). Trace elements in magnetite as petrogenetic indicators. Mineral. Deposita, 49 (7), 785–796. https://doi.org/10.1007/s00126-014-0529-0.
9. Leach, D. L., Bradley, D. C., Huston, D., Pisarevsky, S. A., Taylor, R. D., & Gardoll, S. J. (2010). Sediment-hosted lead-zinc deposits in Earth history. Econ. Geol. 105 (3), 593–625. https://doi.org/10.2113/gsecongeo.105.3.593.
10. Carew, M. J. (2004). Controls on Cu-Au mineralization and Fe oxide metasomatism in the Eastern Fold Belt, N.W. Queensland, Australia. Unpublished Ph.D thesis. James Cook University, Queensland
11. Gosselin, P., Beaudoin, G., & Jébrak, M. (2006). Application of the geochemical signature of iron oxides to mineral exploration. GAC-MAC Annual Meeting Prog Abs 31.

12. Singoyi, B., Danyushevsky, L., Davidson, G. J., Large, R., & Zaw, K. (2006). Determination of trace elements in magnetites from hydrothermal deposits using the LA ICP-MS technique. SEG Keystone Conference, Denver, USA.

13. Beaudoin, G., Dupuis, C., Gosselin, P., & Jébrak, M. (2007). Mineral chemistry of iron oxides: application to mineral exploration. In: Andrew CJ (ed) Ninth Biennial SGA meeting. SGA, Dublin, pp 497–500.

14. Xiao, B., Chen, H., Wang, Y., Han, J., Xu, C., & Yang, J. (2018). Chlorite and epidote chemistry of the Yandong Cu deposit, NW China: metallogenic and exploration implications for Paleozoic porphyry Cu systems in the eastern Tianshan. Ore Geol Rev, 100:168–182.

15. Lockington, J. A., Cook, N. J., & Ciobanu, C. L. (2014). Trace and minor elements in sphalerite from metamorphosed sulphide deposits. Miner. Petrol., 108 (6), 873–890.

16. Franklin, J. M., Gibson, H. L., Jonasson, I. R., & Galley, A. G. (2005). Volcanogenic Massive Sulphide Deposits. 100th Anniversary Volume. The Economic Geology Publishing Company, pp. 523–560.

17. Pirajno, F., (2009). Hydrothermal Processes and Mineral System. Springer, Perth 1–1250.

18. Fox, J. S. (1984). Besshi-type volcanogenic massive sulphide deposits e a review. Canadian Institute of Mining and Metallurgy Bulletin, 77, 57e68.

19. Peter, J. M. & Scott, S. D. (1999). Windy Craggy, Northwestern British Columbia: The world‟s largest Besshi-type deposit – In: Barrie, C. T. & Hannington, M. D. (eds.), Volcanic-associated massive sulfi de deposits. Processes and examples in modern and ancient settings. Rev. Econ. Geol., 8: 261–295.

20. MacLean, W. H., & Kranidiotis, P. (1987). Immobile elements as monitors of mass transfer in hydrothermal alteration; Phelps dodge massive sulfide deposit Matagami, Quebec. Econ Geol, 82:951–962.

21. Sillitoe, R. H. (2010). Porphyry copper systems. Econ Geol, 105:3–41.

22. Zhong, R. C., Li, W. B., Chen, Y. J., & Huo, H. L. (2012). Ore-forming conditions and genesis of the Huogeqi Cu–Pb–Zn–Fe deposit in the northern margin of the North China Craton: evidence from ore petrologic characteristics. Ore Geology Reviews, 44, 107–120.

23. Zhou, Z., Tang, H., Chen, Y. C. Z. (2017). Trace elements ofmagnetite and iron isotopes of the Zankan iron deposit, westernmost Kunlun, China: a case study of seafloor hydrothermal iron deposits. Ore Geol Rev 80: 1191–1205.

24. Bryndzia L. T, & Scott, S. D. (1987). The composition of chlorite as a function of sulfur and oxygen fugacity; an experimental study. Am J Sci, 287: 50–76.

25. Çiftci, E., & Hagni, R. D. (2005). Mineralogy of the Lahanos deposit a Kuroko-type volcanogenic massive sulfide deposit from the eastern Pontides (Giresun, NE Turkey). Geol. Bull. Turk., 48 (1), 55-64.

26. Eyüboğlu, Y., Santosh, M., Keewook, Y., Tüysüz, N., & Korkmaz, S. (2014). The Eastern Black Sea-type volcanogenic massive sulfide deposits: geochemistry, zircon U-Pb geochronology and an overview of the geodynamics of ore genesis. Ore Geology Reviews, 59, 29-54.

27. Revan, M. K., Genc, Y., Maslennikov, V. V., Maslennikova, S. P., Large, R. R., & Danyushevsky, L. V. (2014). Mineralogy and trace-element geochemistry of sulfide minerals in hydrothermal chimneys from the Upper-Cretaceous VMS deposits of the Eastern Pontide orogenic belt (NE Turkey). Ore Geology Reviews, 63, 129–149.

28. Ustaomer, T., & Robertson, A. H. F., (1994). Late Palaeozoic marginal basin and subduction accretion: the Palaeotethyan Kure Complex, Central Pontides, northern Turkey. J. Geo. Soc London, 151, 291–305.

29. Yalçın, C. (2018). Geology and formation of the Gökçedoğan (Kargi-Çorum) Cu ± Zn mineralization. PhD Thesis, İstanbul University, Institute of Graduate Studies in Science and Engineering, 301.

30. Günay, K., Dönmez, C., Oyan, V., Yıldırım, N., & Çiftçi, E. (2018). Geology and geochemistry of sediment-hosted hanönü massive sulfide deposit (Kastamonu – Turkey). Ore Geology Reviews, 101, 652–674.

31. Yalçın, C., Hanilçi, N., Kumral, M., & Kaya, M. (2022). Formation and Tectonic Evolution of Structural Slices in Eastern Kargi Massif (Çorum, Turkey). Bulletin of the Mineral Research and Exploration. Doi: 10.19111/bulletinofmre.1067604.

32. Yalçın, C., Hanilçi, N., Kumral, M., & Kaya, M. (2022). Magnetite Geochemistry of Beshhi-typeCu-Zn Mineralizations in Central Pontides (Kargı-Çorum). 2nd Advanced Engineering Days, 30-32.

33. Mukherjee, I. & Large, R. (2017). Application of pyrite trace element chemistry to exploration for SEDEX style Zn-Pb deposits: McArthur Basin, Northern Territory, Australia. Ore Geology Reviews. 81, 1249–1270.

34. Hu, X., Chen, H.Y., Zhao, L.D., Han, J.S. & Xia, X.P. (2017). Magnetite geochemistry of the Longqiao and Tieshan Fe–(Cu) deposits in the Middle-Lower Yangtze River Belt: Implications for deposit type and ore genesis. Ore Geology Reviews, 89, 822–835.

35. Kampmann, T. C., Jansson, N. F., Stephens, M. B., Olin, P. H., Gilbert, S. & Wanhainen, C. (2018). Syn-tectonic sulphide remobilization and trace element redistribution at the Falun pyritic Zn-Pb-Cu-(Au-Ag) sulphide deposit, Bergslagen, Sweden. Ore Geology Reviews, 96, 48–71.

36. Li, D. F., Fu, Y., Sun, X. M., Hollings, P., Liao, J. L., Liu, Q. F., Feng, Y. Z., Liu, Y. & Lai, C. (2018). LA-ICP-MS trace element mapping: Element mobility of hydrothermal magnetite from the giant Beiya Fe-Au skarn deposit, SW China. Ore Geology Reviews, 92, 463–474.

37. Robertson, A. H. F. (2002). Overview of the genesis and emplacement of Mesozoic ophiolites in the Eastern Mediterranean Tethyan Region. Lithos, 65, 1-67.

38. Robertson, A. H. & Ustaömer, T. (2004). Tectonic evolution of the Intra-Pontide suture zone in the Armutlu Peninsula, Nw Turkey. Tectonophysics, 381, 175–209.

39. Okay, A. I., Tüysüz, O., Satır, M., Özkan-Altıner, S. & Altıner, D. et al. (2006). Cretaceous and Triassic subduction-accretion, HP/ LT metamorphism and continental growth in the Central Pontides, Turkey. Geological Society of America Bulletin, 118, 1247–1269.

40. Okay, A. I., Gürsel, S., Sherlock, S., Altıner, D. & Tüysüz, O. et al. (2013). Early Cretaceous sedimentation and orogeny on the active margin of Eurasia: Southern Central Pontides, Turkey. Tectonics, 32, 1247–1271.

41. Aygül, M., Okay, A. I., Oberhansli, R., Schmidt, A. & Sudo, M. (2015). Late Cretaceous infant intra-oceanic arc volcanism, the Central Pontides, Turkey: petrogenetic and tectonic implications. Asian Journal of Earth Science. https://doi.org/10.1016/j.jseaes.2015.07.005.

42. Aygül, M., Okay, A. I., Oberhänsli, R. & Sudo, M. (2016). Pre-collisional accretionary growth of the southern Laurasian active margin, Central Pontides, Turkey. Tectonophysics, 671, 218–234.

43. Çelik, Ö. F., Chiaradia, M., Marzoli, A., Özkan, M. & Billor, Z. et al. (2016). Jurassic metabasic rocks in the Kızılırmak accretionary complex (Kargı region, Central Pontides, Northern Turkey). Tectonophysics, 672–673, 34–49.

44. Yalçın, C., Hanilçi., N., Kumral, M. & Kaya, M. (2018), Geochemistry of Kömürlükdere and Göçükdibi (Kargı-Çorum) Cu-Zn Mineralization, VIII. Geochemistry Symposium, Abstract books, p. 138-139, 02-06 May, Manavgat, Antalya, Turkey.

45. Nadoll, P., Mauk, J. L., Hayes, T. S., Koenig, A. E. & Box, S. E. (2012). Geochemistry of magnetite from hydrothermal ore deposits and host rocks of the Mesoproterozoic Belt Supergroup, United States. Econ. Geol. 107, 1275–1292.

46. Nadoll, P., Mauk, J. L., Leveille, R. A. & Koenig, A. E. (2015). Geochemistry of magnetite from porphyry Cu and skarn deposits in the southwestern United States. Miner. Depos. 50, 493–515.

47. Makvandi, S., Ghasemzadeh-Barvarz, M., Beaudoin, G., Grunsky, E. C., McClenaghan, M. B., Duchesne, C. & Boutroy, E. (2016). Partial least squares-discriminant analysis of trace element compositions of magnetite from various VMS deposit subtypes: Application to mineral exploration. Ore Geol. Rev. 78, 388–408. https://doi.org/10.1016/j.oregeorev.2016.04.014.

48. Beaudoin, G. & Dupuis, C. (2009). Iron-oxide trace element fingerprinting of mineral deposit types. In: Mumin, H., Corriveau, L. (Eds.), Exploring for Iron Oxide Copper-Gold Deposits: Canada and Global Analogues, Short Course, Geological Association of Canada Annual Meeting, Québec City, 107–121.

49. Yalçın, C., Hanilçi, N., Kumral, M., & Kaya, M. (2022). Magnetite geochemistry of Beshhi-type Cu-Zn mineralizations in Central Pontides (Kargı-Çorum). *Advanced Engineering Days (AED)*, *2*, 30-32.

Engineering Applications

https://publish.mersin.edu.tr/index.php/enap

Measurements and modelling of PM2.5 level in summertime period in Novada Main Shopping Centre Konya, Turkey

Sukru Dursun [*1] [iD], **Mina Naseer Qasim** [1] [iD]

[1]*Konya Technical University, Environmental Engineering Department, Türkiye, sdursun@ktun.edu.tr; mineenviro@gmail.com*

check for updates

Abstract
The people are spending most more the daily time in closed environments in their life. The living atmospheric air quality is important because of this long contact time. Air pollution is the presence of particles in the atmosphere because of the interaction of dust, gas, smoke, water vapor, odor and many chemicals in amounts that can harm living things and other things. This pollution, which is an environmental health problem affecting all countries of the world in recent years, causes the death of 3 million people every year in the world. In another definition, air pollution occurs because of fossil fuel burning, that is, anthropogenic activities such as natural gas, coal, and oil, to power industrial processes and motor vehicles. Industrialized countries expect a modern living place in modern life and living spaces. Their vehicle demands bring along motor vehicles and industrialization close to city centers and this effects a damage the human and environmental health. Konya city center is one of the most crowded plan sections of Turkey, and to finish our preparations together with central planning and industrial planning. People also prefer to spend their spare time doing great shopping that Novada Shopping Centre is one of them. It turns out that the forecasts of this weather arise if it is for the air pollution of the air from the people who come from shoppers and visitors. The basic organization for a good material for obtained air quality preparations. Improvement planning in the current situation achieves the goal of the air quality specialist so that the results obtained can be achieved.

1. Introduction

Looking at the main causes of air pollution, the increasing population, urbanization, and the need for energy from industrialization have led to an increase in the need for fossil fuels [1-2]. As a result of the excessive use of fossil fuels, changes occur in the structure of the atmosphere day by day. People are constantly breathing the air around them all the time. Gases and particles in the air are exhaled together with the inhaled air. These pollutants damage people's heart, lungs, and other organs. When we look at the death cases caused by air pollution in the past, approximately 20 people died in Pennsylvania in 1948, while this event killed 63, 3000 people in Belgium in 1930 and in London in 1952 due to air pollution. Although different pollutants are released into the atmosphere because of natural physical events (volcanoes, fires), anthropogenic (human) activities have been determined as the primary source of air pollution in the environment [3-4].

Indoor air: It is expressed as the air contained in buildings such as workplaces, residences, shopping and living centers, interior spaces of transportation vehicles (bus, car, ship, train, etc.), schools and offices. Indoor air pollution, on the other hand, is the presence of substances that can harm health in the above-mentioned

environments. These respirable substances are generally observed in the form of gas, dust, vapor. The amount and concentration of these substances in the environment differ according to the characteristics of the environment, the building and interior materials used in the construction of the building, and the behaviors of the individuals in it. For example, the increase in dust and particulate matter rates in the corridors caused by the movements of the students in a school building, as well as the equipment such as printing machine and photocopying machine used in a stationery shop, caused the spread of various volatile organic compounds to the environment [5].

The energy saving policies of recent times in countries and the construction of insulated buildings with insufficient ventilation, minimum indoor air circulation, no windows that can be opened to the outside, and air conditioners have had a significant impact on the air quality of these indoor environments. It is a known fact that human performance is affected by indoor air quality. For human comfort and productivity, the indoor environment must be at 19-20°C and the humidity of the air he breathes must be 30-50% [6].

Although indoor pollutants have many types, they differ from each other. Some of these pollutants occur due to indoor cleaning activities (VOC), cooking actions (CO, NO_x, particles), indoor painting processes, cigarette burning (CO, particles) and some activities such as spray perfumes used for odor removal. In addition, it is possible to spread from furniture, building materials, products containing chemicals. In addition, some indoor pollutants can be produced in the outdoor environment and transported to the indoor environment through a window or door [7].

In addition to advantages such as cleaning and hygiene, the effects of disinfectants consisting of chemicals carry a great risk on health. The effect of the volatile organic compounds emitted into the environment during the cleaning activity can also spread in the gas phase after the cleaning is completed and enter the body by inhalation. In addition, the same risk is in question for the individuals who are in the environment as well as the person doing the cleaning [8].

Environmental tobacco smoke (CTS) describes the smoke from the tip of the cigarette when the cigarette is burned by the person who smokes it. The health risks of cigarettes, which are widely used in Turkey and even in the world, cause health problems not only for the users, but also for the individuals around the environmental tobacco smoke emitted during use. Environmental tobacco smoke consists of (mainstream smoke) smoke emitted by the smoker and (side stream smoke) smoke from the end of the cigarette when it is burned [9].

The fact that the emissions from the main combustion smoke are more dominant than the afterburner emissions explain the ETS passive smoking. When we searched many epidemiological studies, it was determined that the effects of passive smoking on health were caused by the risk of lung cancer, breast cancer in women [10-11], affecting the functions of the immune system [12] and impaired sense of smell.

In 2013, The World Health Organization [13] introduced that, because of a study conducted in Turkey in 2000, it was found that approximately 20% of the patients staying in hospitals were caused by smoking and more than half of the male population in the country was consuming cigarettes daily. Turkey implemented the smoke-free policy for the first time in 2008 with a strict management to protect indoor air quality, and successful results were achieved, resulting in a 20% reduction in smoking and a 27% reduction in hospitalization rates [14].

Dursun et al. [15] evaluated the change of PM2.5 values in open environments according to certain hours of the day and different seasons in a study they conducted at Selçuk University. After determining 40 sampling sites on the campus, measurements were made in the morning, noon and evening hours during the winter and spring seasons. As a result, high PM2.5 concentrations were obtained in the morning hours of the winter season. In the spring season, the highest values were found at noon. The collected data were modelled using the ArcGIS program. PM2.5 variations created using the collected data and according to the seasons are presented as pictures. It has been suggested that the reason for the high results obtained in winter is due to the fossil fuels used. It was also observed that there was a difference between weekdays and weekends. Weekend values were lower than weekdays.

PM2.5 exposure threshold has been defined to provide a safe and complete level of protection against all adverse health effects [16]. Nevertheless, in order to limit the health effects of fine particle pollution, the World Health Organization (WHO) has proposed guidelines for annual and short-term (24 hours) human exposure to PM2.5. In addition to these global standards, WHO encourages governments to define and implement national standards [13]. Along with the guideline levels, WHO has defined three intermediate exposure levels to gradually lower PM2.5 concentrations. In addition, WHO recommends the annual average, with priority over the 24-hour average, as sporadic high PM2.5 events are generally less harmful than annual exposure to high PM2.5 levels. The relationship between human diseases and poor air quality has been recognized since ancient times. In the twentieth century, the health effects of air pollution have now entered the world's consciousness. The effect of ultrafine particles on health is more effective and dangerous than coarse particles [17]. Thus, the chemical properties of particles with an aerodynamic diameter of less than 1 μm are of great importance for health [1]. particulate matter affects all population groups, but the sensitivity varies depending on the person's health status and age [18].

PM10 reaches the inside of the lungs, slows down the conversion of carbon dioxide in the blood to oxygen and causes shortness of breath. Meanwhile, there is a great and serious pressure on the heart as it has to work faster in order to eliminate the lack of oxygen [19]. To achieve this aim, particulate matter PM2.5 measurements were

made in the Novada shopping center in Konya, which is called one of the most industrial cities. Modelling was done by mapping the obtained data with Surfer 16 program. The results obtained were interpreted according to three different seasons and then compared with each other.

2. Material and Method

2.1. Material

The variation of the levels of air pollutant concentrations between regions in big cities is shaped depending on the characteristics of the regions [20]. In this study, which was started based on the shopping centers in the Selçuklu district of Konya, were selected for measurements. This places, which were chosen by paying attention to the fact that they are closed environments, is located on the Novada shopping center located in the new development area of the bay was chosen as the second place for data collection.

2.1.1. Working area

Novada outlet shopping and living centre located in the bus station area, which is known as the new development area of the bay, was opened for use in 2015. This shopping centre, with a total area of 33000 m², has 2 outdoor and one indoor parking lots, 51 stores, 12 restaurants and 3 playgrounds. Consisting of 4 floors, this building looks like the letter L when viewed from the satellite image, and 3 of the 4 entrance doors are located on the front of the building facing the main street. For this reason, it is directly exposed to air pollution caused by traffic. The other entrance door is used as a parking garage entrance on the -1 floor and there is no direct exposure to outdoor air pollution. There are cash machines, travel agency and tailor shops on this floor. The first measurement point was chosen right in front of the entrance door (Figure 1).

Figure 1. Novada shopping and living centre [21]

The ground floor (0 in order) has two entrance doors at the same level on the north and south facades. On this floor, there are mostly household goods, electronic goods stores, cosmetics, a small number of cafes and clothing stores. The possible source of pollution was mostly thought of as the exhaust fumes carried in from the open parking lot located at the front of the shopping mall and where both doors open directly there. The first floor consists entirely of clothing stores, and the possible source of pollutants is considered as fabric types and store perfumes. The fourth entrance door is located at the back of this floor. There is a ventilation system on the ceiling and the floor in the entire building is covered with ceramic porcelain.

The third floor consists of restaurants, fast food kitchens and children's playgrounds. The most significant source of pollutants of this floor is emissions from cooking in restaurants. Restaurants are defined as publicly communal indoor environments where many people spend most of their time. For this reason, the clean and healthy air in these areas not only protects the visual appearance, but also protects the health of employees and visiting customers [22]. Small-sized particulate matter (organic and inorganic) and carbon monoxide in kitchens are the main source of combustion in cooking activities [23].

When we look at the playgrounds, the floor coverings that can affect the air quality and cause the spread of volatile organic compounds, the play building materials used, the respiratory rate and mobility during the activities can be listed as the inadequacy of the ventilation system in that area.

This mall has fresh air handling unit on the entrance, first and second floor. The air conditioning system at the entrance and the first floor gives the indoor air to the floors, after taking the air from the outside in normal air temperatures and returns it to the inside by passing it through the filter inside itself (Figure 2).

The first measurement point is located at the entrance of the parking lot on the -1 floor, a single measurement point was considered sufficient due to its area on this floor. The points (2-5) were taken at different points of the

ground floor to show the concentration difference in front of the entrance doors and other parts of the floor. The points (6-11) were taken by choosing certain places along the length of the first floor. (12-17) points were chosen in front of the restaurants and playgrounds on the second floor. Measurement points are shown on the map in Figure 3.
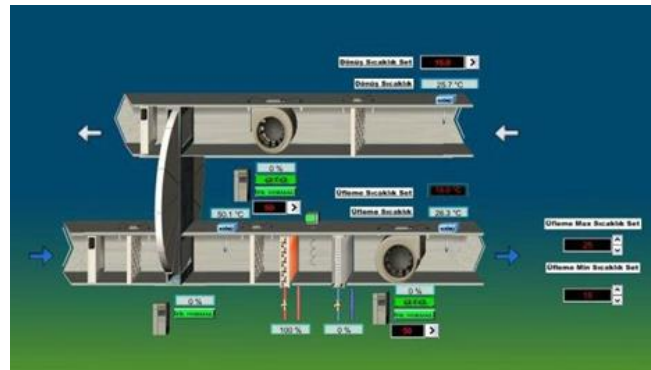
Figure 2. The filter system for aeration of Shopping centre
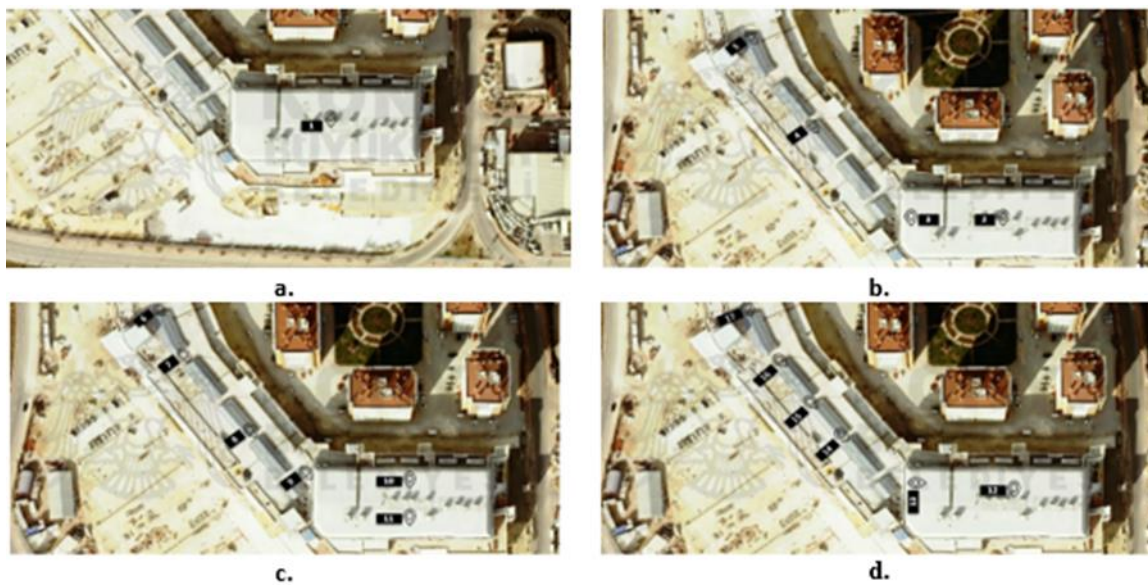
Figure 3. Measurement points according to floors in Novada AVM, a. (-1) floor, b. (0) floor, c. (1) floor, d. (2) fold [14]

2.1.2 Particulate matter measuring device

The measurement methods of dust and particles in the air vary according to the volume of the particles and the desired results in the study. The "particle counter PCE-PCO1" is a laser particle counter and dust measuring device configured to determine the concentration of airborne particles by means of electronic recording. Data can be displayed numerically from the particle counter PCE-PCO1 device (Figure 4). This device is used in clean rooms, indoor air quality, exposure to exhaust, tobacco or cigarette smoke and other harmful air pollutants, and for monitoring airborne dust levels.

Figure 4. Particulate matter measuring device "particle counter PCE-PCO1"

The particle counter was developed to precisely determine the pollution level. The device measures 6 different particle sizes (0.3 μm, 0.5 μm, 1.0 μm, 2.5 μm, 5.0 μm, 10 μm), measurements (more than 5000 measurements) can be saved in the internal memory, A large color LCD with backlight, for image and video recording It includes a built-in camera, sensors to measure air temperature, dew point and relative humidity, displaying temperature measurements in degrees Celsius (°C) or degrees Fahrenheit (°F).

This device, which is deemed suitable for taking measurements at different points in terms of its easy portability, should be charged and prepared before going to the measurement site, and should be zeroed by making (calibration) in a dust-free environment before the measurement. After reaching the measurement area, the device is turned on by pressing the power button and the ENTER button is pressed to switch to the particle counting screen. The covers of the dust and temperature sensors on the top of the device are opened and they are made ready to detect the dust and temperature in the environment and the START / RUN button is pressed. The unit starts measuring for 30 seconds. After the measurement time is over, the data is saved by pressing the F2 button. The device also has 3 different sampling modes: cumulative, differential (differential) and concentration. The desired mode must be selected before measuring. In addition to these features, the date and time, language and screen brightness can be adjusted optionally from the system settings.

2.1.3 Modelling and graphics program surfer 16

This software, produced by Golden software company, consists of a 3D graphics system. It is used for gridding scattered data recorded in different environments, creating contour maps and obtaining 3D images [24]. People from many different disciplines use Surfer. Since 1984, more than 100,000 scientists and engineers worldwide have discovered the power and simplicity of Surfer. The program's exceptional guiding and Shaping capabilities have made it the software of choice for working with XYZ data. Over the years, this program has seen use by hydrologists, engineers, geologists, archaeologists, oceanographers, biologists, geophysicists, climatologists, educators, students, and more. It performs well to visualize XYZ data with stunning clarity and accuracy [25].

This program, which transforms the collected data into information, visualizes the data in high quality while preserving its accuracy and sensitivity. Along with Surfer's extensive modeling tools, interpolation and grating parameters can be adjusted, define errors and breaks, or perform grid calculations such as volumes, transformations, smoothing or filtering [26]. It consists of map types such as contour, calculation, 3D surface, color relief, etc., and provides tools to visualize and model all types of data. The type of map obtained in this study is contour map. After making all the statistical calculations by turning the XYZ data loaded on the worksheet into a grid, the map is created by selecting the desired map type. To make the map more meaningful and readable, the map can be personalized with various customization options, thanks to the window in the lower left corner of the screen. These options include sections, magnifiers, scale bars and edits such as multi-axis, linear or logarithmic colour scales, combining multiple maps, text, line, fill, and symbol properties [26].

2.2 Method

2.2.1 Particulate matter PM2.5 measurement method

The research carried out to determine the particulate matter concentrations, the pollutant sources in the external environment were examined. By comparison, there is little information on indoor particulate matter pollution, its concentrations, sources, and exposure levels to people who spend most of their time in various indoor environments [27]. In this study, which was started to determine the effect of seasonal changes on particulate matter, summer, autumn, and winter seasons were selected to take measurements. In summer and autumn seasons, measurements were made for one week at Selçuk University rainbow social facilities and Novada shopping center, and during the winter season, weekday and weekend measurements were made in both locations. The total measurement period was completed as 4 days.

In all three seasons when the measurements were made, the daily measurement program lasted for 10 hours depending on the working hours of the places, and the measurements were repeated 6 times a day at 2-hour intervals. After taking the coordinates of the measurement points, the data collected at the end of each season are listed in the Excel program in a way that daily, weekly, and hourly averages will be taken. Besides the X and Y coordinates, the Z coordinate represented the measured PM2.5 values. A worksheet was created by transferring X Y coordinates and measurement values to the SURFER 16 program. All statistical calculations were made by making the prepared data into a grid. Then, contour map was selected from the map options to show the contour lines, and the customization window was used to clearly show the high and low concentrations and the distribution lines on the map.

3.Results

Within the scope of the thesis, three measurement periods were determined in the Novada shopping centre located in the Kosovan district. The first measurement period was made in the summer season, the second measurement period in the autumn season, and finally the third measurement period in the winter season. The measurements started one day after they were completed in Novada AVM for the season and ended after 1 week. The first measurement of the day started at 11:00, with a two-hour break between each measurement, a total of 6 measurements were made, and the last measurement was made at 21:00. According to the measurement points made, a separate map was drawn for each floor. As a result of the study, the average values of PM2.5 obtained from the examination of all data on weekdays and weekends are 336.97 μg/m³ and 322.55 μg/m³ for summer, 345.98 μg/m³ and 652.57 μg for autumn, respectively. It was found to be 595.88 μg/m³ and 906.4 μg/m³ for the winter season (Table 1).

Table 1. Seasonal particulate matter PM2.5 weekday and weekend averages in Novada mall

Measurements time	PM$_{2,5}$ weekday average value μg/m³	PM$_{2,5}$ weekend average value μg/m³
Summer	336.97	322.55

The results obtained from the measurements made during the summer season, at 11:00 on weekdays, were found as follows, respectively: minus the first floor 1650 μg/m³, (zero) ground layer 720 μg/m³, first layer 460 μg/m³ and the second layer 720 μg/ m³. At the first measurement hour of the day, the highest PM2.5 concentration was found on the minus first floor Figure 5. This floor, where there are barbers, Attar, PTT, cash machines and tailor machines, has a single door. This door opens to the indoor parking lot of the shopping mall, so it was observed that the vehicle emissions in the parking lot spread into the atmosphere of this floor when the doors were opened, while the pollution level in the indoor environment was expected to disperse to the outside environment. In addition, the fact that the ceiling height of this floor did not exceed approximately 3.5 m caused the particles to be trapped in a narrow space and closer to the respiratory level. Looking at the ground floor, it is seen that the pollution level at the 2nd measurement point in the lower right corner of the building (2nd and 1st measurement points are on different floors and coincides) is more intense than the other parts of the building. This means that the pollution from the minus 1st floor has spread to the 2nd point. When looking at the other floors, lower concentrations are generally observed because the ventilation is working, less visits by people and the cleaning activities have just been done. The maps are shown in Figure 5.

Figure 5. In Novada AVM, summer season is at 11:00 a.m. on weekdays. (-1) floor, b. (0) floor, c. (1) floor, d. (2) floor average

Weekend values were found to be relatively lower than during the week. As a result of the measurements, the PM2.5 concentration in each floor is as follows, respectively: minus 600 μg/m³ for the first layer, (zero) entry layer 430 μg/m³, first layer 560 μg/m³ and second layer 245 μg/m³. Maps indicating weekend concentrations are shown in Figure 6.
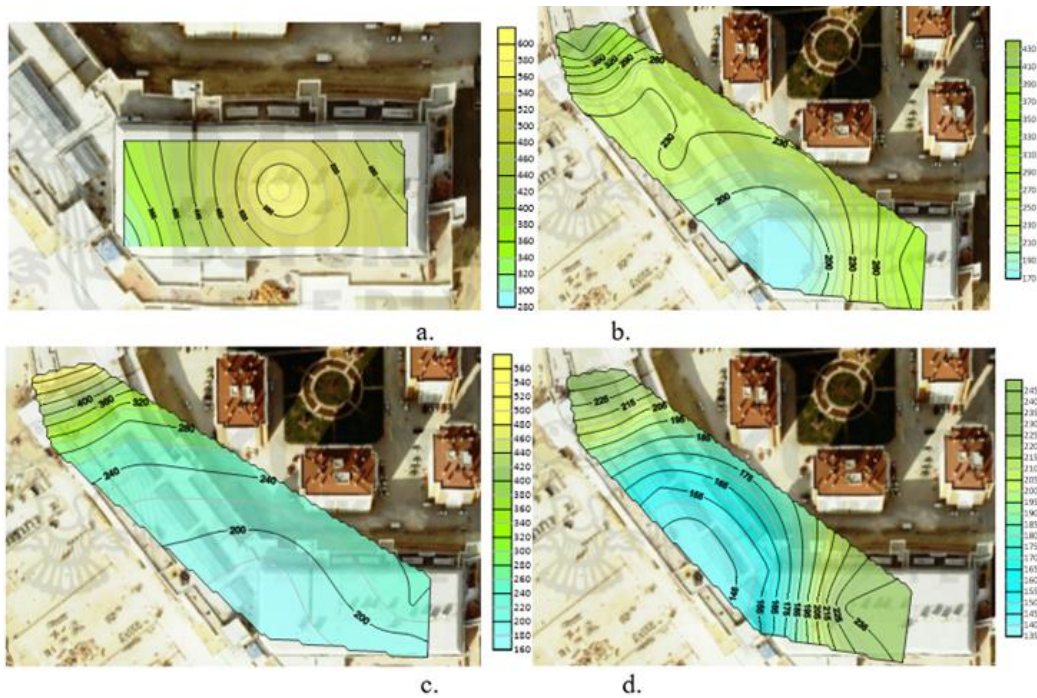
Figure 6. At Novada AVM on summer weekend, at 11:00 a.m. (-1) floor, b. (0) floor, c. (1) floor, d. (2) floor average

PM2.5 concentrations seen in the shopping mall at 13.00, when the second measurement of the day is made, are respectively: minus 1020 µg/m³ for the first floor, (zero) 540 µg/m³ for the ground floor, 400 µg/m³ for the first floor and 680 µg/m³ for the second floor. Again, while the values were found to be high at the first measurement point, lower concentrations were found in the other floors thanks to ventilation. The maps are shown in Figure 7.
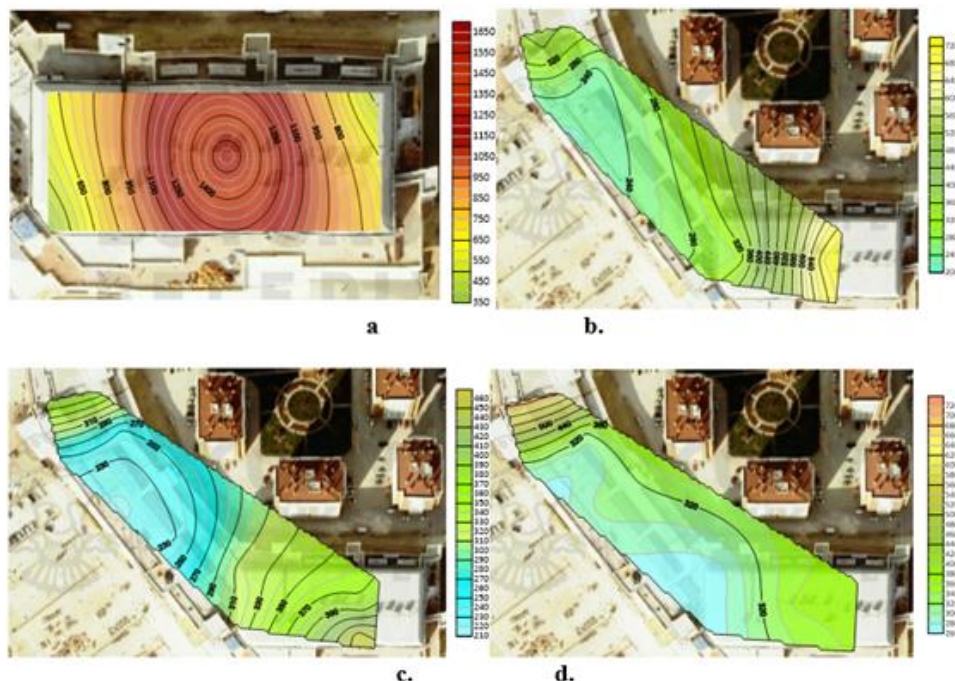

Figure 7. In Novada AVM, summer season is 13.00 a.m. on weekdays. (-1) floor, b. (0) floor, c. (1) floor, d. (2) floor average

At 13.00 on the weekend, PM2.5 concentrations did not show a sharp difference and decreased. Concentrations were found for each coat: minus 640 µg/m³ for first coat, (zero) ground coat 420 µg/m³, first coat 560 µg/m³ and second coat 540 µg/m³. According to the color scale on the particulate matter measuring device, green areas indicate respirable pollution, and as the concentrations increase towards orange and red, it means that the pollution in that environment is dangerous. The maps are shown in Figure 8.

Figure 8. At Novada AVM on summer weekend, 13.00 a. (-1) floor, b. (0) floor, c. (1) floor, d. (2) floor average

The weekday values of the measurements made at 15:00 were found as: minus 1040 µg/m³ for the first layer, 540 µg/m³ for the (zero) entrance layer, 530 µg/m³ for the first layer, and 410 µg/m³ for the second layer, respectively, for each layer. It is similar to the results found at 13:00. The maps are shown in Figure 9.

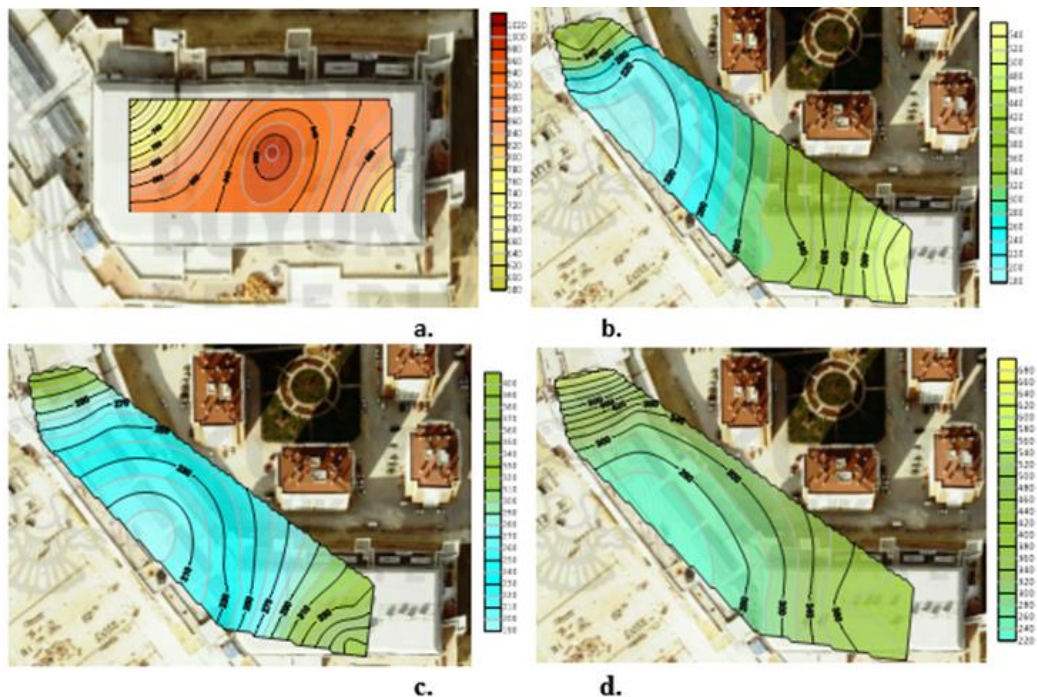**Figure 9**. In Novada AVM, summer season is at 15.00 a.m. on weekdays. (-1) floor, b. (0) floor, c. (1) floor, d. (2) floor average

Lower values were found in the results obtained from the measurements made at the end of the week than the results obtained during the week. Concentrations were found for each layer, respectively: minus the first layer 1040 µg/m³, (zero) ground layer 540 µg/m³, first layer 530 µg/m³ and second layer 410 µg/m³. Distribution maps of PM2.5 concentrations are shown in Figure 10.

Figure 10. Summer season at Novada AVM at 15.00 a.m. on weekends. (-1) floor, b. (0) floor, c. (1) floor, d. (2) floor average

The weekday results of the measurements made at 17.00 were found as follows for each layer, respectively: minus the first layer was 840 µg/m³, (zero) the ground layer was 780 µg/m³, the first layer was 460 µg/m³ and the second layer was 540 µg/m³. Distribution maps of PM2.5 concentrations are shown in Figure 11.

Figure 11. In Novada AVM, summer season is 17.00 a.m. on weekdays. (-1) floor, b. (0) floor, c. (1) floor, d. (2) floor average

The weekend results of the measurements made at 17.00 were as follows: minus 640 µg/m³ for the first layer, 370 µg/m³ for the (zero) ground layer, 560 µg/m³ for the first layer and 315 µg/m³ for the second layer. Distribution maps of PM2.5 concentrations are shown in Figure 12.
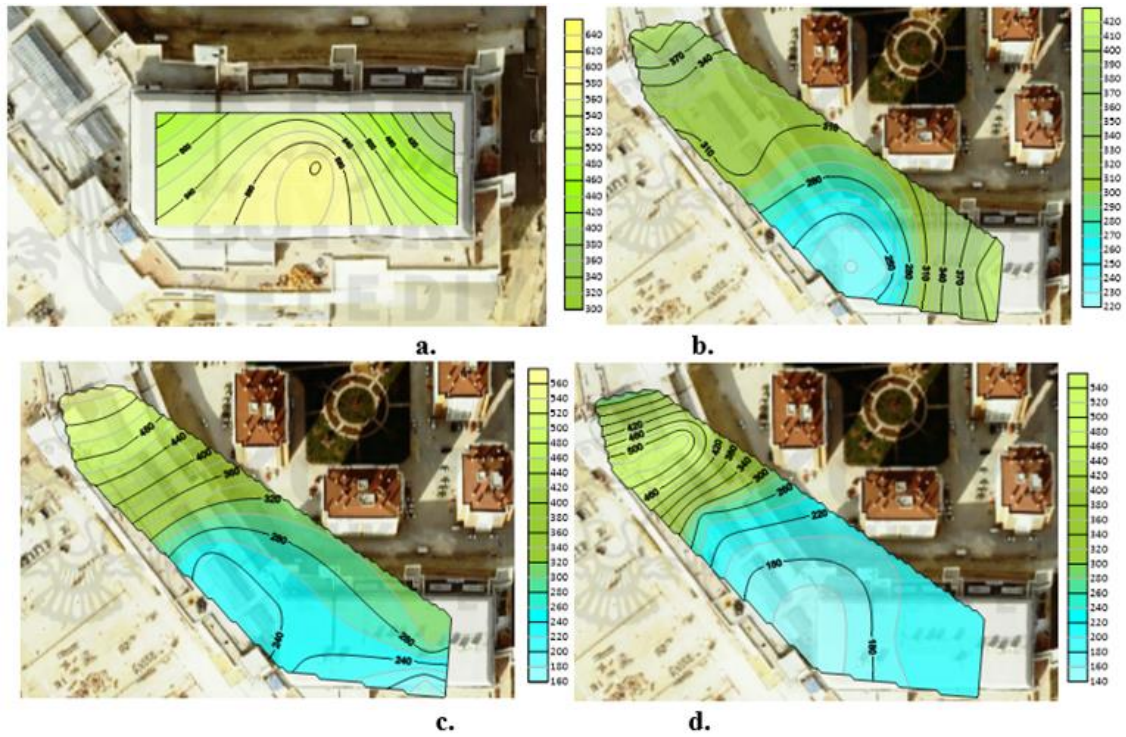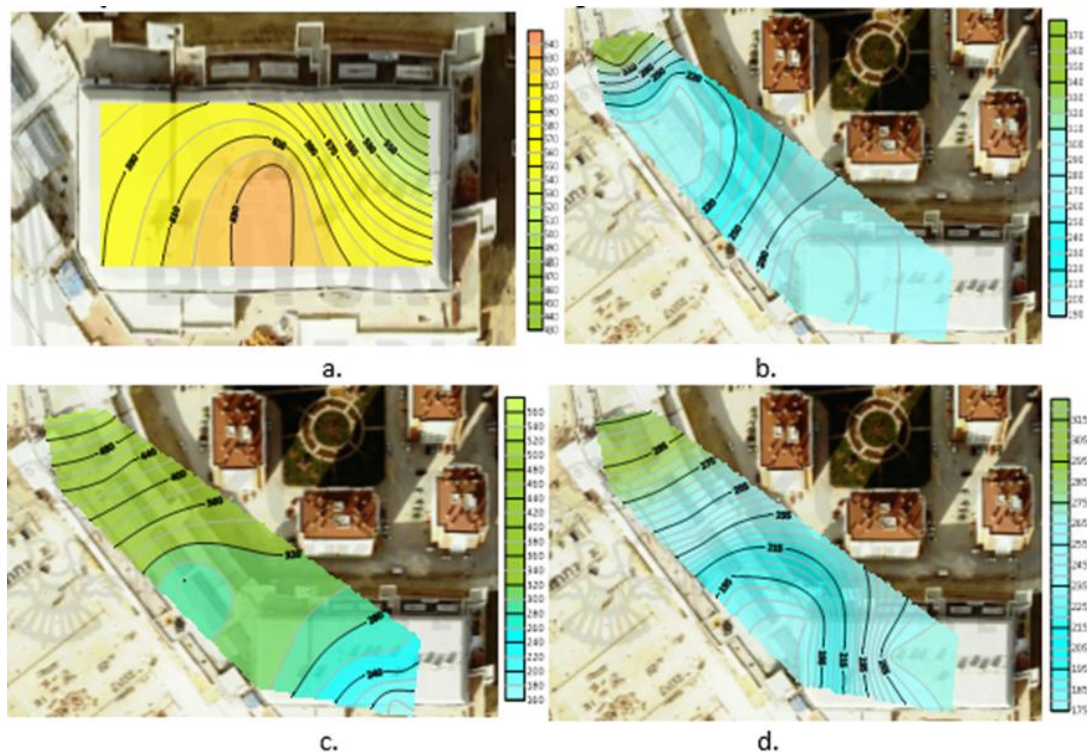
Figure 12. At Novada AVM on the summer weekend at 17.00 a. (-1) floor, b. (0) floor, c. (1) floor, d. (2) floor average

The weekday results of the measurements made at 7:00 pm were found as follows: minus the first floor was 940 µg/m³, (zero) the ground floor was 520 µg/m³, the first floor was 580 µg/m³ and the second layer was 420 µg/m³. Distribution maps of PM2.5 concentrations are shown in Figure 13.
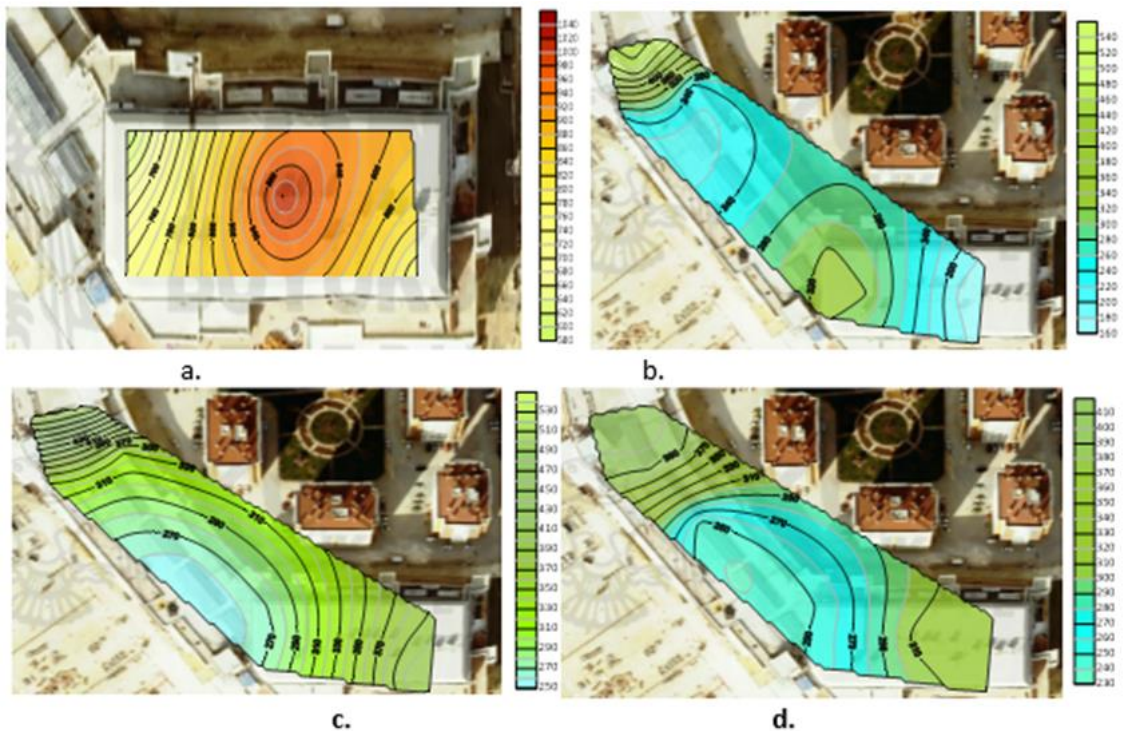

Figure 13. In Novada AVM, summer season is at 19.00 a.m. on weekdays. (-1) floor, b. (0) floor, c. (1) floor, d. (2) floor average

The weekend results of the measurements made at 7:00 pm were found as follows: minus 660 µg/m³ for the first layer, (zero) ground layer 390 µg/m³, first layer 360 µg/m³ and the second layer as 305 µg/m³. Distribution maps of PM2.5 concentrations are shown in Figure 14.
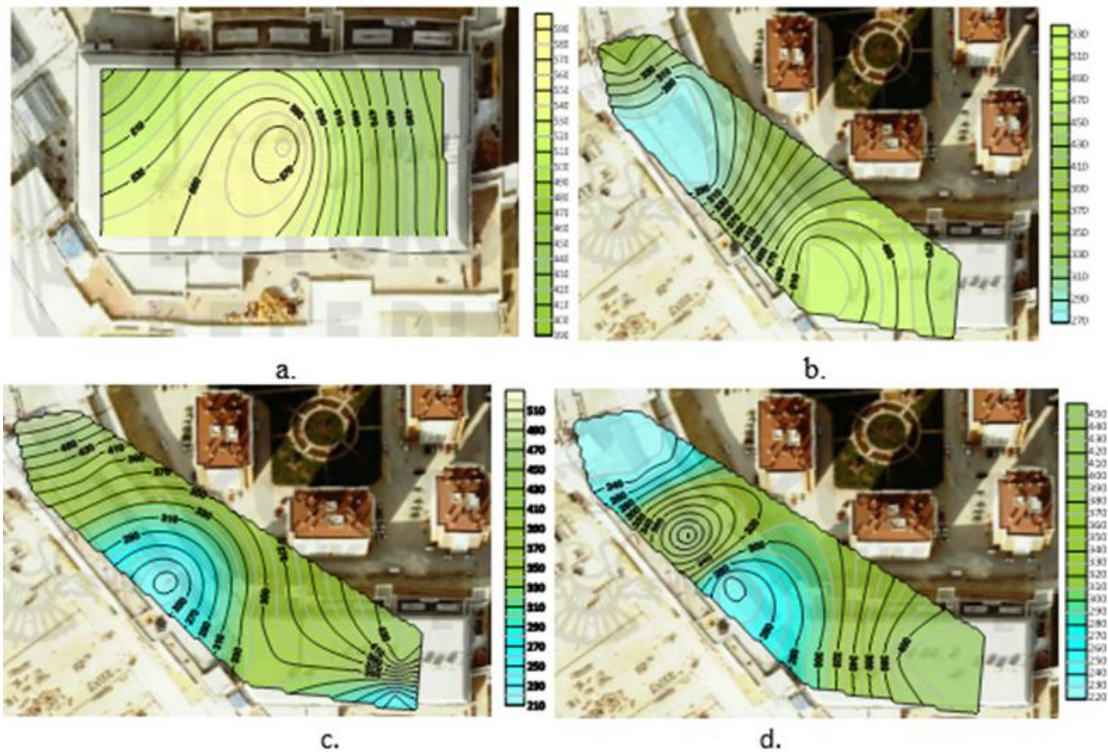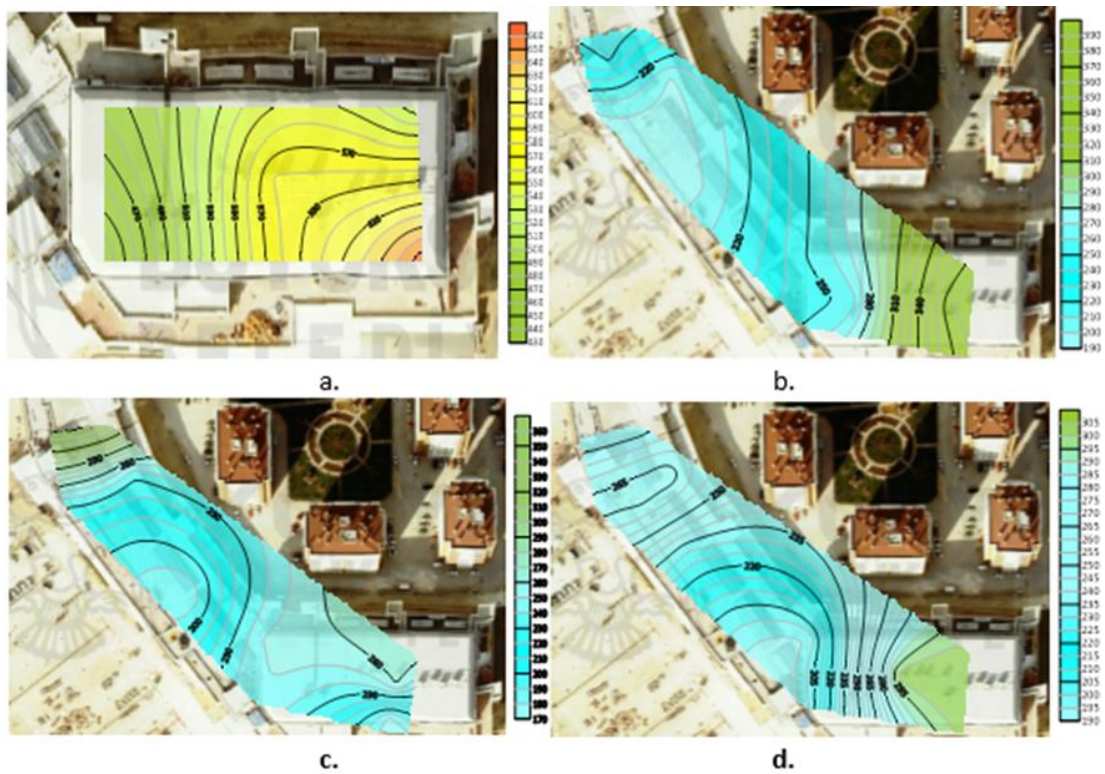
Figure 14. Novada AVM at 19.00 a.m. on the summer season weekend. (-1) floor, b. (0) floor, c. (1) floor, d. (2) floor average

The weekday results of the measurements made at 21:00 were found as follows: minus 1400 µg/m³ for the first layer, 840 µg/m³ for the (zero) ground layer, 1250 µg/m³ for the first layer and 1050 µg/m³ for the second layer. It was observed that the concentrations increased again in the minus first floor. Since the shopping mall was close to closing time, vehicle emissions increased due to the activity in the parking lot, causing PM2.5 values to increase. Rising values were seen on the ground floor, on the first and second floors, on the upper corner of the building. It is thought that the indoor particulate pollution caused by the cooking activities of the restaurants on the second floor is distributed to the first and ground (zero) floors. Distribution maps of PM2.5 concentrations are shown in Figure 15.
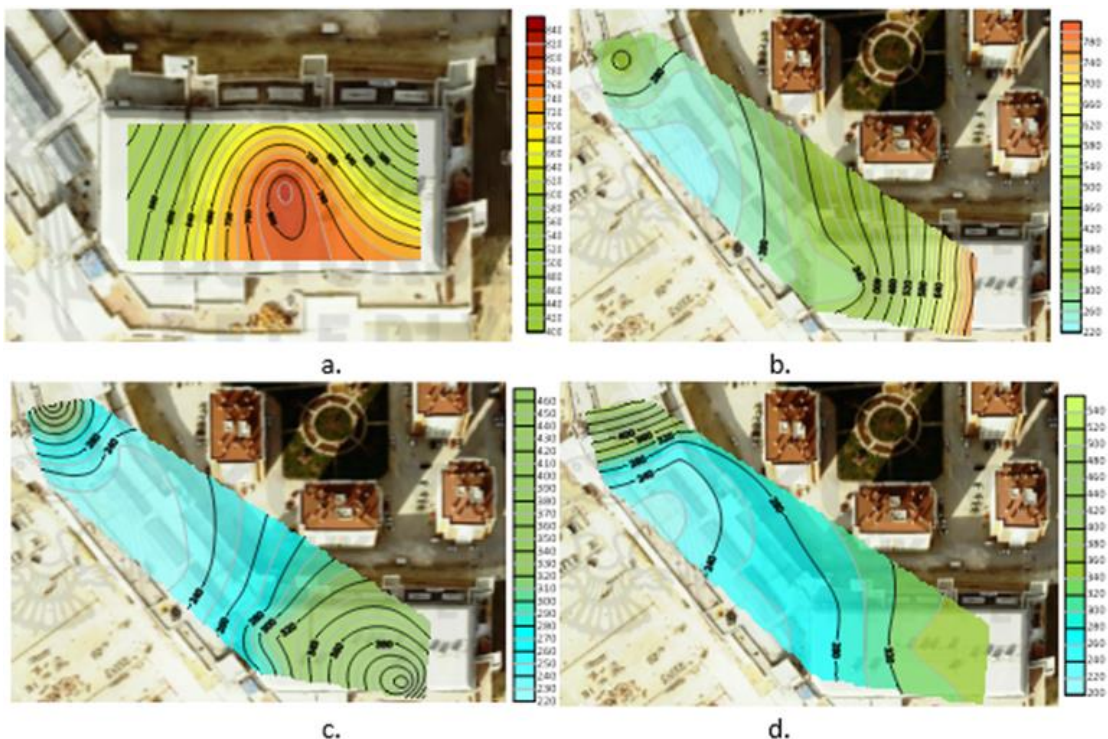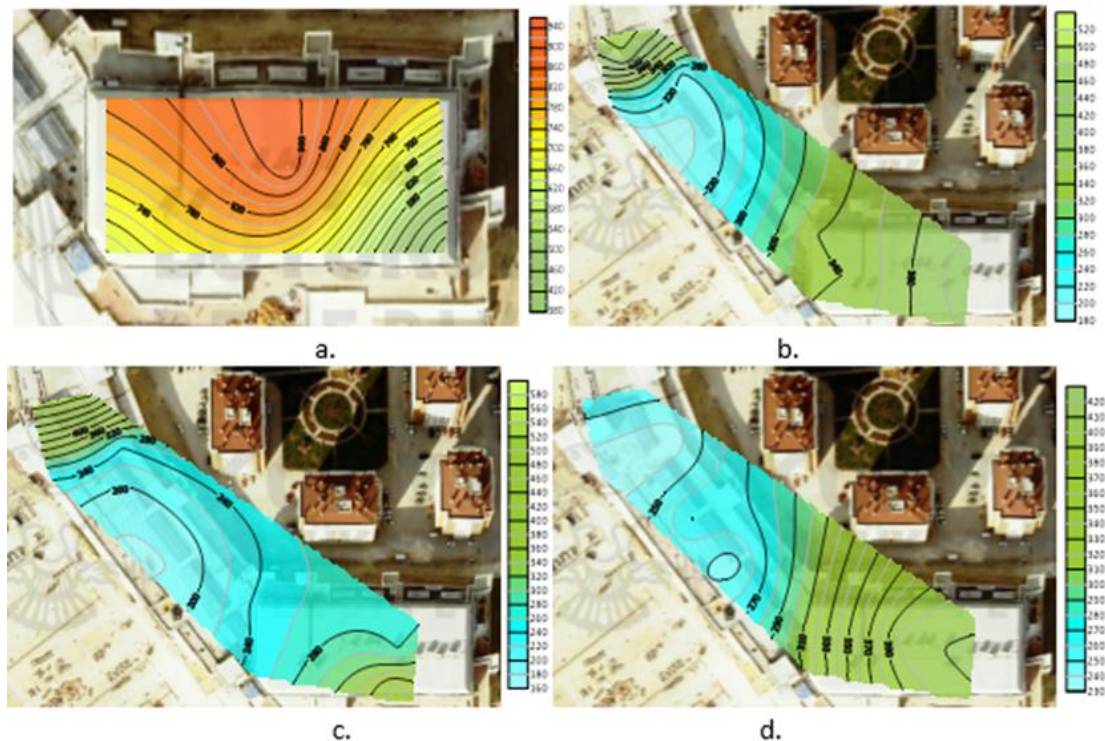

Figure 15. In Novada AVM, summer season is 21.00 a.m. on weekdays. (-1) floor, b. (0) floor, c. (1) floor, d. (2) floor average

The weekend results of the measurements made at 21:00 were found as follows: minus the first floor was 410 $\mu g/m^3$, (zero) the ground floor was 345 $\mu g/m^3$, the first floor was 450 $\mu g/m^3$ and the second floor was 680 $\mu g/m^3$. Distribution maps of PM2.5 concentrations are shown in Figure 16.
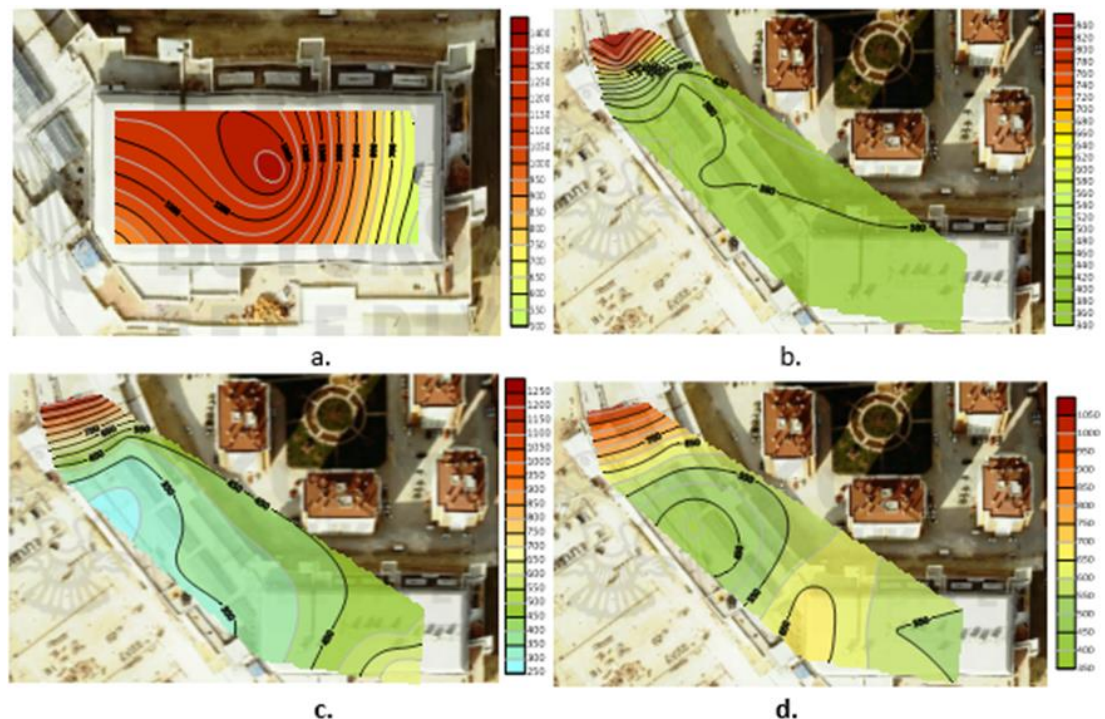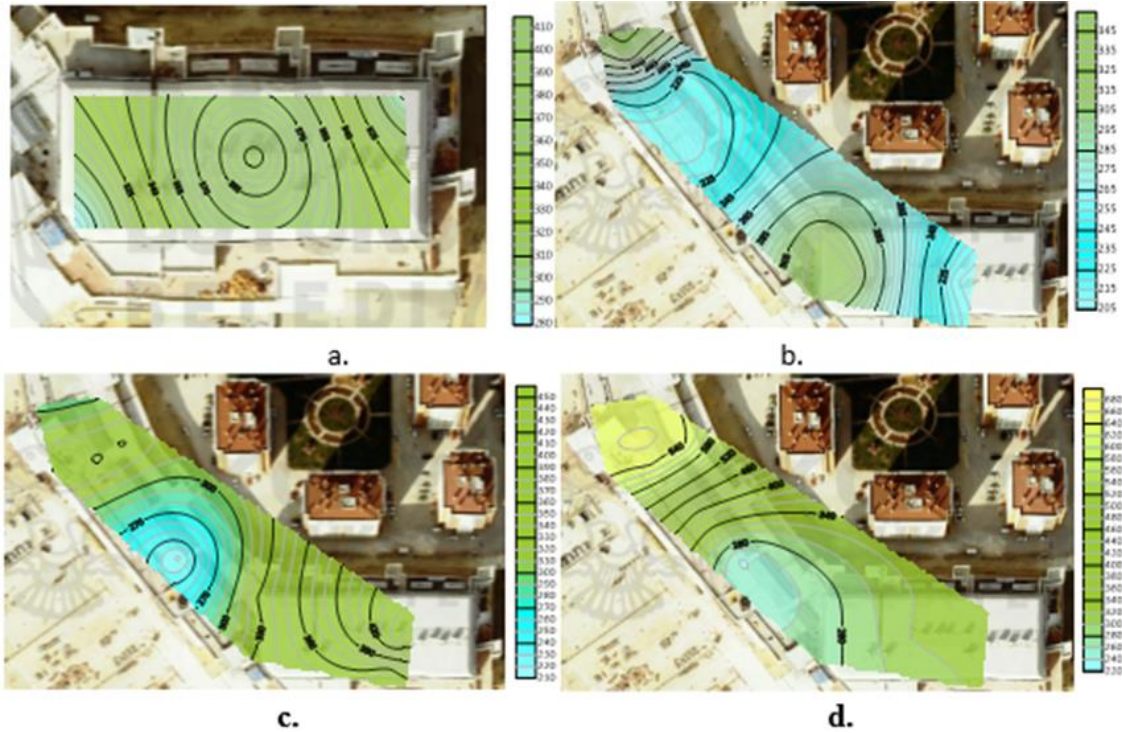

Figure 16. Summer season at Novada AVM at 21.00 a.m. on weekends. (-1) floor, b. (0) floor, c. (1) floor, d. (2) floor average

With a general interpretation, as seen in the maps of the measurements made in Novada AVM during the summer season, PM2.5 concentration averages were found to be higher on weekdays than at weekends. As a result of the measurements made in the summer period, the lowest PM2.5 value is 245 $\mu g/m^3$. This value exceeds the hourly 25 $\mu g/m^3$ limit set by WHO, EEA and EPA for PM2.5. The standard value for PM2.5 in the air quality assessment management and regulation, which was last updated in 2008 in Turkey, is 200 $\mu g/m^3$. The results obtained exceed the HKDYY limit value.

5. Discussion and Recommendations

In this thesis, the importance of indoor air quality, which has started to be noticed in Turkey in the last few years, has been prepared. In this study, which was started in Konya, one of the most important industrial cities of the country, based on shopping centers, particulate matter PM2.5 measurements, which carry serious risk factors on human health, and which is in the second rank among air pollutants by the World Health Organization, were made [28]. Two different environments were selected for the measurements. Rainbow shopping center located on Selçuk University Alaeddin Keykubat campus was chosen as the first location for measurements [29-30]. Novada outlet mall was deemed suitable for the second location. Measurements were made in three separate periods. The first sampling period was carried out between 21.05.2018 - 03.06.2018 in the summer season, the second sampling period was carried out between 24.09.2018 - 07.10.2018 in the autumn season, and the third sampling period was carried out between 25.12.2018 - 07.01.2019 in the winter season. While sampling hours in Novada AVM were held at (09.00-19.00) intervals in all three seasons, they were held at (11.00-21.00) intervals in Novada AVM due to the opening time. How particulate matter PM2.5 affects indoor air quality over three seasons and from what causes it has been examined. The results were mapped and modelled using the Surfer 16 program. While modelling, the results were interpreted as weekday and weekend averages. As a result, the lowest PM2.5 values were found in summer in both shopping malls.

Lower concentrations were obtained in all three seasons in Novada shopping center. Measurements were made on the minus first, entrance, first and second floors of the shopping mall. The highest concentrations were seen in this mall minus the first floor. Opening the only door on this floor where there is no ventilation to the parking garage caused the emissions from the vehicles to spread indoors. The fact that the measurements made in the summer season coincide with the month of Ramadan caused the results to be lower than the weekend values compared to the weekdays. In the autumn and winter measurements, the situation differed, and the weekend averages were generally higher than the weekday results. The fact that the concentrations found in Novada AVM

are lower than that of Rainbow is due to the presence of a clean air plant operating here. These power plants, operating on the entrance, first and second floors, changed the indoor air of the building and helped to breathe quality air. In addition, cleaning activities continue throughout the day. High concentrations are mostly in the food layer; It has been found in areas where restaurants and playgrounds are located. This building, which was put into use in 2015, has less pollution reflected in the environment due to the building material and the age of the building.

For people to breathe healthy air in indoor living spaces where people spend 87% of their day, these environments and the ventilation systems, devices and vehicles in them must be maintained by constantly monitoring and controlling in terms of quality atmosphere. For this reason, it is necessary to implement methods that will ensure an acceptable indoor air quality in shopping malls. These methods are respectively.

• Removal of the source affecting the environment,
• Making central ventilation systems according to standards suitable for the environment in which they will be used, using them appropriately and maintaining them at regular intervals,
• It is recommended to take precautions against smoking in closed environments.
Moreover, Universities should organize lectures, symposiums, and educational seminars in educational institutions about the importance of indoor air quality and its effects on health.

Due to the lack of standards determining indoor air quality in Turkey until today, it is recommended that the relevant institutions act as soon as possible to establish standard values for this air, which has a direct impact on the health of living things.

It should be ensured that the parameters determining the air quality in all provinces of Turkey are measured and modeling maps are created.

Acknowledgement

Funding

Author contributions

Sukru Dursun: Conceptualization, Methodology, -Reviewing and Editing; **Mina Naseer Qasim:** Investigation, Data curation, Writing-Original draft preparation, Modelling.

Conflicts of interest

The authors declare no conflicts of interest.

References

1. Karakaş, B. (2015). İç ve Dış Hava Ortamlarında Partiküler Madde (PM10, PM2.5 ve PM1) Konsantrasyonlarının Değerlendirilmesi. MS Thesis, Hacettepe Üniversitesi, Turkey
2. Kaya, D. & Öztürk, H., (2012). Hava Kalitesi Yönetimi, Umuttepe Yayinlari p. 352.
3. Dursun Ş, (1988). An investigation of the relationship between sulphur dioxide (SO_2), ammonia (NH_3), and smoke concentration, and meteorological factors at the centre Samsun and around Tekkeköy in Turkey. M. Sc. Thesis University of Ondokuz Mayıs, Samsun, Turkey
4. Dursun, S., Ineson, P, Frankland, J. C. & Boddy L., (1996). Sulphur Dioxide Effects on Fungi Growing on Leaf Litter and Agar Media. New Phytologist, 134, 167-176.
5. Dursun, S., Ineson, P., Frankland, J. C., & Boddy, L. (1993). Sulphite and pH effects on CO_2 evolution from decomposing angiospermous and coniferous tree leaf litters. *Soil biology and biochemistry*, *25*(11), 1513-1525.
6. Alyüz, B. & Sevil, V., (2006). İç ortam havasında bulunan uçucu organik bileşikler ve sağlık üzerine etkileri, Trakya Üniversitesi, Türkiye.

7. Mankolli, H., Lika, M., & Dursun, S. (2011). Some air pollution indicators in city of Tirana, Albania. *International Journal of Global Warming*, *3*(1-2), 30-38.

8. Dursun, S., Sagdic, M. & Toros, H. (2022). The impact of COVID-19 measures on air quality in Turkey, Environmental Forensics, 23:1-2, 47-59, DOI: 10.1080/15275922.2021.1892876

9. Organization, W. H. Initiative, T. F., (2007). Protection from Exposure to Second-hand Tobacco Smoke: Policy Recommendations, World Health Organization, p. https://www.who.int [04.04.2019].

10. Morabia, A., Bernstein, M. S., Curtin, F. & Berode, M., (2001). Validation of self-reported smoking status by simultaneous measurement of carbon monoxide and salivary thiocyanate, Preventive medicine, 32 (1), 82-88.

11. Johnson, K. C. (2005). Accumulating evidence on passive and active smoking and breast cancer risk. *International journal of cancer*, *117*(4), 619-628.

12. Castellazzi, A. M., Maccario, R., Moretta, A., De Amici, M., Gasparoni, A., Chirico, G., & Rondini, G. (1999). Effect of active and passive smoking during pregnancy on natural killer–cell activity in infants. *Journal of allergy and clinical immunology*, *103*(1), 172-173.

13. WHO, 2013, World Health Organization (2013). Review of evidence on health aspects of air pollution

14. URL-1, World Health Organization, Turkey – a model of success in tobacco control.;, http://www.euro.who.int/en/health-topics/disease-prevention/tobacco/news/news/2013/06/turkey-a-model-of-success-in-tobacco-control: [03-06-2013].

15. Dursun, Ş., Ayturan, Z., Kunt, F., Ulusoy, Ç., & Mesutoğlu, Ç. (2017). Selçuk Üniversitesi Yerleşkesi Açık Alanlarda Ortam PM2.5 Seviyesinin Belirlenmesi, VII. ulusal hava kirliliği ve kontrolü sempozyumu, 190-202.

16. Kiesewetter, G., Schoepp, W., Heyes, C. & Amann, M. (2015). Modelling PM2. 5 impact indicators in Europe: health effects and legal compliance, Environmental Modelling & Software, 74, 201-211.

17. Alptekin, O., & Çelebi, G. (2015). Toz partiküllerinin iç mekân hava kalitesi üzerindeki etkilerinin incelenmesi. *Kafkas Üniversitesi Fen Bilimleri Enstitüsü Dergisi*, *8*(1), 30-49.

18. Organization, W. H. & UNAIDS, (2006). Air quality guidelines: global update 2005, World Health Organization, p.

19. Süren, P. (2007). Zonguldak kent merkezi atmosferik partikül madde kirliliğinin; PM2, 5 ve PM10 boyut dağılımı, kaynak ve metalik kompozisyon temelinde incelenmesi. MS Thesis, Turkey.

20. Cindoruk, S. S., (2018). Havadaki NO ve NO_2 parametrelerinin marmara temiz hava merkezi ölçümleri kapsamında incelenmesi, Ömer Halisdemir Üniversitesi Mühendislik Bilimleri Dergisi, 7 (2), 600-611.

21. URL-2, Kent rehberi, https://kentrehberi.konya.bel.tr/#/rehber [27-12-2018].

22. Lee, S. C., Li, W.-M. & Chan, L. Y. (2001). Indoor air quality at restaurants with different styles of cooking in metropolitan Hong Kong, Science of the Total Environment, 279 (1-3), 181-193.

23. Morawska, L. & Zhang, J. J. (2002). Combustion sources of particles. 1. Health relevance and source signatures, Chemosphere, 49 (9), 1045-1058.

24. Polat, O. (2002). Golden software surfer v.8 kullanim ile ilgili notlar p, https://docplayer.biz.tr [04.04.2019].

25. Bresnahan, T. & Dickenson, K. (2002). Surfer 8 self-paced training guide, Golden Software Inc. http://www.fca.unesp.br [04.04.2019].

26. URL-3, golden software products, https://www.goldensoftware.com/products: [23-12-2018].

27. Challoner, A. & Gill, L. (2014). Indoor/outdoor air pollution relationships in ten commercial buildings: PM2. 5 and NO_2, Building and Environment, 80, 159-173.

28. Dursun, S., & Naseer Qasım, M. (2022). Measurements and modelling of PM2.5 level in summertime period in Novada main shopping centre Konya, Turkey. 2nd Advanced Engineering Days, 93-95

29. Dursun, S., & Naseer Qasım, M. (2021). Determination and modelling of PM2.5 level in summer time in Selcuk University Shopping Centre Konya. Advanced Engineering Science, 2, 01-08.

30. Dursun, S., & Naseer Qasım, M. (2022). PM2.5 concentration measurements and mapping at Gokusagı Mall for summer 2018, in Konya, Turkey. Advanced Engineering Science, 2, 27-34

31. Dursun, S., & Qasım, M. N. (2022). Measurements and modelling of PM2. 5 level in summertime period in Novada main shopping centre Konya, Turkey. *Advanced Engineering Days (AED)*, *2*, 93-95.
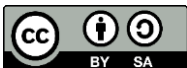
Green concrete production with waste materials as cement substitution: A literature review

Muhammed Tanyıldızı *1 , Erden Ozan Karaca 1 , Nusret Bozkurt 1

¹Bitlis Eren Universitesi, Engineering-Architecture Faculty, Civil Engineering Department, Türkiye
mtanyildizi@beu.edu.tr; eokaraca@beu.edu.tr; nbozkurt@beu.edu.tr

Abstract

In terms of sustainability, using waste material as a cement substitute in concrete has become a global trend. This review article focused on studies that were performed to investigate the effect of some waste materials including eggshell powder (ESP), ceramic waste powder (CWP), rice husk ash (RHA) and corn cob ash (CCA) as cement substitutes on the strength properties of the concrete mixture. The main purpose of this paper is to draw attention to the fact that the use of these waste materials mentioned above as cement substitutes is an environmentally friendly way that prevents their possible harmful effects on both the ecosystem and human beings. In addition, it is aimed to show that cement production, which causes greenhouse gas emissions, which is one of the major causes of global warming, can be reduced as a result of using waste materials as cement substitute material.

1. Introduction

Concrete is the most used construction material in nearly all civil engineering projects due to its versatility and availability around the world [1]. Having a such wide usage area, concrete's sustainability is a major topic of interest in societies. The term sustainability is crucial for societies as it helps to preserve the ecosystem, improve our quality of life, enhance the well-being of societies and prevent the excessive depletion of natural resources [2]. The sustainability of concrete is ensured by its components, primarily cement, and cement, which is the main component of concrete, both affect the cost of concrete and pose a threat to the environment as it releases a significant amount of CO_2 greenhouse gas in its production. For this reason, the construction industry is faced with some challenges in bringing sustainability to production processes, especially cement. This can be achieved by seeking new more environmentally friendly raw materials and products that contribute to the minimization of greenhouse gases released into the environment. In this context, waste from other industrial activities can be a good solution for this purpose [3-6].

Increasing industrialization along with population growth and urbanization produces copious amounts of waste. It is claimed that around 2 billion tons of waste are produced annually all over the world, and it is estimated that by 2050, 3.4 billion tons of waste will be produced annually worldwide [7]. About 62% of these wastes are not handled properly, which causes pollution of the environment and global warming, and threats to public health [8]. An effective way that has emerged is to recycle these wastes. [9]. Recently, the interest in the use of waste materials in the construction industry, especially in concrete production, as a cement substitute has been increasing and remarkable results have been obtained [10]. This review focused on studies performed on the usability of some wastes as cement replacement in the production of green and sustainable concrete. Waste materials such as eggshell powder (ESP), ceramic waste powder (CWP), rice husk ash (RHA), and corn cob ash (CCA) have been subject to this review study. In this regard, the current studies performed about this concern were reviewed and their results on the strength properties of concrete mixtures were submitted comprehensively.

In addition, one of the main purposes of this study is to raise awareness of sustainable waste management in the construction sector and to shed light on researchers and sector representatives on this way.

2. Eggshell powder (ESP)

2.1. Physical and Chemical Properties of ESP

Eggshell is a bio-waste material that emerged from bakers, fast-food restaurants and poultry farms. The food industry produces enormous amounts of eggshells every year, and improper disposal of this waste into the environment causes health problems and environmental pollution due to the release of toxic gases [11]. Bashir et al. [12] stated that eggshell is one of the most environmental problems. There is an urgent need for a way to use eggshells to prevent their harmful effects on the environment and public health. The eggshell is made up of calcium and so it can be used as partial cement replacement material in concrete [13]. The use of eggshell powder as a cement substitute material in concrete is a good way in terms of sustainability. Before using eggshells as a cement replacement material, the cleaning process should be applied to remove the organic wastes from their surface. After the cleaning phase, the eggshell is dried with a help of sunshine or an electrical oven to make grinding easier [14,15]. The physical and chemical properties of eggshells differ based on the sources of the egg. Its specific gravity ranges from 0.85 to 2.66 and is lower than that of cement which has a specific gravity of 3.13 to 3.24 [12,16,17]. ESP mainly consists of $CaCO_3$ and the main oxide of ESP is CaO which reaches 99.8 % by weight [18]. The visual appearance of eggshell and ESP are presented in Figure 1.

Figure 1. Eggshell and Eggshell Powder [19]

2.2. Strength properties of concrete containing ESP as cement replacement

Yerremala [20] replaced cement with ESP in proportions of 0%, 5%, 10% and 15% and investigated compressive and splitting tensile strength changes of concrete mixtures. The water to cement ratio was 0.6 and constant for all mixtures. The concrete specimens were exposed to water curing and the mechanical tests were conducted at 1, 7 and 28 days. From test results, the author state that the strength increased with the curing age for all concretes. When comparing the 1-day strength of concretes, they were nearly the same and comparable to each other. For 7 days, the strength of 5% ESP concrete passed the control concrete. At the end of 28 days of curing, the compressive strength of mixtures was shaped as 22.3, 24, 18.9 and 16.1 MPa for control concrete, 5% ESP, 10% ESP and 15% concrete respectively. It was observed that the concrete with 5% eggshell powder gave the highest compressive strength compared with control concrete. Further increase in ESP content resulted in a decrease in compressive strength. For splitting tensile strength, control concrete and 5% ESP concrete showed the same tensile strength as 2.4 MPa at 28 days. When ESP content reached 10%, the decrease is approximately 4% and nearly negligible. However, 15% introduction of ESP resulted in a 33% decrease in splitting tensile strength of concrete when compared with control concrete.

Kumar et al. [21] analyzed experimentally the effect of cement replacement with ESP on the strength properties of concretes. In this context, the cement was replaced with ESP in levels of 0%, 5%, 10% and 15% by weight. To determine this effect, the mechanical strength test including compressive, flexural and splitting tensile strength was conducted at 7 and 28 days. The compressive strength results of concrete specimens were 17.15, 18.01, 17.83 and 17.61 MPa for concrete mixtures of control, E5%, E10% and E15% respectively. This value increased to 31.52, 35.21, 34.45 and 31.50 MPa respectively at 28 days of curing. From the compressive strength test result, it was concluded that the ESP introduced to concrete enhanced the resistance of the mixture against compression, and the highest compressive strength was obtained with 5% ESP. In the flexural strength test, all ESP incorporated concretes showed better performance compared to control concrete. 5% ESPs flexural strength was higher than control concrete by 5.28% and 6.70% at 7 and 28 days of curing. These values were 6.19 and 2.61, 6.70 and 1.56

for concretes E10% and E15% at 7 and 28 days respectively. Splitting tensile strength of mixtures of control and 5% ESP concrete was nearly the same as 2.11 and 2.12 MPa respectively at 7 days. At 28 days test, a slight difference was obtained as 3.14 and 3.23 MPa for control concrete and 5% ESP concrete respectively. The strength values were 1.89 and 2.56 MPa, 1.65 and 2.31 MPa for concretes 10% and 15% ESP at 7 days and 28 days respectively. When analyzing whole mechanical strength test results, the 5% replacement of cement with ESP comes into view as the optimum percentage to achieve enhanced strength performance compared with control concrete.

Waidya and Bastwadkar [13] made an experimental study of partial replacement of cement with ESP in concrete. In their study, ESP was replaced with cement at 5% intervals from 0% to 20%. After curing specimens, the specimens were subjected to compressive, flexural and splitting tensile strength tests at 7, 14 and 28 days. They reported from experimental analyses that the compressive, flexural and splitting tensile strength increased by 7.15%, 11.62% and 3.5% with the introduction of 10% ESP instead of cement.

Arif et al. [22] conducted a study to analyze the strength performances of concrete mixtures by replacing cement at levels of 0-15% with a 5% increment. The specimens were exposed to water curing for 7 and 28 days and the compressive strength of each mixture was tested. The results of the test were summarized in Figure 2 as shown.
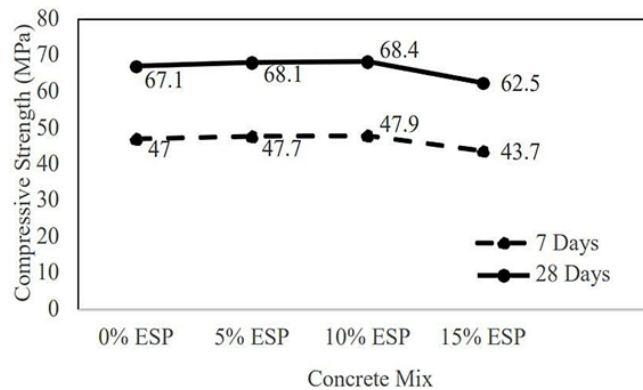
Figure 2. Compressive strength of concrete incorporating ESP [22]

Jhatial [23] performed an experimental study to reduce cement content in concrete by replacing it in ratios of 5%, 10% and 15% by weights. They stated that it was possible to achieve higher strength than control concrete by partial replacement of cement with ESP, and the optimum substitution ratio was declared as 10%. Some studies performed to investigate the effect of cement replacement with ESP were summarized in Table 1.

Table 1. Strength of concrete mixtures containing ESP at 28 days of water curing

Reference	Mix ID	ESP, %	Binder, %	CS (MPa)	FS (MPa)	ST (MPa)
[24]	NC	0	100	52.43		
	E5	5	95	61.25		
	E10	10	90	49.33		
	E15	15	85	44.65		
[25]	CS	0	100	36.50	5.90	
	E10	10	90	37.00	8.10	
	E20	20	80	30.60	6.60	
[26]	C-0	0	100	24.20		2.20
	C-1	6	94	25.00		2.48
	C-2	12	88	27.30		2.10
	C-3	18	82	26.00		1.83
	C-4	24	76	24.80		1.76
[27]	RPC	0	100	26.90	4.30	
	PCF1E5	5	95	26.60	4.28	
	PCF1E10	10	90	25.70	4.14	
	PCF1E15	15	85	24.90	3.98	
	PCF1E20	20	80	23.80	3.80	
[28]	M1	0	100	20.26	4.35	3.34
	M2	2.5	97.5	24.49	4.96	3.47
	M3	5	95	27.38	5.06	4.26
	M4	7.5	92.5	25.53	4.92	3.84
	M5	10	90	24.70	4.82	3.98

***Note: CS** is Compressive Strength, **FS** is Flexural Strength, **ST** is Splitting Tensile Strength*

3. Ceramic waste powder (CWP)

3. 1. Physical and chemical properties of CWP

Ceramic wastes are generated from the ceramic tiles industry and construction sites during the packing and labor process in tremendous amounts yearly [29]. It is estimated that the CWP that is produced globally during the final polishing process of ceramic tiles surpassed 22 billion tons [30]. These wastes are disposed of in landfills and pose a threat to both human health and the environment by causing soil, water and air pollution. There is a need to evaluate this waste in the concern of sustainability, and using it in concrete as cement replacement material is a beneficial way to create a positive environmental impact, reduce the greenhouse effect of cement, and support the sustainability of construction materials [31]. The specific gravity of CWP changes between 2.30 and 2.85. The major oxides of CWP detected with chemical analysis are SiO_2 which constitutes approx. 60-80% of it [32,33]. The other oxides that follow SiO_2 are Al_2O_3 and Fe_2O_3 respectively. The presence of SiO_2, Al_2O_3 and Fe_2O_3 in a noteworthy amount in CWP composition makes it usable as cement replacement material. The visual appearance of ceramic waste and CWP are presented in Figure 3.

Figure 3. Ceramic waste and CWP [34]

3.2. Strength properties of concrete containing CWP as cement replacement

Manigandan and Saravanakumar [33] carried out an experimental study to look into the effect of partial cement replacement with CWP at levels of 10%, 20% and 30% by weight. They produced concrete mixtures, cured in water at 7, 14 and 28 days and tested for compressive strength to compare with the control concrete result. The compressive strength of control concrete was 38.2, 43.3 and 46.6 MPa on 7, 14 and 28 days of curing respectively. These values decreased to 32.4, 36.2 and 40.1 MPa for 7, 14 and 28 days respectively when cement was replaced with CWP in the proportion of 10%. When the replacement was 20% and 30%, the compressive strength was 26.4, 27.13 and 28 MPa for the 20% replacement ratio and 21.5, 23.5 and 24 MPa for the 30% replacement ratio for 7, 14 and 28 days curing respectively.

Bhargav et al. [35] aimed to evaluate the CWP as cement replacement in the concrete to improve the strength properties of mixtures. In this context, cement was substituted with CWP in various ratios ranging from 0% to 20% with an increment of 5%. Each concrete's compressive strength was evaluated at the end of 7, 14 and 28 days of water curing and compared with control concrete. The compressive strength of concretes containing CWP was higher than control concrete for all curing days. The compressive strength increased by 2.75%, 7.05%, 10.89% and 4.40% for ratios of 5% ,10% ,15% and 20% respectively at 28 days.

In another study, El-Dieb et al. [31] conducted a research study to analyze the CWP content effect on the compressive resistance of concrete specimens. The authors reported that the compressive strength increased with the introduction of 20% of CWP. However, when surpassing this ratio, resulted in a decrease in the compressive resistance of concrete specimens. Kannan et al. [36] produced high-strength concrete mixtures by replacing cement in proportions ranging from 10 to 40% with a 10% increment. The authors reported from the experimental analyses that the concrete mixtures containing CWP in large quantities could show high compressive resistance as shown in Figure 4.

Lasseuguette [37] made an experimental analysis to measure the change in compressive strength when cement was partially replaced with CWP at a level of 15%. The compressive strength of concrete mixtures was tested on 7, 28 and 56 days, and results were compared with control concrete. The author indicated that the concrete containing CWP showed higher resistance than control concrete on all test days.

Karthika et al. [38] focused on their study to investigate the effect of cement replacement with CWP ranging from 10% to 40% with a 10% increment on the strength properties of concrete mixtures. They noted that the compressive, flexural and splitting tensile strength increased when cement was replaced with CWP up to a level

of 30%. The optimum strength values in their study were obtained at a 30% substitute ratio as 42.15 MPa, 5.50 MPa and 3.85 MPa at 28 days for compressive, flexural and splitting tensile stress respectively.
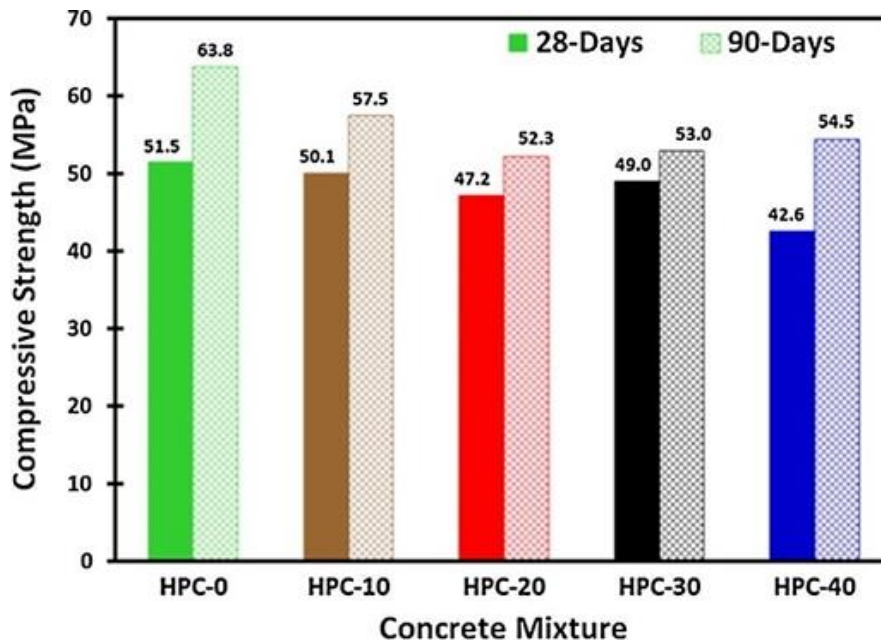
Figure 4. Compressive strength of concrete incorporating CWP [36]

Some studies conducted to investigate the effect of cement replacement with CWP were summarized in Table 2.

Table 2. Strength of concrete mixtures containing CWP at 28 days of water curing

Reference	Mix ID	CWP, %	Binder, %	CS (MPa)	FS (MPa)	ST (MPa)
[39]	0%	0	100	35.11		
	5%	5	95	35.89		
	10%	10	90	37.29		
	15%	15	85	38.34		
	20%	20	80	32.34		
[40]	1	0	100	34.10	5.44	4.38
	2	5	95	35.70	5.51	4.44
	3	10	90	36.40	5.77	4.56
	4	15	85	38.56	5.89	4.61
	5	20	80	33.80	5.38	4.33
	6	25	75	30.60	5.21	4.03
	7	30	70	28.74	5.13	3.73
[41]	Control	0	100	30.00		
	A1	15	85	28.90		
	A2	30	70	27.50		
	A3	35	65	23.50		
	A4	40	60	18.00		
	A5	45	55	16.00		
[42]	1	0	100	50.81		
	2	10	90	56.29		
	4	30	70	40.43		
	5	40	60	39.84		
	6	50	50	30.81		
[43]	1	0	100	38.46		3.10
	2	5	95	37.28		2.92
	3	10	90	37.92		3.12
	4	15	85	38.98		3.42
	5	20	80	36.35		2.78
	6	25	75	36.12		2.66
	7	30	70	35.09		2.52

***Note: CS** is Compressive Strength, **FS** is Flexural Strength, **ST** is Splitting Tensile Strength*

4. Rice Husk Ash (RHA)

4.1. Physical and chemical properties of RHA

Rice husk, which is the outer layer covering the rice grains, is a waste produced from the rice mill process. This is generally thrown away at the landfill without further use, thus, resulting in environmental pollution. It is obtained roughly 200 kg per ton of rice. Rice husk ash is a by-product and obtained by burning rice husk under controlled temperature. And has been taken advantage of in cement replacement materials to form sustainable concrete for years because of its high pozzolanic reactivity [44,45]. It owes its cementitious property to mainly high amorphous content [46]. The specific gravity of RHA generally changes from 2.06 to 2.11 [47,48]. From chemical analyses, the main oxides of RHA were determined as SiO_2 which ranges between 75% to 95% by weight [49-51]. The other oxides that follow the SiO_2 by weight are AI_2O_3 and Fe_2O_3 respectively [52-54]. A visual view of the rice husk and RHA is presented in Figure 5.

Figure 5. Rice Husk and RHA [55]

4.2. Strength properties of concrete containing RHA as cement replacement

Kartini et al. [56] performed a study to evaluate RHA as a cement substitute for producing green concrete. In experimental analyses, six replacement ratios as 0%, 10%, 20%, 30%, 40% and 50% were taken into consideration and compressive strength tests were applied to the mixtures at 28, 60 and 90 days of curing. In this context, two strength classes were targeted as 60 MPa and 70MPa. For the class of 60 MPa, the control concrete attained 73 MPa at 28 days, while 10% RHA concrete attained 68 MPa. When the curing period was prolonged up to 90 days, the compressive strength of the mixture increased. The concrete mixtures containing RHA at levels of 20%, 30%, 40% and 50% showed compressive strength less than 60 MPa at 28 days. For the grade of 70 MPa concrete mixtures, the control concrete gave the compressive strength of 74.4, 77.9 and 82.9 MPa for 28, 60 and 90 days of curing. For 10% RHA concrete, these values decreased by 3%, 5% and 8% for 28, 60 and 90 days. Then for 20% RHA concrete, compressive strength values were lower than control concrete by 19%, 21% and 25% for days 28, 60 and 90 respectively. Further increasing of replacement ratios gave lower strength compared to control concrete. The 30% RHA concrete showed less compressive resistance and the strength values showed a reduction of about 30%, 33% and 36% respectively for 28, 60 and 90 days. For 40% RHA concrete's compressive strength was lower than control concrete approximately 43%, 45% and 47% at 28, 60 and 90 days. The decrease in compressive strength continued with 50% replacement of cement with RHA and the 28, 60 and 90 days of compressive strength was lower at about 51%, 53% and 56% than control concrete respectively.

Takhelmayum [57] aimed to investigate the effect of RHA incorporation into the concrete on the strength properties. In this context, cement was replaced RHA in ratios varies 5 to 30% with an increment of 5%. The specimens were tested at 7 and 28 days and results showed that 10% and 15% RHA concrete gave higher compressive strength compared to control concrete. Zaid et al. [58] performed a study to detect the effect of RHA on the compressive and splitting tensile strength of concrete mixtures at 7 and 28 days. In this manner, the cement was replaced with RHA in levels of 5 to 20% with an increment of 5%. The test results showed a steady reduction obtained with increasing content of RHA for both tests.

Saand et al. [59] conducted research to produce aerated concrete by replacing cement in ratios ranging from 0 to 15 with an increment of 2.5%. The test results demonstrated that the optimum replacement ratio was 10%. At this ratio, the compressive strength increased by 22.22% when compared with control concrete. Zareei and Ahmadi [44] studied to evaluate rice husk ash as cement substitute material in high strength concrete in ratios ranging from 5 to 25% with an increment of 5%. The specimens were tested at the end of 7 and 28 days. The compressive strength of control concrete was 50.84 and 83.36 MPa for 7 and 28 days respectively. The strength values of control concrete increased by about 2.12% and 2.11% for 7 and 28 days when RHA was incorporated

into concrete for 5%. This increase was shaped as 4.25% and 4.24% for 10% RHA concrete. The increase in compressive strength continued with RHA replacement in ratios of 15% and 20% and the strength increased by 10.99% and 10.97%, 11.47% and 11.90% for 7 and 28 days for 15% RHA and 20% RHA concrete respectively. After the 20% replacement ratio, the compressive strength decreased but still was higher than control concrete approximately 6.90% and 6.88% for 7 and 28 days as shown in Figure 6.
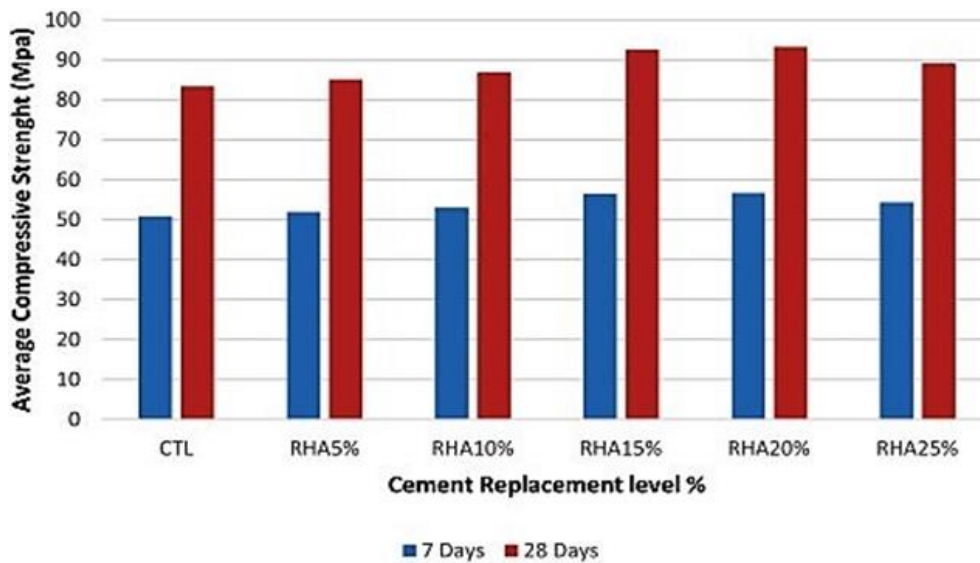

Figure 6. Compressive strength of concrete incorporating RHA [44]

Some studies carried out to investigate the effect of cement replacement with RHA were summarized and given in Table 3.

Table 3. Strength of concrete mixtures containing RHA at 28 days of water curing

Reference	Mix ID	RHA, %	Binder, %	CS (MPa)	FS (MPa)	ST (MPa)
[45]	0%	0	100	27.47		
	10%	10	90	25.80		
	20%	20	80	22.73		
	30%	30	70	19.60		
[60]	0%	0	100	27.75		1.53
	5%	5	95	30.86		1.65
	10%	10	90	31.72		1.68
	15%	15	85	32.78		1.70
	20%	20	80	32.00		0.96
	25%	25	75	28.80		0.78
[61]	0%	0	100	27.00	2.11	2.28
	5%	5	95	24.80	2.53	2.36
	10%	10	90	29.30	1.94	2.52
	15%	15	85	17.60	-	2.11
	20%	20	80	16.03	-	1.97
[62]	0%	0	100	48.12		
	5%	5	95	36.76		
	10%	10	90	33.79		
	15%	15	85	25.47		
	25%	25	75	17.32		
[63]	Control	0	100	25.72		
	RHA10%	10	90	22.28		
	RHA15%	15	85	25.12		
	RHA20%	20	80	24.43		

Note: CS is Compressive Strength, FS is Flexural Strength, ST is Splitting Tensile Strength.

5. Corn Cob Ash (CCA)

5.1. Physical and chemical properties of CCA

The corn cob, which is an agricultural waste product obtained from maize, is the remainder of the corn cob after the corn kernels have been peeled and constitute about 75-85% of the corn cob's weight. Corn cob is burnt

in a furnace at approximately 650°C to take its ash form. Corn cob ash (CCA) is can be used as cement supplementary material to produce green and sustainable concrete [64, 65]. The specific gravity of CCA is ranging from 1.95 to 2.55 [66,67]. The main component of CCA is SiO_2 which constitutes 60-80% of it by weight obtained from chemical analyses [68,69]. The other oxides that follow the SiO_2 are AI_2O_3 and Fe_2O_3. The abundant oxides of SiO_2, AI_2O_3 and Fe_2O_3 in the composition of CCA affect the pozzolanic characteristics namely the cementitious properties of CCA and enable to use it as a cement substitute material. Using CCA in concrete to minimize the usage of cement is a beneficial way to protect the environment and human health [70,71]. The visual appearance of corn cob and CCA are presented in Figure 7.

Figure 7. Corn Cob and CCA [72]

5.2. Strength properties of concrete containing CCA as cement replacement

Adebisi et al. [64] performed a study by using CCA as partial cement replacement materials to produce green and sustainable concrete. In this manner, the cement was replaced with CCA at levels of 0%, 5%, 10%, 20% and 30%. Compressive strength tests were applied to specimens at ages 28, 56, 90 and 120 days. From the test results, they observed that the compressive strength of concrete mixtures decreased at all curing ages with increasing CCA content. At 28 days of curing, the compressive strength of mixtures of 5%, 10%, 20% and 30% were lower than control concrete by 7.28%, 14.94%, 22.99% and 42.91% respectively. These values were 13.14%, 24.23%, 28.35% and 49.74% at age of 120 days.

Tiza [73] conducted a study on the usability of CCA as a partial cement replacement material in the production of concrete. In this context, CCA was replaced with cement in proportions of 0%, 5%, 10%, 15%, 20%, and 25%. The compressive strength of concrete obtained from cube specimens at the end of the 28 days of water curing decreased by 5.05% for 5% CCA, 13.49% for 10% CCA, 23.03% for 15% CCA, 33.12% for 20% CCA concrete mixtures. The reduction in flexural tensile strength also at the end of the 28-day water curing was 7.51% for 5% CCA, 20.48% for 10% CCA, 27.52% for 15% CCA, 39.20% for 20% CCA and 46.99% for 25% CCA concrete mixtures.

Singh et al. [74] studied the effect of cement replacement with CCA on the compressive strength of concrete. Five concrete mixtures were produced by replacing cement at levels of 0%, 5%, 10%, 15% and 20%. The authors tested the compressive strength of concrete mixtures at 28 days of room temperature curing. The compressive strength of the control concrete was 36.43 MPa. The strength of concrete decreased to 32.47 MPa when incorporating CCA by 10% of cement. The more CCA content resulted in more decrease in compressive strength. When replacing cement with CCA at levels of 15% and 20%, the strength of control concrete decreased from 36.43 MPa to 23.07 and 20.15 MPa for a mixture of 15% and 20% respectively.

Bala et al. [75] investigated the compressive strength changes of concretes when replacing cement with CCA in ratios ranging from 3 % to 12% with an increment of 3%. The compressive strength of concrete mixtures was tested at the age of 7, 14, 21 and 28 days, and it increased with prolonged age for all mixtures. However, it decreased compared to control concrete when CCA was incorporated as shown in Figure 8.

Adesanya and Raheem [76] tested the effect of cement replacement with CCA in proportions of 0%, 2%, 4%, 6%, 8%, 10%, 15%, 20% and 25% by weight. They concluded that the optimum content for strength improvement emerged as 8%.

Some studies made to investigate the effect of cement replacement with CCA were summarized and presented in Table 4.
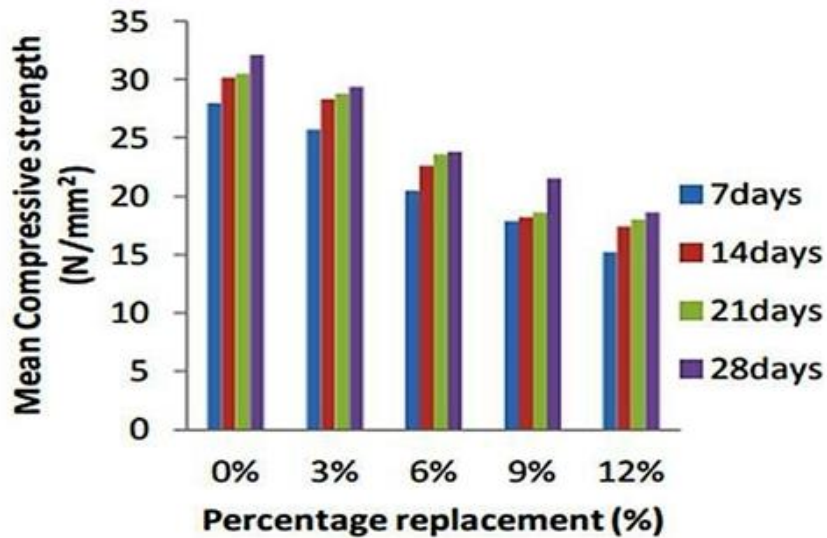
Figure 8. Compressive strength of concrete incorporating CCA [75]

Table 4. Strength of concrete mixtures containing CCA at 28 days of water curing

Reference	Mix ID	CCA, %	Binder, %	CS (MPa)	FS (MPa)	ST (MPa)
[77]	0%	0	100	24.69		2.01
	10%	10	90	20.00		1.72
	20%	20	80	13.78		1..15
[78]	Control	0	100	61.60	3.60	
	5%	5	95	49.00	3.50	
	7.5%	7.5	92.5	51.30	2.30	
	10%	10	90	37.90	2.80	
	15%	15	85	34.30	1.30	
	20%	20	80	23.50	2.10	
	25%	25	75	18.90	1.60	
	30%	30	70	19.30	2.20	
[79]	0%	0	100	17.78		
	10%	10	90	17.70		
	20%	20	80	17.11		
	30%	30	70	18.44		
[80]	0%	0	100	24.04	4.75	4.06
	10%	10	90	22.68	4.68	4.29
	20%	20	80	21.85	4.51	3.84
	30%	30	70	20.87	4.19	3.51
[81]	CS	0	100	29.33	13.77	6.30
	CCA 5	5	95	28.40	12.88	5.65
	CCA 10	10	90	26.22	11.55	5.09
	CCA 15	15	85	22.60	9.77	4.10

***Note: CS** is Compressive Strength, **FS** is Flexural Strength, **ST** is Splitting Tensile Strength.*

6. Conclusion

This review study focused on prior studies that were performed to investigate the effects of ESP, CWP, RHA and CCA replacement with cement on the strength properties of concrete mixtures. And with this study, it is aimed to raise awareness about green and sustainable concrete production among both researchers and concrete industry representatives. The accumulation of these waste materials in landfills causes toxic gases and poses a threat to the environment and public health. Therefore, the use of these wastes as cement substitutes is a useful way to reduce environmental pollution and protect the health of living things. In addition, minimizing the use of cement in concrete production is an effective way to reduce greenhouse gas emissions to the ecosystem, where

cement production is a major threat in terms of triggering global warming. The following can be deduced from this article;

1. ESP can be used as a cement replacement up to a level of 10% to improve the strength properties of concrete.

2. CWP can be utilized as a cement substitute up to a level of 10% to enhance the mechanical strength of the concrete mixture.

3. RHA generally decreased the strength of concrete mixtures when replaced with cement. But, up to a level of 5% substitution is applicable when compared with control concrete.

4. CCA's replacement with cement has a negative effect on the strength properties of concrete. However, the replacement ratio of 5% is feasible to produce green and sustainable concrete.

Author contributions

Muhammed Tanyıldızı: Conceptualization, Methodology, Software, Investigation, Validation, Writing-Reviewing and Editing, Visualization **Erden Ozan Karaca:** Data curation, Writing-Original draft preparation, Software, Validation.

Conflicts of interest

The authors declare no conflicts of interest.

References

1. Güneyisi, E., Gesoglu, M., Akoi, A. O. M., & Mermerdas, K., (2014). Combined effect of steel fiber and metakaolin incorporation on mechanical properties of concrete. Construction and Building Materials, 56, 83-91.
2. Naik, T. N. (2008). Sustainability of concrete construction. Practice Periodical on Structural Design and Construction, 3(2).
3. Pereira, C. L., Savastano, H. J., Paya Bernabeu, J. J., Santos, S. F., Borrachero Rosado, M. V., Monzó Balbuena, J. M., & Soriano Martinez, L. (2013). Use of highly reactive rice husk ash in the production of cement matrix reinforced with green coconut fiber. Industrial Crops and Products. 49, 88-96.
4. İpek, S. (2022). Macro and micro characteristics of eco-friendly fly ash-based geopolymer composites made of different types of recycled sand. Journal of Building Engineering, 52. https://doi.org/10.1016/j.jobe.2022.104431.
5. Öz, H. Ö., Yücel, H. E., Güneş, M., Köker, T. Ş., (2021). Fly-ash-based geopolymer composites incorporating cold-bonded lightweight fly ash aggregates. Construction and Building Materials, 272. https://doi.org/10.1016/j.conbuildmat.2020.121963.
6. Niş, A., Eren,N. A., & Çevik, A. (2022). Effects of recycled tyre rubber and steel fibre on the impact resistance of slag-based self-compacting alkali-activated concrete. European Journal of Environmental and Civil Engineering. https://doi.org/10.1080/19648189.2022.2052967.
7. Wang, X., Ji, Guanyu., Zhang, Yi., Guo, Y., & Zhao, J. (2021). Research on High- and Low-Temperature Characteristics of Bitumen Blended with Waste Eggshell Powder. Materials, 14.
8. Dastjerdi, B., Strezov, V., Kumar, R., He, J., & Behnia, M. (2020). Comparative Life Cycle Assessment of System Solution Scenarios for Residual Municipal Solid Waste Management in NSW, Australia. Science of the Total Environment, 767.

9. Talan, A., Tiwari, B., Yadav, B., Tyagi, R. D., Wong, J. W. C., & Drogui, P. (2021). Food waste valorization: Energy production using novel integrated systems. Bioresource Technology, 322.

10. Cimpan, C., Rothmann, M., Hamelin, L., & Wenzel, H. (2015). Towards increased recycling of household waste: Documenting cascading effects and material efficiency of commingled recyclables and biowaste collection. Journal of Environmental Management, 157, 69-83.

11. Hamada, H. M., Tayeh, B. A., Al-Attar, A., Yahaya, F. M., Muthusamy, K., & Humuda, A. M. (2020). The present state of the use of eggshell powder in concrete: A review. Journal of Building Engineering, 32.

12. Bashir, A. M., & Manusamy, Y. (2015). Characterization of Raw Egg Shell Powder (ESP) as A Good Bio-filler. Journal of Engineering Research and Technology, 2, 1.

13. Vaidya, N., & Bastwadkar, M. P. (2019). Experimental Study of Partial Replacement of Cement with Eggshell Powder in Concrete. International Journal of Engineering Development and Research, 7(4).

14. Parthasarathi, N., Prakash, M., & Satyanarayanan, K. S. (2017). Experimental study on partial replacement of cement with egg shell powder and silica füme. Rasayan Journal of Chemistry, 10(2), 442-449.

15. Panchal, M., Raghavendra, G., Prakash., M. O., & Ojha., S. (2017). Effects of environmental conditions on erosion wear of eggshell particulate epoxy composites. Silicon, 10, 1-8.

16. Bakis, A. (2021). Interlocking paving stones made of limestone sand and volcanic ash aggregates. Road Materials and Pavement Design.

17. Demirhan, S., & Demiral, Ö. (2021). Investigation of microstructural properties of high-volume fly ash blended cement mortars including micronized calcite. Journal of the Faculty of Engineering and Architecture of Gazi University, 36(4), 2255-2269.

18. Abdulabbas, Z. H. (2016). Investigation of drying shrinkage and compressive strength of cement mortar with partial replacement of cement by egg shell powder and milled glass. Al-Qadisiyah Journal for Engineering Sciences, 9, 316-330.

19. Tan, Y. Y., Chin, S. C., & Doh, S. I. (2018). Eggshell as a partial cement replacement in concrete development. Magazine of Concrete Research, 70(13), 662-670. https://doi.org/10.1680/jmacr.17.00003.

20. Yerremala, A. (2014). Properties of concrete with eggshell powder as cement replacement. The Indian Concrete Journal, 94-102.

21. Kumar, P., Sarathy, V., & Ravindraraj, J. (2015). Experimental Study on Partial Replacement of Cement with Egg Shell Powder. International Journal of Innovations in Engineering and Technology, 5(2).

22. Arif, S. M., Rokiah, O., Khairunisa, M., Chong, B. W., Chek, Y. C., Youventharan, D., ... & Doh, S. I. (2021, February). Compressive Strength of Concrete containing Eggshell Powder as Partial Cement Replacement. In *IOP Conference Series: Earth and Environmental Science* (Vol. 682, No. 1, p. 012031). IOP Publishing.

23. Jhatial, A. A., Sohu, S., Memon, M. J., Bhatti, N. U. K., & Memon, D. (2019). Eggshell powder as partial cement replacement and its effect on the workability and compressive strength of concrete. International Journal of Advanced and Applied Sciences, 6(9), 71-75.

24. Teara, A., Doh, S. I., Chin, S.C., Ding, Y. J., Wong, J., & Jiang, X. X. (2019). Investigation on the durability of use fly ash and eggshells powder to replace the cement in concrete productions. IOP Conf. Series: Earth and Environmental Science, 244.

25. Dezfouli, A. A. (2020). Effect of Eggshell Powder Application on the Early and Hardened Properties of Concrete. Journal of Civil Engineering and Materials Application, 4(4), 209-221.

26. Allie, M. A., & Anand, E. (2018). Behaviour Of Concrete Containing Egg Shell Powder As Cement Replacing Material. International Journal of Scientific Development and Research – IJSDR, 3(5).

27. Hama, S. M. (2017). Improving mechanical properties of lightweight Porcelanite aggregate concrete using different waste material, Internation Journal of Sustainable Built Environment, 6, 81-90.

28. Soumyan, K., & Wiswanath, A. K. (2016). Experimental Study to Check the Effect of Egg Shell Powder and Rice Husk Ash on the Property of Concrete. International Journal of Engineering Research & Technology (IJERT).

29. Alsaif, A. (2021). Utilization of ceramic waste as partially cement substitute – A review. Construction and Building Materials, 300.

30. El-Dieb, A. S., & Kanaan, D. M. (2018). The Use of Ceramic Waste Powder (CWP) in Making Eco-Friendly Concretes. Ceramic Materials - Synthesis, Characterization, Applications and Recycling.

31. El-Dieb, A. S., & Kanaan, D. M. (2018). Ceramic waste powder an alternative cement replacement – Characterization and evaluation. Sustainable Materials and Technologies, 17. https://doi.org/10.1016/j.susmat.2018.e00063.

32. Higashiyama, H., Yagishita, F., Sano, M., & Takahashi,O. (2012). Compressive strength and resistance to chloride penetration or mortars using ceramic waste as fine aggregate, Construction and Building Materials, 26(1),96-101.

33. Manigandan, S., & Saravanakumar, G. S. (2017). Experimental Study on Partial Replacement of Cement by Using Ceramic Waste Powder, International Journal for Research in Applied Science & Engineering-Technology (IJRASET).

34. Tanyıldızı, M. (2022). Capillarity of Concrete Incorporating Waste Ceramic Powder. Muş Alparslan University Journal of Science, 10 (1), 925-930.

35. Bhargav, M., & Kansal, R. (2020). Experimental investigation to Substitue of cement with ceramic tile powders in Concrete. International Research Journal of Engineering and Technology (IRJET), 45.98.

36. Kannan, D. M., Aboubakr, S. H., El-Dieb, A.S., & Reda Taha, M. M. (2017). High performance concrete incorporating ceramic waste powder as large partial replacement of Portland cement. Construction and Building Materials, 144, 35-41. https://doi.org/10.1016/j.conbuildmat.2017.03.115.

37. Lasseuguette, E., Burns, S., Simmons, D., Francis, E., Chai, H. K., Koutsos, V., & Huang, Y. (2017). Recycling Ceramic Waste to Produce Green Concrete. 1st International Conference on Construction Materials for Sustainable Future.

38. Katrhika, V., Sathanandham, T., Sathes, K. K., & Manikandan, M. (2015). Strength characteristics on concrete with ceramic waste as a partial replacement of cement. Journal of Chemical and Pharmaceutical Sciences, 8(4).

39. Uniyal, A., & Singh, K. (2019). Partial Replacement of Cement in Concrete using Ceramic Waste. International Journal of Engineering Research & Technology (IJERT).

40. Daniel, S., & Raju, A. A. (2018). A Study of Properties of Concrete Making Partial Replacement of Cement by Ceramic waste Powder. International Research Journal of Engineering and Technology (IRJET), 5(3).

41. Arthi, A. J. J. (2016). Effective Replacement of Cement by Ceramic Waste in Concrete for Sustainable Development. International Journal of Research in Engineering and Technology, 5(11).

42. Rani, M. S. (2016). A Study on Ceramic Waste Powder. SSRG International Journal of Civil Engineering (SSRG – IJCE), 3(7).

43. Devi, C., & Venkateswarlu, D. (2015). A Study on Various Properties of Concrete by Using Ceramic Dust Powder as a Partial Replacement of Cement. International Journal of Engineering and Technical Research (IJETR), 3(12).

44. Zareei, S. A., Ameri, F., Dorostkar, F., & Ahmadi, M. (2017). Rice husk ash as a partial replacement of cement in high strength concrete containing micro silica: Evaluating durability and mechanical properties. *Case studies in construction materials*, *7*, 73-81.

45. Oyejobi, D. O., Abdulkadir, T. S., & Ajibola, V. (2014). Investigation of Rice Husk Ash Cementitious Constituent in Concrete. International Journal of Agricultural Technology, 10(3), 533-542.

46. Siddika, A., Al Mamun, A., Alyousef, R., & Mohammadhosseini, H. (2021). State-of-the-art-review on rice husk ash: A supplementary cementitious material in concrete. Journal of King Saud University - Engineering Sciences, 33(5), 294-307. https://doi.org/10.1016/j.jksues.2020.10.006.

47. Gansean, K., Rajagopal, K, & Thangavel, K. (2008). Rice husk ash blended cement: Assessment of optimal level of replacement for strength and permeability properties of concrete. Construction and Building Materials, 22, 1675-1683. https://doi.org/10.1016/j.conbuildmat.2007.06.011.

48. Habeeb, G. A., & Fayyadh, M. M. (2009). Rice Husk Ash concrete: The effect of RHA average particle size on mechanical properties and drying shrinkage. Australian Journal of Basic and Applied Sciences, 3(3), 1616-1622.

49. Memon, S. A., Shaikh, M. A., & Akbar, H. (2011). Utilization of rice husk ash as viscosity modifying agent in self compacting concrete, Construction and Building Materials, 25(2), 1044-1048. https://doi.org/10.1016/j.conbuildmat.2010.06.074.

50. Chopra, D., & Siddique, R. (2015). Strength, permeability and microstructure of self-compacting concrete containing rice husk ash, 130, 72-80. https://doi.org/10.1016/j.biosystemseng.2014.12.005.

51. Le, H. T., Nguyen, S. T., & Ludwig, H. M. (2014). A study on high performance fine-grained concrete containing rice husk ash. International Journal of Concrete Structures and Materials volume, 8, 301-304.

52. Corderio, G. C., Filho, R. D. T, & Fairbairn, E. M. R. (2009). Use of ultrafine rice husk ash with high-carbon content as pozzolan in high performance concrete. Materials and Structures, 42, 983-992.

53. Sua-iam, G., & Makull, N. (2013). Utilization of limestone powder to improve the properties of self-compacting concrete incorporating high volumes of untreated rice husk ash as fine aggregate. Construction and Building Materials, 38, 455-464. https://doi.org/10.1016/j.conbuildmat.2012.08.016.

54. Givi, A. N., Rashid, S. A., Aziz, F. N. A., & Salleh, M. A. M. (2011). Assessment of the effects of rice husk ash particle size on strength, water permeability and workability of binary blended concrete. Construction and Building Materials, 24(11), 2145-2150. https://doi.org/10.1016/j.conbuildmat.2010.04.045.

55. https://gharpedia.com/blog/rice-husk-ash-in-concrete-pros-cons/. Accessed Date: 2.04.2022

56. Kartini, K., Nazierah, N. M. Y., Zaidahtulakmal, M. Z., & Aisyah, S. G. (2012). Effects of Silica in Rice Husk Ash (RHA) in producing High Strength Concrete. International Journal of Engineering and Technology, 2(12).

57. Takhelmayum, G., Prasad, R., & Savitha, A. L. (2014). Experimental Study on the Properties of cement concrete using Rice Husk Ash. International Journal of Engineering Science and Innovative Technology (IJESIT), 3(6).

58. Zaid, O., Ahmad, J., Siddique, M. S., & Aslam, F. (2021). Effect of Incorporation of Rice Husk Ash Instead of Cement on the Performance of Steel Fibers Reinforced Concrete. Frontiers in Materials. https://doi.org/10.3389/fmats.2021.665625.

59. Saand, A., Ali, T., Keerio, M. A., & Bangwar, D. K. (2019). Experimental Study on the Use of Rice Husk Ash as Partial Cement Replacement in Aerated Concrete. Engineering, Technology & Applied Science Research, 9(4), 4534-4537.

60. Patil, V., & Paliwal, P. M. (2020). Partial Replacement of Cement with Rice Husk Ash in Cement Concrete. International Journal of Engineering Research & Technology, 9, 12.

61. Krishna, N. K., Sandeep, S., & Mini, K. M. (2016). Study on concrete with partial replacement of cement by rice husk ash. IOP Conf. Series: Materials Science and Engineering, 149.

62. Musau, M. K., Shitanda, D., Githinji, M., & Mwende, C. (2021). Use Of Rice Husks Ash as Partial Replacement of Cement in Concrete Paving Blocks. Journal of Engineering in Agriculture and the Environment, 7(1).

63. Hussin, T. A. R., & Parasuraman, J. (2018). Partial Replacement of Cement with Commercial Available Rice Husk Ash In Concrete, 6(1).

64. Adebisi, O., Taiwo, A. M., Nathaniel, O., & Olusola, A. E. (2019). Suitability of Corn Cob Ash as Partial Replacement for Cement in Concrete. International Journal of Scientific & Engineering Research Volume, 10(10).

65. Murthi, P., Poongodi, P., & Gobinath, R. (2020). Effects of Corn Cob Ash as Mineral Admixture on Mechanical and Durability Properties of Concrete – A Review. IOP Conf. Series: Materials Science and Engineering, 1006.

66. Shazim, Ali., Memon, M.K.K. (2017). Ash blended cement composites: eco-friendly and sustainable option for utilization of corn cob ash. Cleaner Production. https://doi.org/10.1016/j.jclepro.2017.12.050.

67. Price, A., Yeargin, R., Fini, E., & Abu-Lebdeh., T. (2014). Investigating effects of introduction of corncob ash into Portland cements concrete: Mechanical and thermal properties. American Journal of Engineering and Applied Science, 7, 133-144.

68. Pranav, H. D. (2018). Experimental study on corn cob ash powder as partial replacement of cement in concrete. International research Journal of Engineering and Technology, 5(6), 724-728.

69. Udoeyo, F. F., & Abubakar, S. A. (2003). Maize-cob ash as filler in concrete. Journal of Materials in Civil Engineering, 15, 205- 208.

70. Akila, S., Manila, A., Meera, D., Nathigamani, G., & Ramya, S. (2018). A partial replacement of cement with corn cob ash in concrete production International Journal of Advanced Research Trends in Engineering and Technology, 226-233.

71. Murthi, P., Poongodi, K., & Gobinath, R. (2020). Effects of Corn Cob Ash as Mineral Admixture on Mechanical and Durability Properties of Concrete –A Review. IOP Conf. Series: Materials Science and Engineering.

72. Memon, S. A., Javed, U., & Khushnood, R. A. (2019). Eco-friendly utilization of corncob ash as partial replacement of sand in concrete. Construction and Building Materials, 195, 165-177. https://doi.org/10.1016/j.conbuildmat.2018.11.063.

73. Tiza, M. T. (2016). Partial Replacement of Cement with Corn Cob Ash. International Journal for Innovative Research in Multidisciplinary Field, 2(7).

74. Singh, K., Singh, J., & Kumar, S. (2017). A Sustainable Environmental Study on Corn Cob Ash Subjected to Elevated Temperature. Current World Environment, 13(1), 144-150.

75. Bala, A., Aminulai, H. O., Abubakar, M., Abdulrahman, H. S., & Musa, U. (2015). Partial Replacement of Cement with Corn Cob Ash in Concrete Production. Department of Civil Engineering, Federal University of Technology, Minna, Nigeria, Technical Note.

76. Adesanya, A. D., & Raheem, A. A. (2009). A study of the workability and compressive strength characteristics of corn cob ash blended cement concrete. Construction and Building Materials, 23(1), 311-317. https://doi.org/10.1016/j.conbuildmat.2007.12.004.

77. Oladipupo, O., & Festus, O. (2012). Strength Properties of Corn Cob Ash Concrete. Journal of Emerging Trends in Engineering and Applied Sciences (JETEAS), 3(2), 297-301.

78. Kamau, J., Ahmed, A., Hirst, P., & Kangwa, J. (2016). Suitability of Corncob Ash as a Supplementary Cementitious Material. International Journal of Materials Science and Engineering, 4(4).

79. Oluborode, K.D., & Olofintuyi, I.O. (2015). Strength Evaluation of Corn cob ash in a blended Portland cement. International Journal of Engineering and Innovative Technology (IJEIT), 4(12).

80. Desai, P. H. (2018). Experimental Study on Corn Cob Ash Powder as Partial Replacement of Cement In Concrete. International Research Journal of Engineering and Technology (IRJET), 5(6).

81. Selina,R. G., Dinesh, S., Bharath, R. P., & Kishorenandha, S. (2020). Assessment on Influence of Corncob Ash as a Partial Replacement of Cement in Concrete. International Journal of Innovative Technology and Exploring Engineering (IJITEE), 9(8).

82. Tanyıldızı, M., & Karaca, E. O. (2022). An investigation on the effect of cement replacement with waste materials on the strength properties of concretes. *Advanced Engineering Days (AED)*, *2*, 62-64.

PV connected pumped-hydro storage system

Ayşenur Oymak*1 , Mehmet Rida Tür 2 , Nouha Bouchiba 3

¹Batman University, Electrical Electronics Engineering Department, Türkiye, aysenur.oymak@batman.edu.tr
²Batman University, Electrical and Energy Department, Türkiye, mrida.tur@batman.edu.tr
³Université de Moncton, Department Faculty of Engineering, Moncton, Canada, bouchibanouha@gmail.com

Abstract
Storage systems are needed to increase the number of renewable energy sources that can be integrated into distribution systems in smart grids and to ensure the continuity of energy. Energy storage can support system operators and provide many services such as energy time shifting, capacity backup, outage management, transmission congestion relief and power quality improvements. Batteries and storage are used due to interruptions and waves in renewable energy sources such as wind and solar. In order to expand the use of clean energy and to ensure energy continuity, mechanical storage methods are emphasized in large power systems. Storage studies have been carried out to increase efficiency, reduce costs and improve storage time. In this study, pumped storage and compressed air storage systems, which are mechanical storage methods, are briefly mentioned. Then, the PV integrated pumped storage system model is emphasized. PHS has been said that the system in which solar are used as a hybrid is advantageous in providing high profitability in the energy market. Thanks to its integration with the sun carbon emissions are reduced. The system will also be useful in meeting irrigation and water needs.

1. Introduction

Transitions from systems based on carbon-intensive fossil fuels that harm the environment to lower-carbon energy or renewable energy sources are becoming the policies of countries [1]. Commonly used renewable energy sources are solar, wind, hydroelectric, geothermal, etc. can be sorted. There is hourly, daily, monthly and annual fluctuations in renewable and clean energy sources. For example, wind power is the speed of the wind; ocean energy to changes in tide level by waves and currents; solar energy to solar radiation intensity; In hydroelectric power plants, it also depends on the flow rate of the stream [2]. Therefore, energy storage systems are required to provide quality power and to efficiently hold solar and wind power in grids. Global electricity production of about 200,000 TWh per year will be needed when developing countries overtake the energy consumption per capita in today's developed economies. Assuming electricity is generated by a conjunction of solar (60%), wind (30%) and other methods (10%), a total of 81 TW of solar energy and 17 TW of wind energy will be required. To remove fossil fuels by 2050, the distribution rates of solar and wind would need to increase by a factor of 20. Assuming that one day's energy storage is required with sufficient storage power capacity to be delivered over 24 hours, then approximately 500 TWh and 20 TW of storage energy and power will be necessary [3]. This shows the need for studies on storage. Energy storage is a necessary technology that uses stored electrical energy when there is peak load demand. Intelligent energy storage systems are used to provide continuous, flexible and quality power. The development of energy storage technologies is of great importance in solving power quality problems such as

voltage drops and interruptions, both at the system and equipment level. However, energy storage; It also has benefits such as increasing system efficiency, enabling the integration of renewable energy sources, increasing grid stability and reliability [4, 5, 38].

The conversion and storage of energy is done with batteries, compressed air, flywheels, thermal power, ultra/super capacitors, superconductors, and fuel cells [6]. Mechanical energy storage technologies include pumped water-based energy storage systems, compressed air energy storage systems and flywheels. Mechanical energy storage is generally preferred in large power plants. The most preferred mechanical energy storage methods are compressed air storage and pumped hydro storage. Pumped hydro and compressed air storage system is a new energy storage system that can be combined with electricity generation from renewable energy sources such as wind and solar.

Energy storage systems, which have many methods, have a wide area today. Pumped hydro storage technology, which is more useful and has a larger storage area than energy storage systems, is a system with a large energy storage area [7]. It is preferred in high energy demands. Hydroelectric reservoirs can use limited sources of energy and storage energy produced from other renewable sources to increase the applicability of the electrical system. Looking at the studies done;

Dong et al. [8] conducted to evaluate the performance of pumped hydro and compressed air storage system in terms of energy associated with power generation from photovoltaic (PV) system. The proposed system can both store energy and generate electricity. Marefati et al. [9] In their work, performance study of a new energy storage system, namely Pumped-Hydro and Compressed Air storage system, combined with organic Rankine cycle (ORC) and Linear Fresnel solar reflector (LFR). As a result, it has been shown that the energy needed by the pump for isothermal operation and the energy level in the container are 3.24 and 2.43 MJ/m3, respectively. It has been stated that the isentropic process requires less solar collector area than the isothermal process. Mousavi et al. [10] A real-time energy management strategy has been proposed for pumped hydro storage systems in farmhouses to manage excess renewable energy. It considers the state of the microgrid to efficiently adjust the pump power and turbine flow rate. It has been tested in fuzzy logic and artificial neural network to solve the prediction error problem. As a result, they observed that artificial neural networks reduce the electricity cost better. Al-Masri et al. [11] The effect of different photovoltaic models was investigated for a combined solar array and pumped hydro storage system. Two-diode (TD), single-diode (SD) and ideal single-diode (ISD) solar models were evaluated in terms of solar array size, reliability and ecological effects. As a result of the evaluations, they observed that the TD model was reliable with a reliability index of 98,558%. Bhayo et al. [12] studied, the analysis and optimization of a stand-alone hybrid renewable energy system to power a residential unit of 3,032 kWh/day was made and examined in 4 cases. it has been shown that as a result there will be less dependence on battery storage. Punys et al. [13], examined power databases to determine production in mixed pumped storage facilities from renewable and non-renewable energy sources. Yildiz et al. [14] examined a pumped hydroelectric storage power plant according to day-ahead electricity market values in Turkey. An optimization algorithm has been developed with linear programming method in order to optimize day-ahead market offers of the power plants. When the generation and revenues of the power plants controlled with the optimization method are examined, it is observed that the annual income has enhanced by approximately 2.737% with the operation of the wind power plants alone and productions have shifted to the hours when the demand power is high. In the study by Makhdoomi and Askarzadeh [15], the crow CSA algorithm was developed and observed to reduce the cost of a grid-connected hybrid system consisting of PV and pumped hydro storage.

In this study, pumped hydro storage and air pressure storage, which are mechanical storage methods, are mentioned in order to better understand the subject. Then, pumped hydro storage connected to solar energy, which is our main topic, is explained in detail and the stages of creating a mathematical model are expressed. As a result, implementation of local adaptation actions to reduce the risks from climate change is a critical and urgent issue. In order to leave a livable environment for future generations, it is foreseen to focus and implement this system, which provides fully renewable environmentally friendly storage at great powers. It will be able to contribute to Turkey in terms of cost, frequency regulation and water needs. The intermittent nature of renewable resources requires longer storage usage. With this storage, both the continuity of the energy will be ensured and the supply-demand balance will be ensured. The drop height, hydraulic slope, network connection and geological structure of hydroelectric reservoirs in Turkey are suitable for the installation of these solar connected pumped hydro storage facilities.

2. Material and Method

There has been an increased interest in renewable energy sources to reduce carbon dioxide absorption and fossil fuel use. However, electrical energy storage systems were needed to ensure the stability and reliability of the electricity grid and to use renewable energy resources efficiently due to the intermittent nature of renewable energy resources [16]. This need; This can be met either by the implementation of conventional storage hydroelectric power plants or by the implementation of other energy storage systems that can keep fossil fuel power plants in reserve so that they can be commissioned within minutes. Popular uses include fossil fuel

generators, batteries, flywheels, supercapacitors and compressed air systems. Storage of electrical energy is necessary for better use of renewable energy resources through electricity transmission and distribution infrastructure [17]. Energy storage systems, which eliminate fluctuations associated with energy production, can facilitate the integration of renewable energy systems. The energy storage system can support system reliability and additionally offer some ancillary facilities such as load tracking, rotary reserve. In addition, energy storage systems can contribute to the stabilization of peak loads and in this way reduce generator failures. The amount of energy stored can play an important role in balancing the peak load. The capacity factor of the base generating units can be increased in this way, it is also a positive factor for the use of stored energy at a low price. In addition, energy balance is very important in power systems. This balance also emphasizes that it requires keeping the frequency at 50 Hz. This is made possible by smart grid integration. Energy storage systems can also contribute to the stabilization of peak loads, thus reducing generator failures. Energy storage systems are an important key to adapting to the diversity of new technology, changing consumer habits and actions, and the changing mechanism of electricity generation and distribution in recent years.

Energy storage technologies are developing day by day. Among the popular ones are fossil fuel generators, batteries, flywheels, supercapacitors. Energy storage technologies can generally be examined under three headings: mechanical, electrochemical and electromagnetic storage. Mechanical energy storage technologies include pumped water-based energy storage systems, compressed air energy storage systems, and flywheels. Flywheels store kinetic energy. Pumped hydro storage and compressed-air energy storage is used as potential energy storage.

2.1. Compressed air energy storage

The oldest compressed air energy storage (CAES) plant was built in 1978 in Hundorf, Germany. It is planned to come cross the highest energy needs and allow a nuclear power plant to maintain a constant capacity factor [18]. Compressed air storage compressors are used to compress air and store it in an underground or aboveground piping system [19]. It can provide above 100 MW of energy with a single unit. When there is low power demand, the compressor is operated and the ambient air is compressed and stored in the underground impermeable caverns, and electricity is produced by operating the turbines with compressed air at times of need. The energy produced from electricity or a different source is stored in large air tanks [20]. Efficiency varies between 70% and 89% as it is related to compressor and turbine efficiencies. It can self-discharge. It has a useful life of about 40 years [18] When the power generation cannot meet the load demand, the stored compressed air is released and the heat released by the combustion of fossil fuel or the heat gained as a result of the compression process can be converted into electrical energy by heating it with a heat source and applying it to turbines as a pressure [19]. Energy storage with compressed air can be used from small scale to large scale power capacity. It can also be integrated into a large-scale power plant that includes grid applications for load shifting, voltage and frequency control. Disadvantage; It is difficult to find suitable geographical areas with underground natural caves. The system is incineration with the use of fossil fuels.
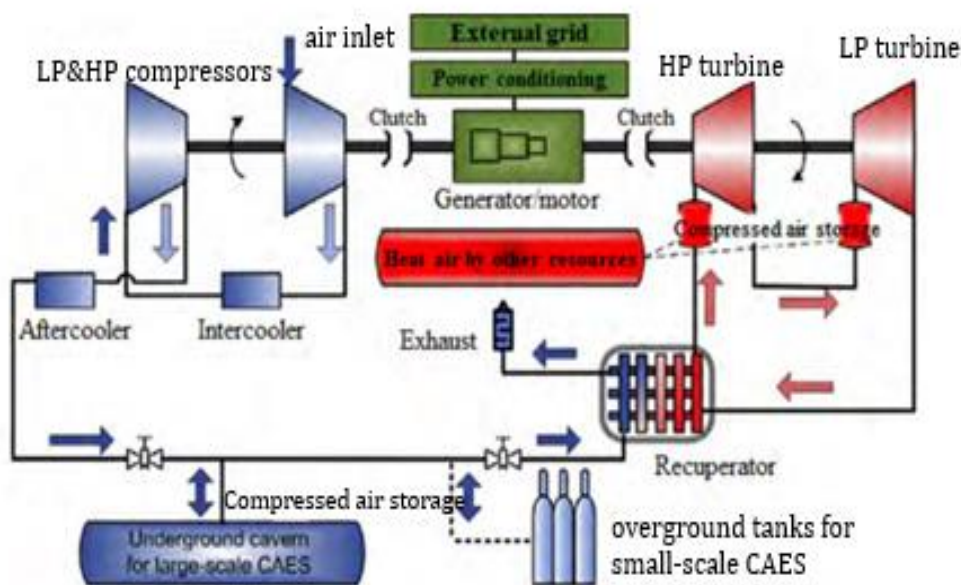

Figure 1. Compressed air of principle scheme [21]

2.2. Pumped hydro storage

Pumped storage hydroelectric power plants for the first time in the world emerged in the 1890s in the mountainous zones of Switzerland, Austria and Italy. In the early models, an independent pump wheel and turbine generator were used. Later, in line with the developments, the use of reversible pump turbines increased in pumped storage systems [22].

Pumped hydroelectric storage power plant is a system that provides consumption when electricity demand is high, by storing electricity when electricity demand is low in facilities that are difficult to stop and costly, such as nuclear and thermal power plants [23]. In pumped storage hydroelectric power plants, there are 2 reservoirs, the upper and lower reservoirs. River, natural lake, dam, sea or artificial pool are chosen as reservoirs.

Figure 2 shows the schematic of pumped hydro storage. Pumped hydroelectric storage power plants provide storage as potential energy by pumping water from the lower reservoir to the upper reservoir [24]. When the energy demand is rise, electrical energy is produced by reducing the water accumulated in the upper reservoir to the lower reservoir [25]. When the energy demand is decrease, water is transported from the downer reservoir to the upper reservoir by pump. When the demand is low, when it needs to be operated at low capacities, the electrical energy to be obtained from discontinuous energy sources such as the sun and wind is stored using the electricity and the minimum load is pulled up. By producing electricity at times of high demand and expensive electricity, the maximum load is lowered and the ratio of minimum load to maximum load is increased. Thus, the amount of peak load is reduced, the base load value is increased, and the consumption in the peak load periods is shifted to the minimum consumption periods. In this way, the system load factor is increased and efficiency is increased [26]. It can be made a more useful system by integrating with renewable energy sources.

PHES is used for improving plant performance, regulating storage capacity, and power quality assurance. PHES has great power and energy, long service life, high efficiency and very small discharge losses [27]. PHES can adapt for the volatile situations of renewable resources by reacting quickly. A quantity of energy stored is rate to the height distinction between the two reservoirs and the volume of water stored. Thanks to small evaporations, the storage time of PHES can vary from hours to years. Considering evaporation losses, 71% to 85% of the electrical energy used to pump water into the upper reservoir can be recovered [28]. Pumped storage is classified three main categories [29]:

Closed circuit: consists of two reservoirs, separated by a vertical distance, both of which are not connected to another body of water.

Semi-open: consists of an artificial or modified reservoir and a lake or river dam in continuous mode.

An open system (back pumping) is a system in which there is a continuous flow of water from both the upper and lower reservoirs. Most of the lands are far from the river when the terrain is examined for the installation of the pumped hydro storage system. Therefore, the non-river PHES system consists of a pair of artificial reservoirs placed several kilometers apart and connected by aqueducts, pipes and tunnels. Reservoirs can be custom built or existing reservoirs can be used [3, 37]. A combination of high head, low separation of reservoirs, and low dam wall volumes result in relatively low capital costs
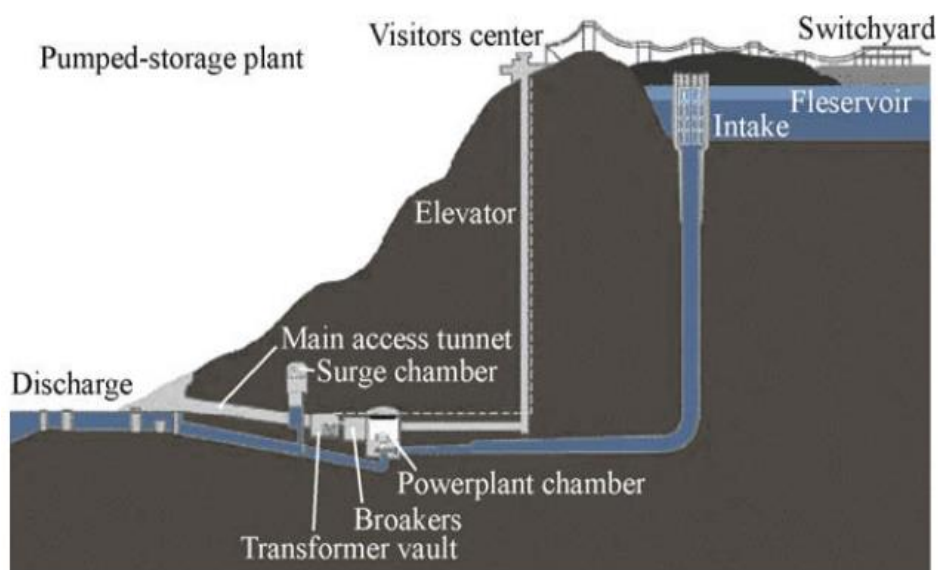

Figure 2. Pumped hydroelectric storage diagram [27]

Table 1 shows the advantages, disadvantages and usage areas of mechanical energy storage methods, pumped hydro storage and compressed air storage, which are used in high-power systems and provide potential energy storage.

Table 1. Mechanical energy storage methods advantage, disadvantage and usage area [29]

Mechanical Energy Storage Technology	Advantage	Disadvantage	Usage Area
Pumped Hydro Storage	High capacity, low unit energy cost	The need for large and private space	Time shift energy applications, Integration of large-powered renewable energy sources
Compressed-air Storage	High capacity, low unit energy cost	Large underground space needed, additional fuel cost	Time shift energy applications, Integration of large-powered renewable energy sources

2.3. Solar Powered Pumped Hydro Storage

In PV solar energy, a storage is needed due to the fact that the sun is not continuous, only for daytime production. Pumped hydroelectric storage (PHES) uses mechanical storage to maximize solar energy use and prevent outages [30]. A continuous supply of electricity can be provided by this solar-connected pumped hydro storage. In addition, the integration of pumped hydro storage with solar also supports supply and demand balance.

During low demand, the pumping process and hydroelectric generation are done during peak demand. Therefore, consumption during off-peak hours is covered by the sun. In the remaining period, power generation is completed from hydro if insufficient solar production is confirmed. Excess solar energy that is not used for consumption in the system is used for storage. In this way, the purchase prices of electricity from the grid are likely to decrease [31].

The working principle of the hybrid PHES can be briefly explained as follows. As shown in Figure 3, when solar generation is higher than energy demand, the excess energy is used to pump water from a lower reservoir to an upper reservoir. Storing energy in the form of gravitational potential energy of water (charge/pumping mode, Figure 3a). When energy generation is needed, water is permitted to flow back down through the turbines and the stored energy is transferred to the load (production mode, Figure 3b) [32].
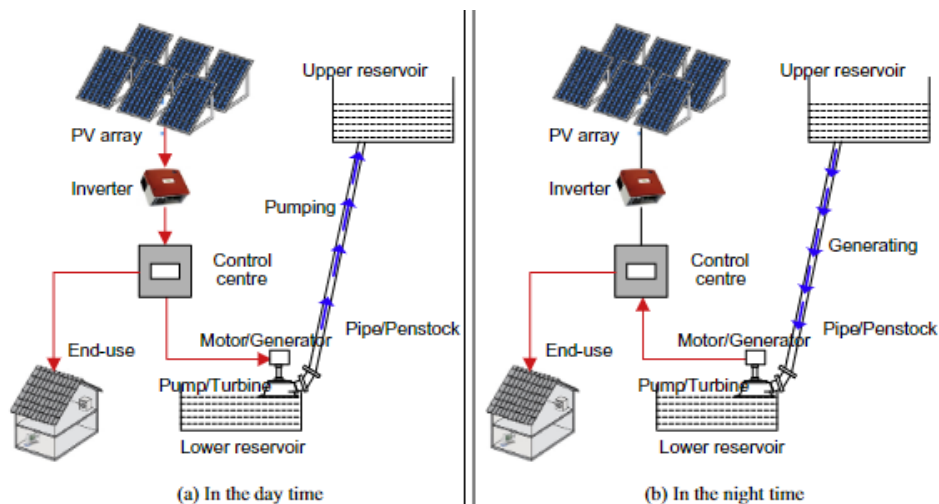

Figure 3. System schematic of a solar connected pumped storage system

System modeling is a critical step before system design, simulation and optimization.

2.3.1. Energy model of the system components

The studied system consists of different stages that can convert solar radiation into hydro potential energy. First, the photovoltaic cell system works as an energy source. The output of the first stage is processed by a dc-dc converter to feed and electromechanical pump-hydro stage. It follows from this that the pumping system is able to raise a column of water through a water recovery pipe from the bottom to the upper reservoir [33].
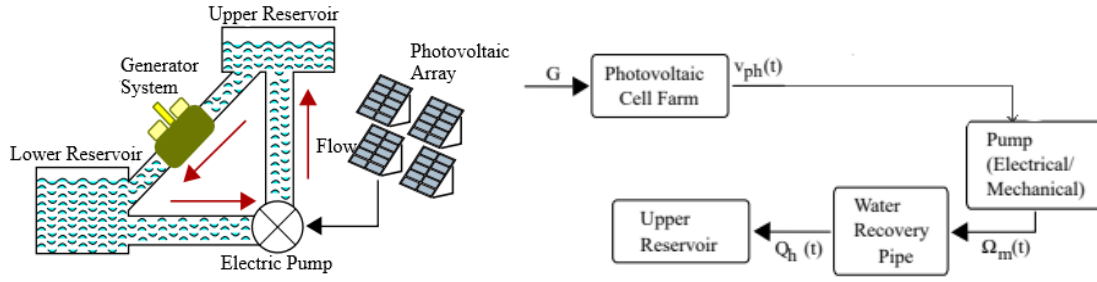
Figure 4. a) Model of the solar-powered pumped-hydro system for energy storage b) System blog diagram

The complete system is illustrated in Figure 4a with a more detailed block diagram given in Figure 4b, where the inputs and outputs of each of the subsystems (domains) are presented. In Figure 4b we see that the system has as input the current due to the sun's G radiation and as output the hydraulic flow Qc. A solar cell, also known as a photovoltaic cell, is an electronic system that converts solar energy into electricity using the photovoltaic effect.
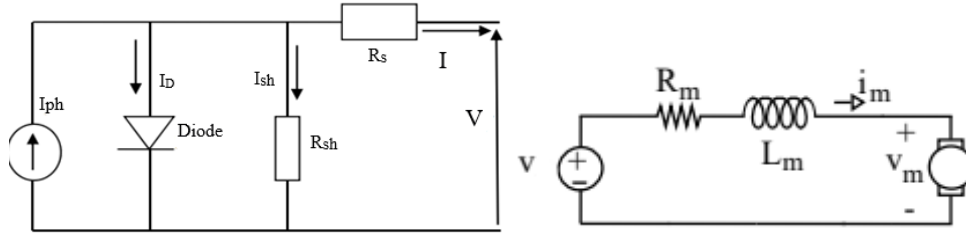
Figure 5. Photovoltaic cell circuit diagram and Pump circuit diagram

A single diode PV circuit diagram is used in the solar model. V output will be the pump voltage. The relationship between the outputs current (I) and voltage (V) of the PV panel for a single unit is expressed as follows [34, 35].

$$I = I_{Ph} - I_0 \left(e^{\frac{V+IR_S}{aV_T}} - 1 \right) - \frac{V+IR_S}{R_{sh}} \tag{1}$$

A pump is defined electrically and mechanically to store water from the bottom to the upper reservoir. First, the equivalent circuit for the electric field is shown in Figure 5. Inductance Lm stores kinetic energy and in Figure 4 the dynamics of the system is described.

$$L_m \dot{i}_m = -R_m i_m + v - v_m \tag{2}$$

According to the Biot-Savart Law, the magnetic flux can be expressed as:

$$\emptyset_m = L_m i_m \tag{3}$$

The dynamics of the system, the q_m related to charge storage in the circuit are used. q_m is expressed as the ratio of magnetic flux to inductance.

If we make mathematical modeling to determine the hydroelectric power;

The power output from the hydro system is rely on the condition of the water tank due to precipitation and previous pumped storage. The water stored within one hour will be used to generate power when the power from the PV is not sufficient to meet the load demand [12]. It will be used to generate hydroelectricity during rainy hours. It is divided by 3600s to run continuously for 1 hour. Hydroelectric output can be expressed with Equation 4 and 5.

$$Q_r(t) = \frac{R_{rain} \cdot dt_{rain} \cdot A_{catch} \cdot \tau_{catch}}{36 \times 10^5} \tag{4}$$

$$P_H(t) = \rho \cdot g \cdot Q_r(t) \cdot (h - h_f) \cdot \tau_{Ho} \tag{5}$$

$$Q_{pump}(t) = \frac{P_{excess}(t) \cdot \tau_{pump}}{\rho \cdot g \cdot (h - hf)} \tag{6}$$

$$V_m(t) = (Q_{pump}(t) \times 3600) + (R_{rain} \cdot dt_{rain} \cdot A_{catch})/1000 \tag{7}$$

Where Qr denotes the water flow rate enters to hydro turbine in m³/s, Qmax is the maximum limit of water flow to be used in hydro turbine in m³/s, Q_{pump} is the pumped water flow rate in m³/s, R_{rain} indicate rain in millimeters (mm), dt_{rain} represents the rainfall time duration in number of minutes in an hour. A_{catch} is the

accumulate area in m^2, V is the effective volume of water in the upper reservoir. τ_{catch} is the efficiency of rainfall basin, ρ means water density (1000 kg/m^3), h shows the gross water head in m, hf is head loss due to friction in m, and τ_{Ho} is the overall efficiency of hydropower system.

In PV solar energy, a storage is needed due to the fact that the sun is not continuous, only for daytime production. A continuous supply of electricity can be provided by this solar-connected pumped hydro storage. In addition, the integration of pumped hydro storage with solar also supports supply and demand balance.

During low demand, the pumping process and hydroelectric generation are done during peak demand. Therefore, consumption during off-peak hours is covered by the sun. In the remaining period, power generation is completed from hydro if insufficient solar production is confirmed. Excess solar energy that is not used for consumption in the system is used for storage. In this way, the purchase prices of electricity from the grid are likely to decrease [36]. In order to make the energy management very well in system design, the output power estimations of the PV system are made by methods such as ANN and Fuzzy Logic. The planning and operating process of the power system are a good measure to increase the reliability of these systems. These performance values are examined for the processes of meeting the load demand for hybrid renewable systems. This is due to the power imbalance of the hybrid renewable energy source. Optimization methods are used to correct this. While optimizing the reliability of the system, the process is taken as a constraint or a target to be achieved. The value of the reliability index (IR) can be checked using optimization methods to find the optimal size of the hybrid renewable resource's configuration.

3. Conclusion

There is a need for new studies in the field of energy storage in order to ensure the efficiency of existing energy sources and to meet the energy need in a healthy way. This need can be met with new studies to be carried out in the field of energy storage by using developing technological opportunities. However, it is important to consider environmental factors, low cost and high efficiency in such studies. Among the energy storage systems, the pumped hydroelectric storage system and compressed air storage from mechanical storage systems provide frequency and voltage stability. Considering the location definitions for PHES applicability, it may be beneficial to use rivers and shores as reservoirs. Because the use of rivers and shores in low reservoirs can be efficient in terms of construction and cost. The use of large rivers as sub-reservoirs increases efficiency by providing a large increase in the amount of water, while it is also used for hydroelectric power plants. It is predicted that pumped storage can meet the hourly energy needs with its integration with the PV solar energy system. A brief review of the solar coupled hybrid pump hydro storage system is given. As a result of these investigations; It is said that optimization methods are used to solve the solar problems of the hybrid system and as a result, the ANN model is better. It is stated that this hybrid system provides a good balance in situations where supply-demand variability is high. The hybrid system can generate and store electricity at low cost in a standalone solution that faces climate change and reduces its carbon footprint.

Author contributions

Ayşenur Oymak: Conceptualization, Methodology, Software **Mehmet Rida Tür:** Data curation, Writing-Original draft preparation, Software, Validation. **Nouha Bouchiba:** Visualization, Investigation, Writing-Reviewing and Editing.

Conflicts of interest

The authors declare no conflicts of interest.

References

1. Barbour, E., Wilson, I. G., Radcliffe, J., Ding, Y., & Li, Y. (2016). A Review of Pumped Hydro Energy Storage Development in Significant International Electricity Markets. Renewable and Sustainable Energy Reviews, 61, 421-432.
2. Vilanova, M. R. N., Flores, A. T., & Balestieri, J. A. P. (2020). Pumped Hydro Storage Plants: A Review. Journal of The Brazilian Society of Mechanical Sciences and Engineering, 42(8), 1-14.
3. Blakers, A., Stocks, M., Lu, B., & Cheng, C. (2021). A review of pumped hydro energy storage. Progress in Energy.
4. Kocaman, B. (2013). Akıllı Şebekeler ve Mikro Şebekelerde Enerji Depolama Teknolojileri. *Bitlis Eren Üniversitesi Fen Bilimleri Dergisi*, *2* (1), 119-127.
5. Tur. M.R., Yaprdakdal, F. Yenilenebilir Enerji Kaynaklarına Dayalı Bir Sistemde Güç Kalitesi Analizi, Kontrolü ve İzlemesi, Gazi Üniversitesi Fen Bilimleri Dergisi Part C: Tasarım ve Teknoloji, 8 (2020), Sayı 3, 572-587.
6. Nehrir, M. H., Wang, C., Strunz, K., Aki, H., Ramakumar, R., Bing, J., & Salameh, Z. (2011). A review of hybrid renewable/alternative energy systems for electric power generation: Configurations, control, and applications. IEEE transactions on sustainable energy, 2(4), 392-403.
7. Rehman, S., Al-Hadhrami, L. M., & Alam, M. M. (2015). Pumped Hydro Energy Storage System: A Technological Review. Renewable and Sustainable Energy Reviews, 44, 586-598
8. Dong, L., Xing, T., Song, J., & Yousefi, A. (2021). Performance analysis of a novel hybrid solar photovoltaic-pumped-hydro and compressed-air storage system in different climatic zones. Journal of Energy Storage, 35, 102293.
9. Marefati, M., Mehrpooya, M., & Pourfayaz, F. (2021). Performance analysis of an integrated pumped-hydro and compressed-air energy storage system and solar organic Rankine cycle. Journal of Energy Storage, 44, 103488.
10. Mousavi, N., Kothapalli, G., Habibi, D., Lachowicz, S. W., & Moghaddam, V. (2020). A Real-time Energy Management Strategy for Pumped Hydro Storage Systems in Farmhouses. Journal of Energy Storage, 32, 101928.
11. Al-Masri, H. M., Magableh, S. K., Abuelrub, A., Saadeh, O., & Ehsani, M. (2020). Impact of Different Photovoltaic Models on The Design of A Combined Solar Array and Pumped Hydro Storage System. Applied Sciences, 10(10), 3650.
12. Bhayo, B. A., Al-Kayiem, H. H., Gilani, S. I., & Ismail, F. B. (2020). Power management optimization of hybrid solar photovoltaic-battery integrated with pumped-hydro-storage system for standalone electricity generation. Energy Conversion and Management, 215, 112942.
13. Punys, P., Baublys, R., Kasiulis, E., Vaisvila, A., Pelikan, B., & Steller, J. (2013). Assessment of Renewable Electricity Generation by Pumped Storage Power Plants in EU Member States. Renewable and Sustainable Energy Reviews, 26, 190-200.
14. Yıldız, C., & Şekkeli, M. (2016). Türkiye Gün Öncesi Elektrik Piyasasında Rüzgar Enerjisi ve Pompaj Depolamalı Hidroelektrik Santral için Optimum Teklif Oluşturulması. Pamukkale Üniversitesi Mühendislik Bilimleri Dergisi, 22(5), 361-366.
15. Makhdoomi, S., & Askarzadeh, A. (2020). Daily Performance Optimization of A Grid-connected Hybrid System Composed of Photovoltaic and Pumped Hydro Storage (PV/PHS). *Renewable Energy*, 159, 272-285.
16. Luo, X., Wang, J., Dooner, M., & Clarke, J. (2015). Overview of current development in electrical energy storage technologies and the application potential in power system operation. Applied energy, 137, 511-536.
17. Rehman, S., Al-Hadhrami, L. M., & Alam, M. M. (2015). Pumped hydro energy storage system: A technological review. Renewable and Sustainable Energy Reviews, 44, 586-598.
18. Amirante, R., Cassone, E., Distaso, E., & Tamburrano, P. (2017). Overview on recent developments in energy storage: Mechanical, electrochemical and hydrogen technologies. Energy Conversion and Management, 132, 372-387.
19. Zhao, H., Wu, Q., Hu, S., Xu, H., & Rasmussen, C. N. (2015). Review of energy storage system for wind power integration support. Applied energy, 137, 545-553.
20. Kutucu, N., Terzi, Ü. K., & Ayirga, H. Y. (2017, April). Technical and economic analysis of energy storage systems in smart grids. In 2017 5th International Istanbul Smart Grid and Cities Congress and Fair (ICSG) (pp. 166-170). IEEE.
21. Faisal, M., Hannan, M. A., Ker, P. J., Hussain, A., Mansor, M. B., & Blaabjerg, F. (2018). Review of energy storage system technologies in microgrid applications: Issues and challenges. Ieee Access, 6, 35143-35164
22. Yang, C. J. (2016). Pumped Hydroelectric Storage. In Storing Energy (pp. 25-38). Elsevier
23. Gürsakal, H., & Uyumaz, A. (2021). Pompaj Depolamalı Hidroelektrik Santrallerin Optimizasyonunda Karlılık Analizi Ve Çalışma Süresi Tayini. Mühendislik Bilimleri Ve Tasarım Dergisi, 9 (2), 436-452.
24. Guittet, M., Capezzali, M., Gaudard, L., Romerio, F., Vuille, F., & Avellan, F. (2016). Study of The Drivers and Asset Management of Pumped-Storage Power Plants Historical and Geographical Perspective. Energy, 111, 560-579.
25. Chauhan, A., & Saini, R. P. (2014). A review on Integrated Renewable Energy System Based Power Generation for Stand-alone Applications: Configurations, Storage Options, Sizing Methodologies and Control. Renewable and Sustainable Energy Reviews, 38, 99-120.

26. Ünver, Ü., Bilgin, H., & Güven, A. (2015). Pompaj Depolamalı Hidroelektrik Sistemler. Mühendis ve Makina, 56 (663), 57-64.
27. Zhao, H., Wu, Q., Hu, S., Xu, H., & Rasmussen, C. N. (2015). Review of Energy Storage System for Wind Power Integration Support. Applied Energy, 137, 545-553.
28. Chen, H., Cong, T. N., Yang, W., Tan, C., Li, Y., & Ding, Y. (2009). Progress in Electrical Energy Storage System: A Critical Review. Progress in Natural Science, 19(3), 291-312.
29. Kabalcı, E., Bayındır R., & Tur, M.R. (2021). Mikroşebekeler ve Dağıtık Üretim Sistemleri. ISBN:978-625-439-718-9.
30. Javed, M. S., Ma, T., Jurasz, J., & Amin, M. Y. (2020). Solar and Wind Power Generation Systems with Pumped Hydro Storage: Review and Future Perspectives. Renewable Energy, 148, 176-192.
31. Simão, M., & Ramos, H. M. (2020). Hybrid pumped hydro storage energy solutions towards wind and PV integration: Improvement on flexibility, reliability and energy costs. Water, 12(9), 2457.
32. Ma, T., Yang, H., Lu, L., & Peng, J. (2015). Pumped storage-based standalone photovoltaic power generation system: Modeling and techno-economic optimization. Applied energy, 137, 649-659.
33. Phillips-Brenes, H., Pereira-Arroyo, R., & Muñoz-Arias, M. (2019, November). Energy-based model of a solar-powered pumped-hydro storage system. In 2019 IEEE 39th Central America and Panama Convention (CONCAPAN XXXIX) (pp. 1-6).
34. Al-Masri, H. M., Magableh, S. K., Abuelrub, A., Saadeh, O. (2020). Impact of different photovoltaic models on the design of a combined solar array and pumped hydro storage system. Applied Sciences, 10(10), 3650.
35. Tur, M.R. S. Ay, A. Shobole, M. Wadi, Güç Sistemlerinde ünite tahsisi için döner rezerv gereksinimi optimal değerinin kayıp parametrelerin dikkate alınarak hesaplanması, Journal of the Faculty of Engineering & Architecture of Gazi University. Vol. (2018) Issue 18, Part 2, p1-20. 20p.
36. Simão, M., & Ramos, H. M. (2020). Hybrid pumped hydro storage energy solutions towards wind and PV integration: Improvement on flexibility, reliability and energy costs. Water, 12(9), 2457.
37. Stocks, M., Stocks, R., Lu, B., Cheng, C., & Blakers, A. (2021). Global Atlas of Closed-loop Pumped Hydro Energy Storage. Joule, 5(1), 270-284.
38. Hossain, E., Tür, M. R., Padmanaban, S., Ay, S., & Khan, I. (2018). Analysis and mitigation of power quality issues in distributed generation systems using custom power devices. IEEE Access, 6, 16816-16833.
39. Oymak, A., Tür, M. R., & Bouchiba, N. (2022). PV connected Pumped-Hydro Storage System. *Advanced Engineering Days (AED)*, *2*, 10-12.

Geochemical and geological approach to the carbonate-hosted barite deposits in Dadağlı (Kahramanmaraş), Turkey

Cihan Yalçın*1

1Ministry of Industry and Technology, General Directorate of Industrial Zones, Türkiye, cihan.yalcin@sanayi.gov.tr

Abstract
In terms of its geological structure, Kahramanmaraş is a complex region where various tectonic units are observed simultaneously. Many thrust and fault zones identified with the closure of the southern branch of the Neotethys Ocean are observed in this region. There are units existing to the Amanos Group in the vicinity of Dadağlı (Kahramanmaraş). Paleozoic aged rocks and Mesozoic aged carbonates are observed on them. There is vein type barite mineralization in the fracture lines of the Upper Triassic-Lower Jurassic Küreci dolomitic limestones in the north of Dadağlı. Paragenesis consists of galena, sphalerite, pyrite, smithsonite, calcite and quartz, individually. The mineralization is roughly 1 m thick and 200 meters long. The BaO value amounts to a peak of 65.07% in the specimens gathered from the ore zone. Although the ore zone is poor in SrO, it is rather rich in SiO_2. Barite samples from the study area exhibit similar many other vein type barite deposits with SrO% contents. Since this region is extremely close to both East Anatolian Fault (EAF) and suture belt of Taurides and Arabian Platform, it is considered that EAF may have an effect on barite formation in fractures and cracks.

1. Introduction

Barite ($BaSO_4$) is an essential industrial raw material because it is an intense mineral. Barite, which generally observed in marine environments [1-2], is still involved in the paragenesis of Pb, Zn, Cu and Au deposits in low, medium and high sulfidation classes [3-4]. Barite-bearing fluids occur in sedimentary processes, specifically in marine environments, including magmatic [5], hydrothermal [6] and metamorphic [7] fluids [2, 8-9]. For barite formation: fluid cooling or bacterial process [10], intense liquid-rock interaction [11] and mixing of two or more liquids [12] are effective.

Turkey's important barite deposits were formed as a result of the Alpine and Hercynian Orogeny [13]. For this reason, barite mineralization is located in major tectonic belts. Among these deposits, the Isparta barite deposits, which have the largest distribution, are observed in Paleozoic aged carbonate and pelitic rocks in the Western Taurus [14-19]. Cansu and Öztürk [20] explained the formation and origin of barite deposits associated with Paleozoic sediments located in both the Tauride-Anatolide belt (Şarkikaraağaç, Hüyük and Tordere deposits) and the Arabian platform (Şekeroba and Önsen deposits, Kahramanmaraş). The barite mineralization observed in the Dadağlı region is very close to this district.

In this paper, we present geochemical data obtained from Dadağlı barite mineralization using X-ray fluorescence (XRF) methods.

2. Material and Method

In terms of its geological structure, Kahramanmaraş is a complex region where various tectonic units are observed simultaneously. Many thrust and fault zones identified with the closure of the southern branch of the Neotethys Ocean are observed in this region [21]. Suture belts were formed by both the closure of the ocean and the convergence of the Tauride and Arabian plates [22]. With the depletion of the ocean floor, allochthonous units were thrusted onto the Arabian platform in the south and suture belt and suture belts were formed between these two continents [23]. Rigo De Righi and Cortesini [24] and Gül [25] divided the tectonostratigraphic units in the Southeastern Anatolia Region into orogenic belts.

The Dadağlı barite mineralization is situated in the margin fold belt of the Arabian Platform in the south of the Taurus Orogenic Belt (Figure 1). It has been stated that in the Middle Miocene, when the Arabian Plate collided with the Anatolian Plate in this region, allochthonous units emplaced in the shallow Miocene basin and caused the basin to partially turn into land [26]. Gül [27] stated that the collision of the Anatolian and Arabian plates took place in the Upper Cretaceous and a compressional regime was active in the region during the Paleocene-Early Eocene period. Yılmaz and Yiğitbaş [28] stated that as a result of the movement of the Arabian continent towards the Anatolian plate between the Upper Cretaceous-Miocene, the region gained a nappe character. In this tectonically active region, rock groups of different origins are observed together. Rocks belonging to the Amanos Group are widely observed in the Dadaglı region.
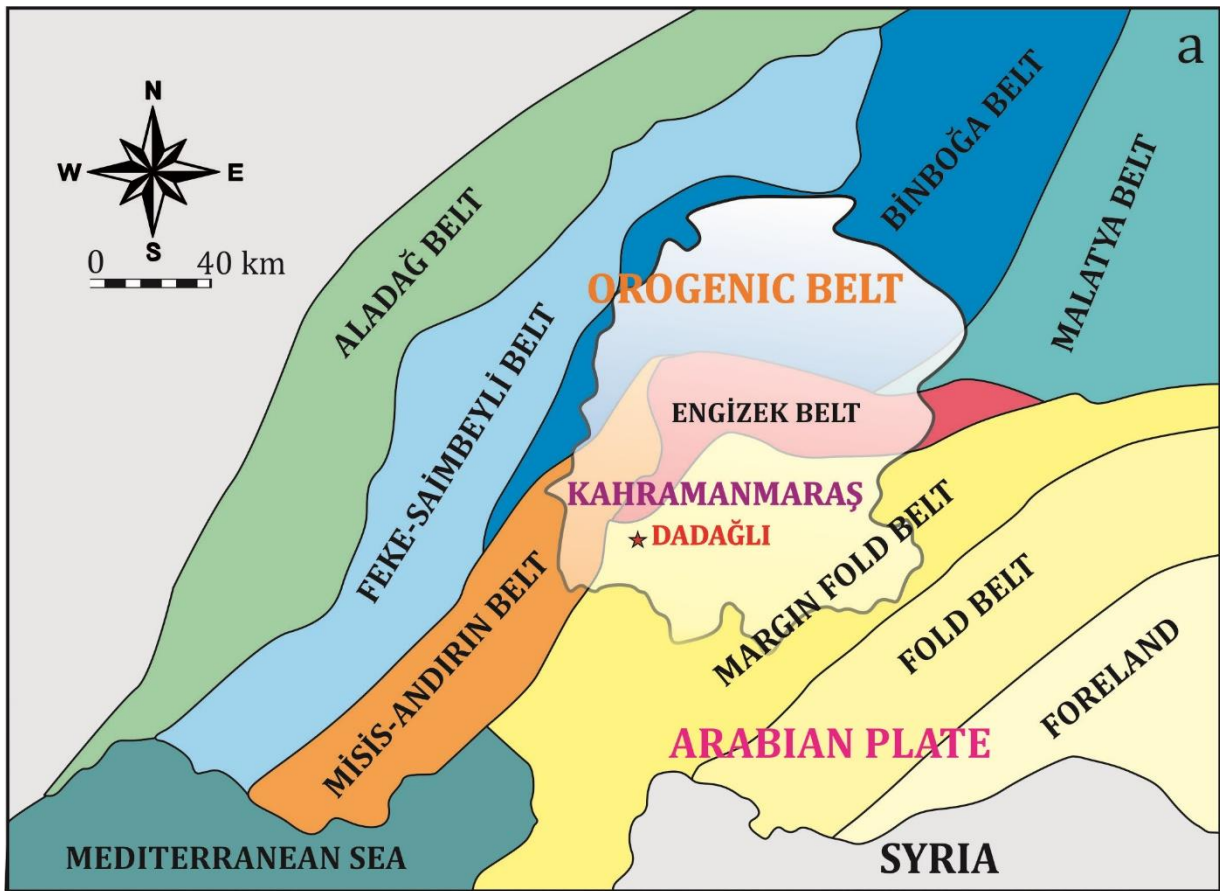
Figure 1. Tectonic location of the study area [25]

2.1. Geological background

Seydişehir formation forms the basement of the study area. The unit mainly consists of shale, siltstone, metasandstone and quartzite [29-30]. Lithologies of this unit crop out in Altınova, Dadaglı and Hopurlu regions (Figure 2) respectively. On this unit, Mesozoic aged carbonates are overlying with angular unconformity. Küreci dolomitic limestones and Karadağ limestones are observed around Önsenhopuru and Dadağlı (Figure 2) districts. These units of Amanos are overlain by Upper Miocene aged basalts with angular unconformity [31-32]. Quaternary alluviums represent the youngest lithologies of the region.

The study area is very close to the East Anatolian Fault (EAF), which is one of the most important faults of Turkey in terms of tectonics. For this reason, the origin of the deformations in this region may be the EAF as well as the tectonic structures before the formation of the EAF. This warning was made for the importance of factors

such as faults and joints, which are effective in the formation of ore in the region. Because many faults are observed in the region (Figure 2). The rocks were deformed by the effect of these faults. Depending on the movement of fluids in deformed rocks, vein type mineralizations are found. Around these veins, crushed zones and altered zones have developed in the rocks.

The study area is very close to the area where the southern branch of the Neotethys Ocean was closed [21] and as a result Tauride and Arabian plates converged to form suture belts [33-38]. It should also be taken into account that this region has undergone a north-south oriented compression period.
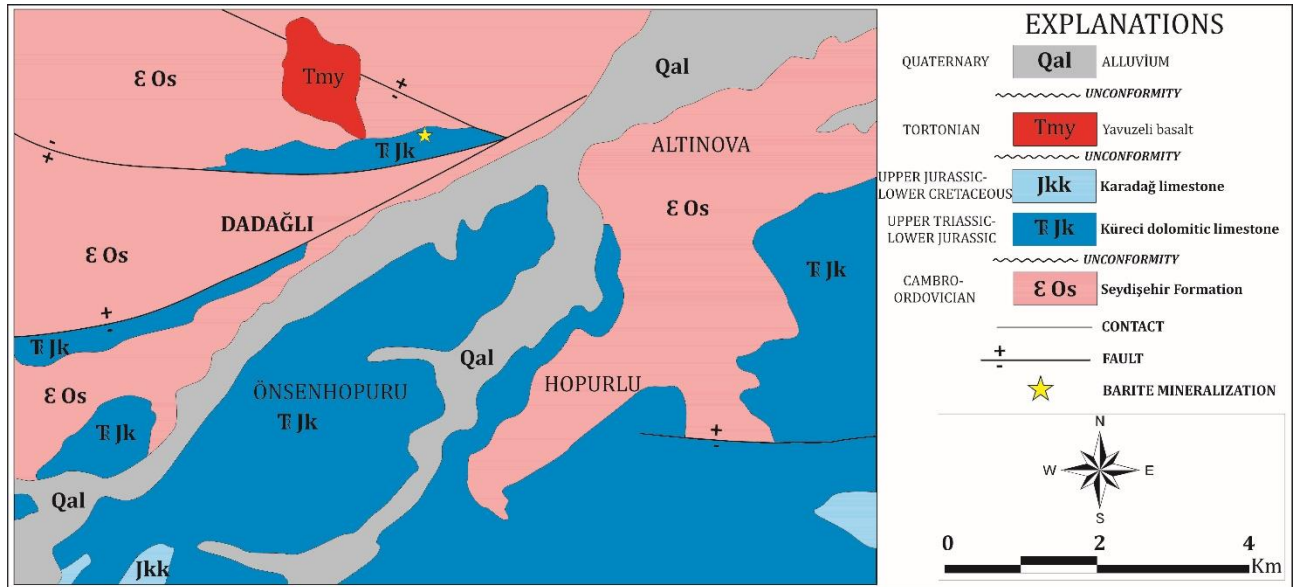
Figure 2. Geological map of the study area [39]

2.2. Mineralization

In Dadağlı region, Upper Triassic-Lower Jurassic Küreci limestones overlie the Paleozoic basement with angular unconformity. Vein type barite mineralizations are observed in the limestones in the north of Dadadağlı (Figure 3).
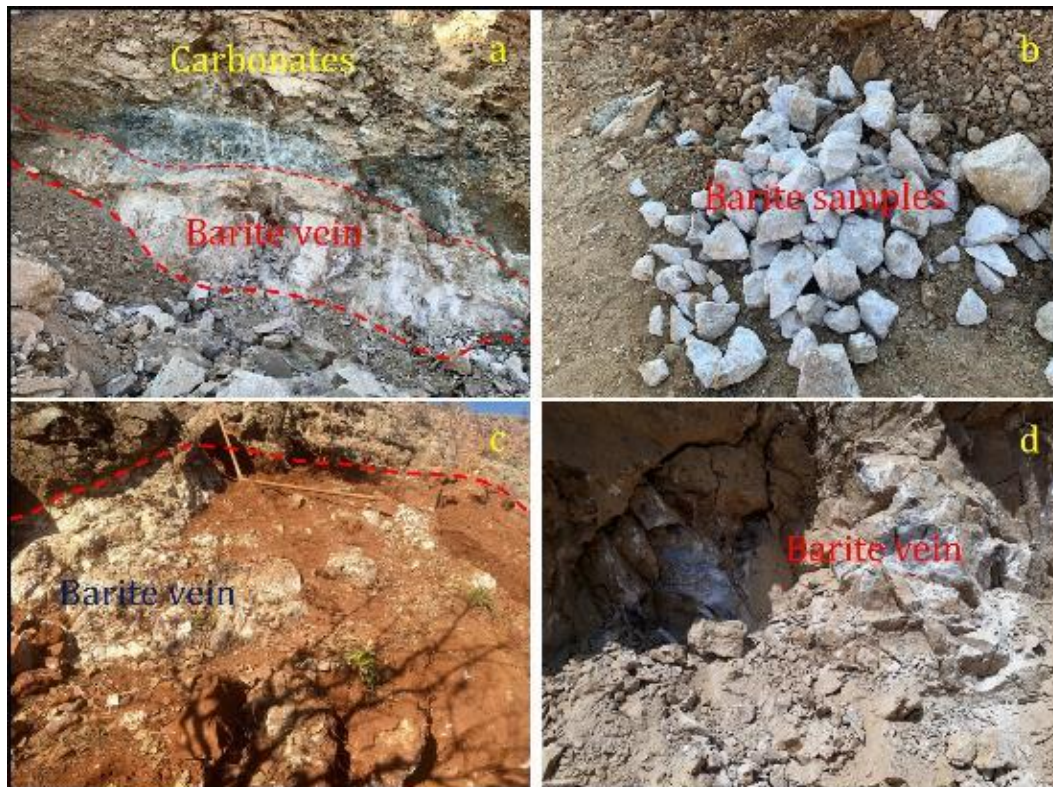
Figure 3. General view of barite mineralization.

Barite mineralization is observed in faults and joints of carbonate units. These fault zones are easily distinguished by their brecciated texture. In addition, altered zones are observed in some areas along the ore vein.

In the mineralization with epigenetic formation, quartz, calcite and smithsonite are still observed along with galena, sphalerite and pyrite, respectively. In the ore petrography, it was determined that quartz veins cut the calcite veins and the sphalerites were transformed into smithsonite (Figure 4 a,b,c). Pyrites are commonly converted to goethite (Figure 4b) and galenas to serousite (Figure 4d). Galena and sphalerites are generally anhedral and scattered, while smithsonites are euhedral.
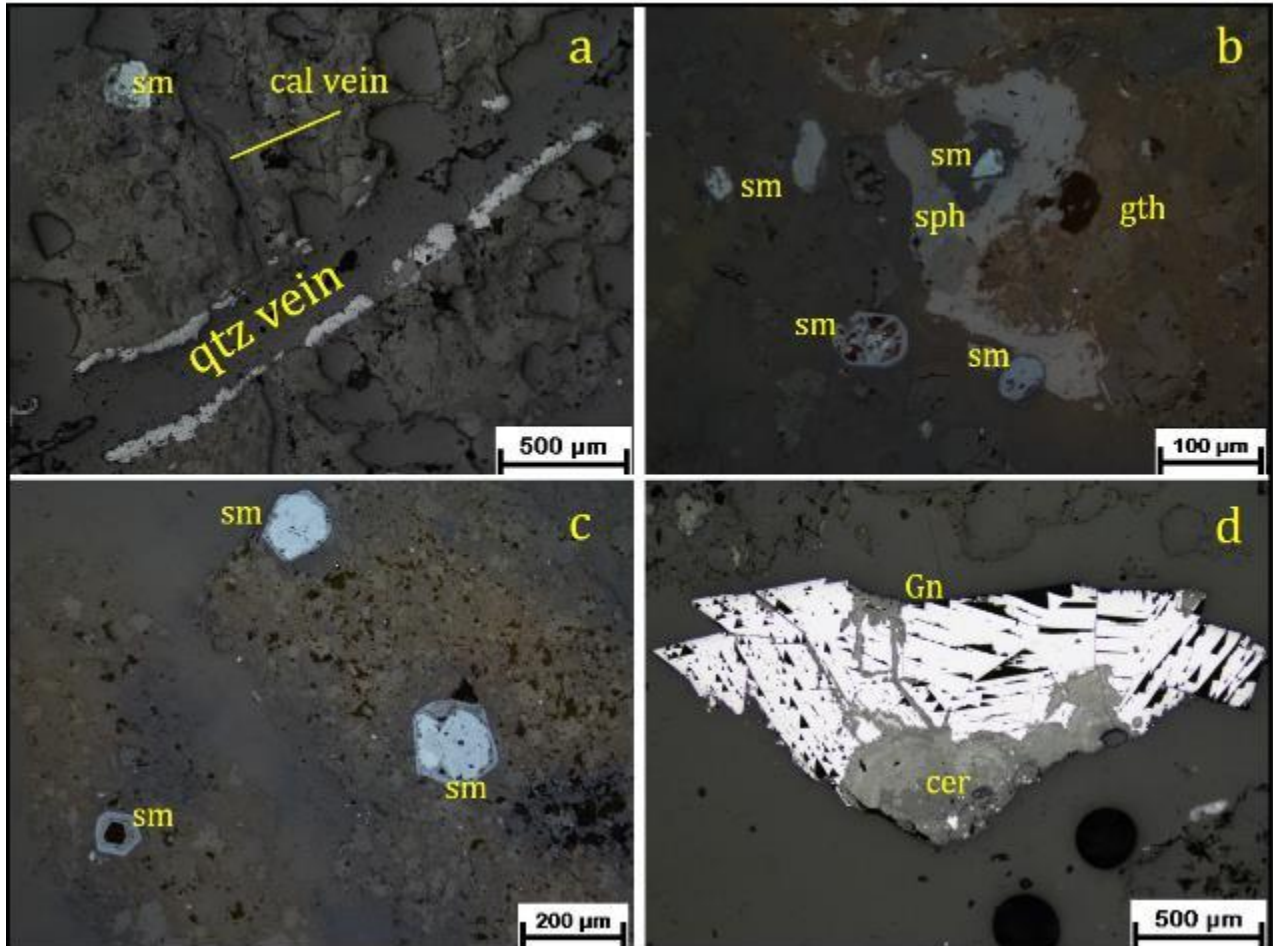
Figure 4. Microscope images of the polished sections. Abbreviations: (sm) smithsonite, (cal vein) calcite vein, (qtz vein) quartz vein, (sph) sphalerite, (gth) goethite, (Gn) galenite, (cer) cerussite

3. Geochemistry

In this region, 8 samples were taken and geochemical analyzes were made. Major oxide element analyzes were carried out in ITU-JAL. Analysis results are given in Table 1.

As showed in Table 1, BaO is between 0.49-65.07% (average 29.52%) and SrO is between 0.06-1.78% (average 0.64%) in the ore zone. Some of the compiled samples are rather rich in SiO_2. CaO is between 0.26-12.77% (average 2.88%) and Fe_2O_3 is between 0.12-15.97% (average 4.15%). The high Fe_2O_3 values in some barite samples are related the presence of ferrous minerals (pyrite and goethite). In K1, K2, K5, K6, and K7 samples, the high SiO_2 composition, which indicates quartz gangue in barite ore as observed in polish sections.

Samples have low Al_2O_3, MnO, Na_2O, K_2O, TiO_2 and P_2O_5 contents respectively. The presence of strontium oxide in barite deposits can be used to determine and compare the genesis of the deposit. Barite samples from the study area exhibit similar many other vein type barite deposits.

4. Discussion

Important barite deposits are both sedimentary stratiform, hydrothermal and biogenic deposits [40]. In sedimentary deposits, sulfur minerals are not involved in paragenesis [41-43]. In hydrothermal formation, it is similar to the sedimentary exhalative (SEDEX) model containing some sulfate minerals and base metal sulfides [44]. Also known as 'Mississippi Valley type mineralization', epigenetic barite ore occurs in platform carbonate

sequences [45]. It has been suggested that basin fluids with a temperature of <200 °C and concentrated along the faults cause to Mississippi Valley type deposits of lead, zinc and barite [46-48].

Table 1. Major oxide analysis of barite mineralization

Formula	K1	K2	K3	K4	K5	K6	K7	K8
Na_2O	0,13	0,89	0,48	0,48	0,05	0,33	0,00	0,38
MgO	3,95	0,82	0,20	0,05	0,42	0,13	0,61	0,12
Al_2O_3	1,80	22,70	1,27	0,25	1,28	0,45	1,72	0,65
SiO_2	38,79	42,44	6,62	2,32	87,74	32,18	86,78	9,28
P_2O_5	0,27	0,66	0,03	0,00	0,02	0,04	0,03	0,03
K_2O	0,47	5,51	0,10	0,00	0,24	0,10	0,28	0,10
CaO	12,77	0,26	1,13	0,61	1,46	2,23	2,32	2,31
$TiO2$	0,13	3,97	0,12	0,01	0,06	0,16	0,06	0,10
MnO	0,20	0,03	0,02	0,00	0,81	0,00	1,84	0,07
Fe_2O_3	2,41	15,97	0,30	0,12	0,86	11,38	1,63	0,53
SO_3	8,56	0,13	26,77	28,44	1,47	17,43	0,31	25,58
BaO	16,71	0,49	60,97	65,07	2,51	31,07	0,96	58,41
Cr_2O_3	0,00	0,01	0,00	0,00	0,00	0,00	0,00	0,00
SrO	0,57	0,06	1,12	1,78	0,06	0,57	0,02	0,94
LOI	13,22	5,86	0,83	0,81	2,96	3,89	3,38	1,47
TOTAL	99,99	99,80	99,96	99,94	99,94	99,97	99,93	99,97
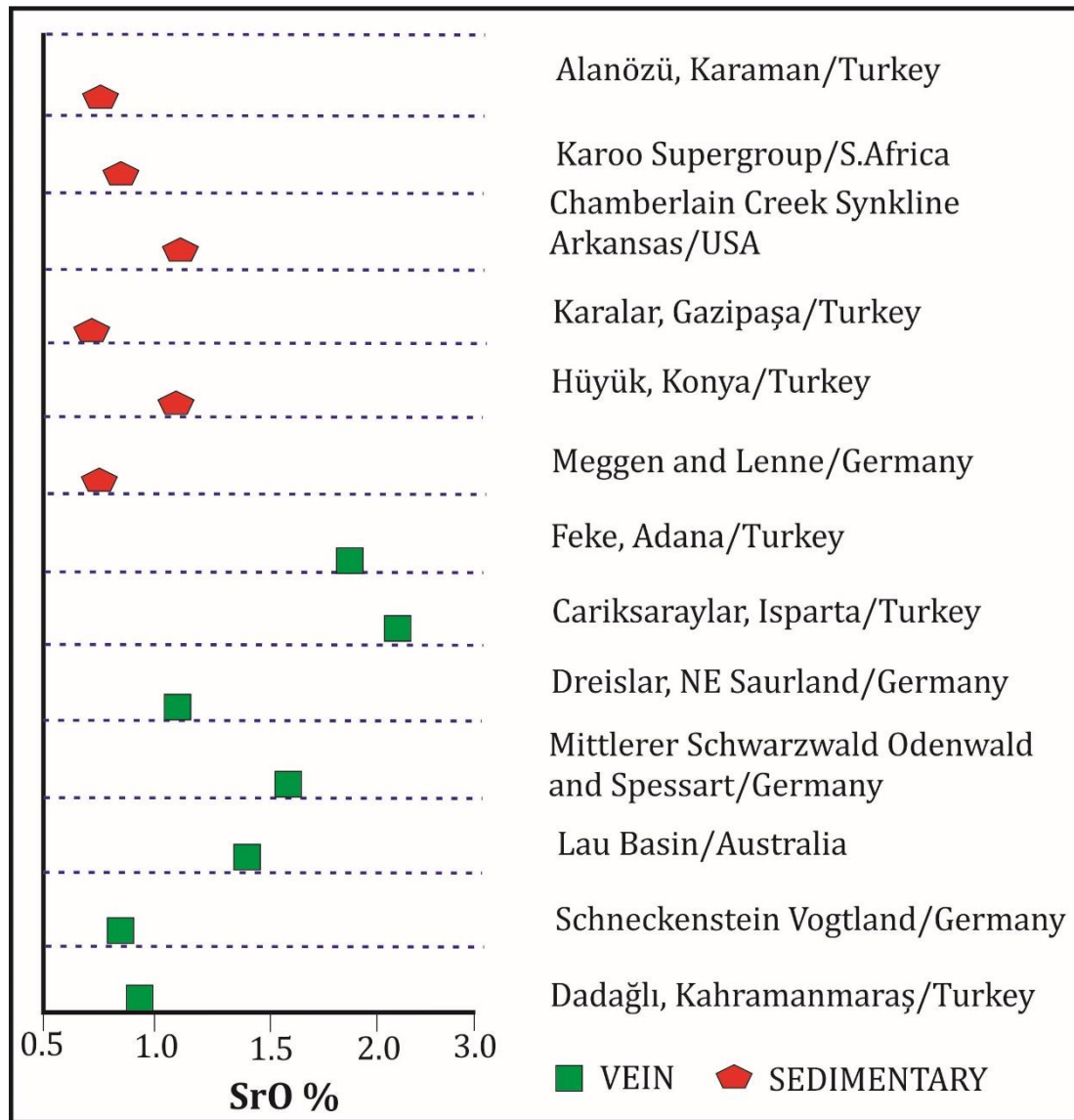
Figure 5. Several deposit types of barite, percentage of strontium oxide amounts [49]

In Turkey, there are many barite deposits associated with carbonate rocks in the Taurus Orogenic belt and the Arabian Plate. In the paragenesis of these barite deposits, chalcopyrite is sometimes found together with galena and sphalerite. Since this study area is very close or related to the barite formation belts described above, the data obtained is important for the Turkish barite deposits.

5. Conclusion

The Dadağlı region is located within the margin fold belt of the Arabian plate. There is vein type epigenetic barite mineralization in the Mesozoic aged carbonates from the Amanos Group units here. The mineralization observed in the fractures and cracks of the carbonates in this region is 200 meters long, with an average thickness of 1 meter. Corresponding to the preliminary data, lead-zinc minerals and their carbonated forms are observed in the ore paragenesis. Major oxide results indicate a mineralization that is poor in Sr but rich in silica. Rich Al_2O_3 values in specimens with poor BaO content may be associated with argillization in fault zones. The positive correlation between SO_3 and BaO in the analysis results is remarkably strong to be ignored.

Since this region is extremely close to both EAF and suture belt of Taurides and Arabian Platform, it is considered that EAF may have an effect on barite formation in fractures and cracks.

In order to elucidate the formation of the barite deposit, isotope studies, trace element and Rare Earth element analyzes as well as liquid inclusion studies should be performed. Apart from the fluid inclusion study, the host rocks should not be ignored in other studies. Each analysis made should be correlated with the host rock.

Conflicts of interest

The authors declare no conflicts of interest.

References

1. Goldberg, E. D., & Arrhenius, G. O. S. (1958). Chemistry of pelagic sediments. *Geochimica et cosmochimica acta,* 13, 153–212.
2. Griffith, E. M., & Paytan, A. (2012). Barite in the ocean-occurrence, geochemistry, and palaeoceanographic applications. Sedimentology 59, 1817–1835.
3. White, N., & Hedenquist, J. (1995). Epithermal gold deposits: Styles, characteristics and exploration. EG Newsletters, 23, 1, 9–13.
4. Wang, Le, Ke-Zh Qin, G.-X. & Song, G.-M. Li. (2019). A review of intermediate sulfidation epithermal deposits and subclassification. Ore Geology Reviews, 107, 434–456.
5. Williams-Jones, A. E., Samoson, I. M., & Olivo, G. R. (2000). The genesis of hydrothermal fluorite-REE deposits in the Gallinas Mountains, New Mexico. Economic Geology. 95, 327–341.
6. Hanor, J. S. (2000). Barite-celestine geochemistry and environments of formation. Reviews in Mineralogy and Geochemistry, 40 (1), 193–275.
7. Kontak, D. J., Kyser, K., Gize, A., & Marshall, D. (2006). Structurally controlled vein baryte mineralization in the Maritimes Basin of Eastern Canada: geologic setting, stable isotopes, and fluid inclusions. Economic Geology, 101, 407–430.
8. Baioumy, H. M. (2015). Rare earth elements, S and Sr isotopes and origin of barite from Bahariya Oasis, Egypt: Implication for the origin of host iron ores. *Journal of African Earth Sciences,* 106, 99–107.
9. Monnin, C. & Cividini, D. (2006). The saturation state of the world's ocean with respect to (Ba, Sr)SO4 solid solutions. *Geochimica et cosmochimica acta*, 70, 3290–3298.
10. Pfaff, K., Hildebrandt, L. H., Leach, D. L., Jacob, D. E., & Markl, G. (2010). Formation of the Wiesloch Mississippi Valley-type Zn-Pb-Ag deposit in the extensional setting of the Upper Rhinegraben, SW Germany. Miner. Deposita, 45 (7), 647–666. https://doi. org/10.1007/s00126-010-0296-5.

11. Marchev, P., & Moritz, R. (2006). Isotopic composition of Sr and Pb in the Central Rhodopean ore fields: inferences for the genesis of the base-metal deposits. Geologica Balcanica, 35 (3–4), 49–61.

12. Valenza, K., Moritz, R., Mouttaqi, A., Fontignie, D., & Sharp, Z. (2000). Vein and karst barite deposits in the western Jebilet of Morocco: fluid inclusion and isotope (S, O, Sr) evidence for regional fluid mixing related to Central Atlantic rifting. Economic Geology, 95 (3), 587–606.

13. Okay, A. I. (2008). Geology of Turkey: A Synopsis. Anschnitt 21, 19–42.

14. Ayhan, A. (1986). The properties of barite occurences in the Lower-Middle Cambrian sedimentary sequences around Huyuk (Konya). Selçuk University Engineering Faculty Bulletin. 1, 20–45.

15. Ayhan, A. (2001). Stratiform Barite Deposits between Şarkikaraagaç (Isparta) and Hüyük (Konya) in Sultandag Region, Turkey. Chemie der Erde Geochemistry, 61, 54–66.

16. Çopuroğlu, İ. (1994). Mineralogical-petrographical and genetic exploration of Karalar- Gazipaşa (Antalya) galenite-barite deposit. Bullet. Min. Res. Explor. 116, 29–36

17. Cengiz, O., & Kuşçu, M. (2002). Geochemical properties and the source of barite deposits between Şarkikaraağaç (Isparta) and Hüyük (Konya). Bulletin of The Mineral Research and Exploration, 123–124, 67–89.

18. Cengiz, O., Uçurum, A., & Muchez, P. (2008). Determination of the source of Sarkikaraagaç (Isparta), Hüyük, Beyşehir (Konya) ve Gazipasa (Antalya) barite deposits by fluid inclusion and S, O, C, Sr ve Pb isotope studies. The Final Report of TUBITAK Project 104Y032, p. 211.

19. Elmas, N., Kumral, M., Suner, F., & Taşdelen, S. (2012). Stratiform barite deposits hosted in metamorphic assemblages of Dinek and surrounding regions, Isparta, Turkey. *Journal of Asian Earth Sciences*, 48, 150–159.

20. Cansu, Z., & Öztürk, H. (2020). Formation and genesis of Paleozoic sediment-hosted barite deposits in Turkey. Ore Geology Reviews, 125, 103700.

21. Şengör, A. M. C., & Yılmaz, Y. (1981). Tethyan evolution of Turkey, a plate tectonic approach. Tectonophysics 75, 181–241.

22. Robertson, A. H. F., & Dixon, J. E. (1984). Introduction: aspects of the geological evolution of the Eastern Mediterranean. In: Dixon JE, Robertson AHF (eds) The Geological Evolution of the Eastern Mediterranean, Geol Soc London, Spec Publ 17:1–74.

23. Yılmaz, Y., Gürpınar, O., Kozlu, H., Gül, M. A., Yiğitbaş, E., Yıldırım, M., Genç, C., & Keskin, M. (1987). Maraş kuzeyinin jeolojisi (Andırın- Berit-Engizek-Nurhak-Binboğa Dağları) yapı ve jeolojik evrimi. İstanbul Üniversitesi, Mühendislik Fakültesi.

24. De Righi, M. R., & Cortesini, A. (1964). Gravity tectonics in foothills structure belt of southeast Turkey. *AAPG Bulletin*, *48*(12), 1911-1937.

25. Gül, M. A. (2000). Kahramanmaraş Yöresinin Jeolojisi. Hacettepe Üniversitesi, Fen Bilimleri Enstitüsü, Doktora Tezi, 304 s.

26. Gözübol, A. M. & Gürpınar, O. (1980). Kahramanmaraş Kuzeyinin Jeolojisi ve Tektonik Evrimi. Türkiye 5. Petrol Kong., Jeoloji-Jeofizik Bild., s. 21-29, Ankara.

27. Gül, M.A. (1987). Kahramanmaraş Yöresinin Jeolojisi ve Petrol Olanakları. T.P.A.O. Rap. No: 2359, (Yayınlanmamış), Ankara.

28. Yılmaz, Y. & Yiğitbaş, E. (1990). SE Anadolu'nun Farklı Ofiyolitik Metamorfik Birlikleri ve Bunların Jeolojik Evrimdeki Rolü Türkiye 8. Petrol Kong. Bild. s. 128-140, Ankara.

29. Blumenthal, M. M. (1947). Geologie der Taurusketten im Hinterland von Seydişehir und Beyşehir, M. T. A., Ankara.

30. Dean, W. T., & Monod, O. (1990). Revised stratigraphy and relationships of Lower Palaeozoic rocks, eastern Taurus Mountains, south central Turkey. *Geological Magazine*, *127*(4), 333-347.

31. Yoldemir, O. (1987). Suvarlı-Haydarlı-Narlı-Gaziantep Arasında Kalan Alanın Jeolojisi ve Petrol Olanakları. T.P.A.O. Rap. No: 2275, Ankara (yayınlanmamış).

32. Ulu, U., Genç, Ş., Giray, S., Metin, Y., Çörekçioğlu, E., Örçen, S., Ercan, T., Yaşar, T. & Karabıyıkoğlu, M., (1991). Belveren-Araban-Yavuzeli-Nizip-Birecik Alanının Jeolojisi, Senozoyik Yaşlı Volkanik Kayaçların Petrolojisi ve Bölgesel Yayılımı. M.T.A. Enst. Derleme Rap. No: 9226 (Yayınlanmamış), Ankara.

33. Robertson, A. H. F. & Dixon, J. E. (1984). Introduction: aspects of the geological evolution of the Eastern Mediterranean. In: Dixon JE, Robertson AHF (eds) The Geological Evolution of the Eastern Mediterranean, Geol Soc London, Spec Publ, 17:1–74.

34. Yılmaz, Y. (1993). New evidence and model on the evolution of the southeast Anatolian orogen. *Geological Society of America Bulletin*, 105:251–271.

35. Yılmaz, Y., Gürpınar, O., Kozlu, H., Gül, M. A., Yiğitbaş, E., Yıldırım, M., Genç, C. & Keskin, M. (1987). Maraş kuzeyinin jeolojisi (Andırın- Berit-Engizek-Nurhak-Binboğa Dağları) yapı ve jeolojik evrimi. İstanbul Üniversitesi, Mühendislik Fakültesi.

36. Yılmaz, Y., Yiğitbaş, E., Gürpınar, O. & Yiğitbaş, E. (1988). Amanos Dağları ve Maraş Dolaylarında Miyosen Havzalarının Tektonik Evrimi. T.P.A.O. Bülteni C.1/1, 52-72.

37. Yiğitbaş, E. (1989). Engizek dağı (K.Maraş) dolayındaki tektonik birliklerin petrolojik incelenmesi; Doktora tezi, İstanbul Üniversitesi. Fen. Bilimleri Enstitüsü, 347 s.

38. Robertson, A. H. F., Ünlügenç, U. C., İnan, N. & Taslı, K. (2004). The Misis–Andırın Complex: a Mid Tertiary mélange related to late-stage subduction of the Southern Neotethys in S Turkey. Journal of Asian Earth Sciences, 22:413–453.
39. Herece, E. (2008). Atlas of East Anatolian Fault, General Directorate of Mineral Research and Exploration, Special Publication Series-13, 359, 13 appendices as separate maps. ISBN / ISSN: 9786054075126.
40. Clark, S. H. B., Poole, F. G., & Wang, Z. (2004). Comparison of some sediment-hosted stratiform barite deposits in China, the United States, and India. Ore Geology Reviews, 24, 85–101.
41. Jewell, P. W. (1994). Paleoredox conditions and the origin of bedded barites along the Late Devonian North American continental margin. The Journal of Geology, 102, 151–164.
42. Jewell, P. W., & Stallard, R. F. (1991). Geochemistry and paleoceanographic setting of central Nevada bedded barites. Journal of Geology, 99, 151–170.
43. Torres, M. E., Brumsack, H. J., Bohrman, G., Emeis, K. C. (1996). Barite fronts in continental margin sediments: a new look at barium remobilization in the zone of sulphate reduction and formation of heavy barites in diagenetic fronts. Chemical Geology, 127, 125–139.
44. Binns, R. A., Parr, J. M., Gemmell, J. B., Whitford, D. J., & Dean, J. A. (1997). Precious metals in barite-silica chimneys from Franklin Seamount, Woodlark Basin, Papua New Guinea. Marine Geology 142, 119–141.
45. Leach, D. L., Bradley, D. C., Huston, D., Pisarevsky, S. A., Taylor, R. D., & Gardoll, S. J. (2010). Sediment-hosted lead-zinc deposits in Earth history. Economic Geology, 105, 593–625.
46. Sverjensky, D. A. (1986). Genesis of Mississippi Valley-type lead-zinc deposits. Annual Review of Earth and Planetary Sciences, 14, 177–199.
47. Ravenhurst, C. E., Reynolds, P. H., Zentilli, M., Kreuger, H. W., & Blenkinsop, J. (1989). Formation of Carboniferous Pb-Zn and barite mineralisation from basin-derived fluids, Nova Scotia, Canada. Economic Geology, 84, 1471–1488.
48. Williams-Jones, A. E., Schrijver, K., Doig, R., & Sangster, D. F. (1992). A model for epigenetic BaPb-Zn mineralization in the Appalachian thrust belt, Quebec: evidence from fluid inclusions and isotopes. Economic Geology, 87, 154–174.
49. Özdoğan, A. T., Uras, Y. & Öner, F. (2017). Geochemistry of the barite deposits near Adana-Feke area (Eastern Taurides). Russian Geology and Geophysics, 58, 1351–1367.
50. Yalçın, C. (2022). Preliminary Datas of Carbonate-rock hosted barite Mineralization in Dadağlı (Kahramanmaraş) area, Turkey. *Advanced Engineering Days (AED)*, *2*, 33-35.

Investigation of seismic base isolation systems and their properties

Erden Ozan Karaca *1 [iD]**, Muhammed Tanyıldızı** 1 [iD]**, Nusret Bozkurt** 1 [iD]

1 *Bitlis Eren University, Engineering and Architecture Faculty, Civil Engineering Department, Türkiye, eokaraca@beu.edu.tr; mtanyildizi@beu.edu.tr; nbozkurt@beu.edu.tr*

Abstract
The use of various seismic isolators instead of changing the dimensions of the structural elements is an increasingly common practice in the design of buildings against earthquakes. The differences in soil properties, inadequacy in inspections and workmanship errors negatively affect the earthquake performance of the structures. Similarly, the complexity of earthquake forces that cannot be formulated adequately makes structural engineering solutions difficult. All these factors can be counted as the reasons that make the insulators, which enable the structure to make different displacements from the ground, stand out as a solution tool. In this study, the types and properties of seismic base isolation systems were investigated.

1. Introduction

Earthquakes are a natural disaster that does not show any symptoms before and can cause great loss of life and property due to the lack of an early warning system [1]. Alpid Belt, one of the two important earthquake belts in the world; It extends from Spain, Italy and Greece to Northern India and Afghanistan, and Turkey is located in the so-called Mediterranean Earthquake Belt on this belt. There are two major fault zones in Turkey, 92% of which is on this seismic belt. These are East Anatolian and North Anatolian faults. Turkey can be divided into the following four seismotechnical regions [2];

1. North Anatolian Fault Zone
2. East Anatolian Fault Zone
3. Bitlis Thrust Zone and East Anatolian Compression Zone
4. Aegean (Western Anatolia) Grabens Zone.

The fact that most of the existing building stock in Turkey is not built-in accordance with the current earthquake regulations, workmanship-material defects, the inhomogeneity of the soil properties and the lack of public awareness about earthquakes increase the loss of life and property in earthquakes. Reasons such as increasing urban population, unplanned construction considering today's facilities and technology, it is not acceptable to experience loss of life in a possible earthquake. This situation causes the concept of earthquake resistant building design to gain importance. Contemporary regulations prepared to meet current needs allow for quality building design and production, and our latest earthquake regulation [3] which came into force in 2018, is a good example of this. However, the fact that the earthquake has a complex structure limits its deterministic features to be used in engineering solutions. For this reason, it is necessary to use approximate data in engineering calculations and to stay on the safe side at the highest degree in proportion to these. This undoubtedly increases the cost. Earthquake resistant building design can be roughly summarized for two purposes and these are; The structure is of sufficient quality and the cross-sectional forces that will occur during the earthquake are calculated

in such a way that they can be met at a sufficient rate [4]. In the traditional design approach; It is expected that the seismic energy coming into the structure will be damped by the inelastic deformations that the structure will exhibit before it collapses. It is expected that the structure designed for this purpose will be damaged at a level that can be repaired in a moderate earthquake, and that collapses that will cause loss of life in a severe earthquake will not occur [5]. In summary, the traditional approach aims to meet the seismic loads that will affect the structure with damage that will occur at a level that will not collapse. Increasing the rigidity of the structure for less damage; It will also increase the earthquake forces that will affect it. This situation creates the need for a different way to design earthquake resistant structures. Today, this need has been met by means of special elements that absorb the energy that affects the structure in the event of an earthquake. The techniques for protecting the structure from seismic loads acting on it can be divided into active and passive protection systems. Active control methods, in general terms, are systems in which an energy source is used to keep the displacement of the structure at the desired level. Passive control methods mentioned above; It provides the energy acting on the structure with special elements that absorb and absorb it [6]. In this study, seismic isolation systems, which are one of the passive protection methods, are emphasized and an example image of them is presented in Figure 1 [7].
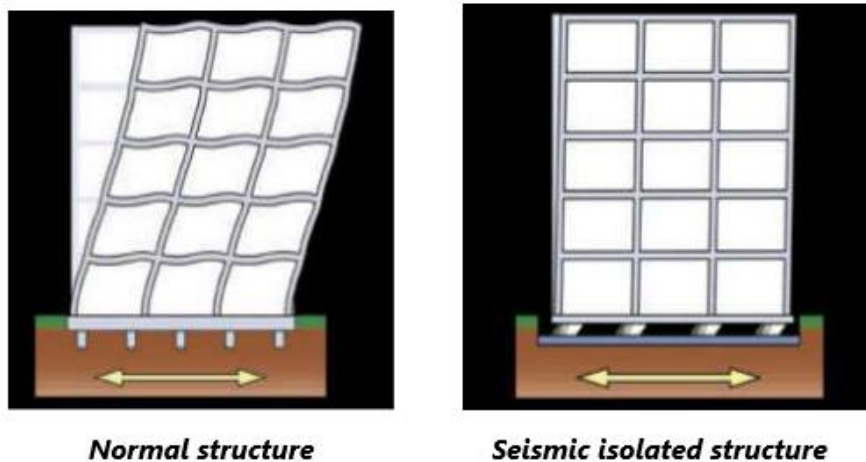
Figure 1. Behavior of normal and seismically isolated structures during an earthquake

Protecting from the devastating effects of earthquakes has been a problem that all civilizations established in earthquake regions wanted to solve, and they sought a solution to this issue. The seismic isolation provided by today's special elements has tried to be applied in different ways in historical buildings. Considering that the working principle of the seismic isolator in the building is to roughly separate the ground and the building, reducing the effect of the shaking on the building, it is possible to see an application in this logic in the Dikili Taş monument in Istanbul (Figure 2). The granite stones under the pedestal can be considered as a historical isolation system made in order to reduce the shaking that will occur on the monument during earthquake shaking [8]. Today, in parallel with the development of the properties of insulators, the number of structures using isolators against earthquakes is increasing rapidly. If the advantages of seismic isolators are examined; minimizing the damage to the structure, protecting the goods-equipment inside the building and reducing the relative floor acceleration. Also, as disadvantages; high cost, the presence of nearby buildings, and the difficulties encountered in the design of water and natural gas installations in a structure where insulators are used [9].
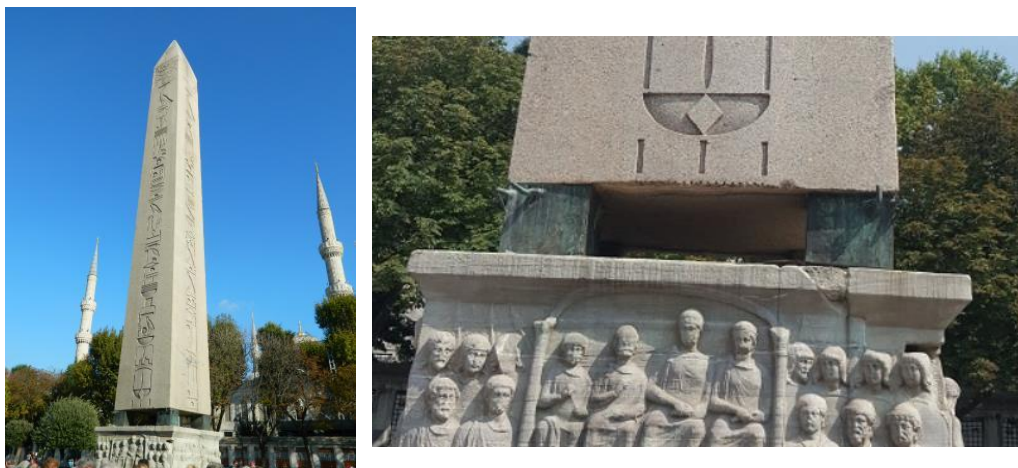
Figure 2. Dikili Taş monument, İstanbul

Element sizes are enlarged in order to increase the rigidity of the structure in earthquake resistant structure design. This reduces the ductility of the structure and causes it to exhibit an inelastic behavior. A structure with low ductility makes sudden and rapid displacements during an earthquake. It is not desirable for the building to behave in this way. Seismic isolators used as a solution; they are elements with low lateral rigidity used between the structure and the ground and increase the natural period of the structure. By keeping the rigidity of the structural elements small, the vibration period can be brought to the desired range. As a result, earthquake effects are reduced. For this purpose, the dominant period of the region and the natural period of the structure are kept away from each other in order to avoid the resonance phenomenon. This applies, for example, to the construction of short-term and low-rise structures in areas with hard floors and long periods. The seismic isolation tools to be used will change the dynamic behavior of the structure and reduce the force acting (Figure 3).
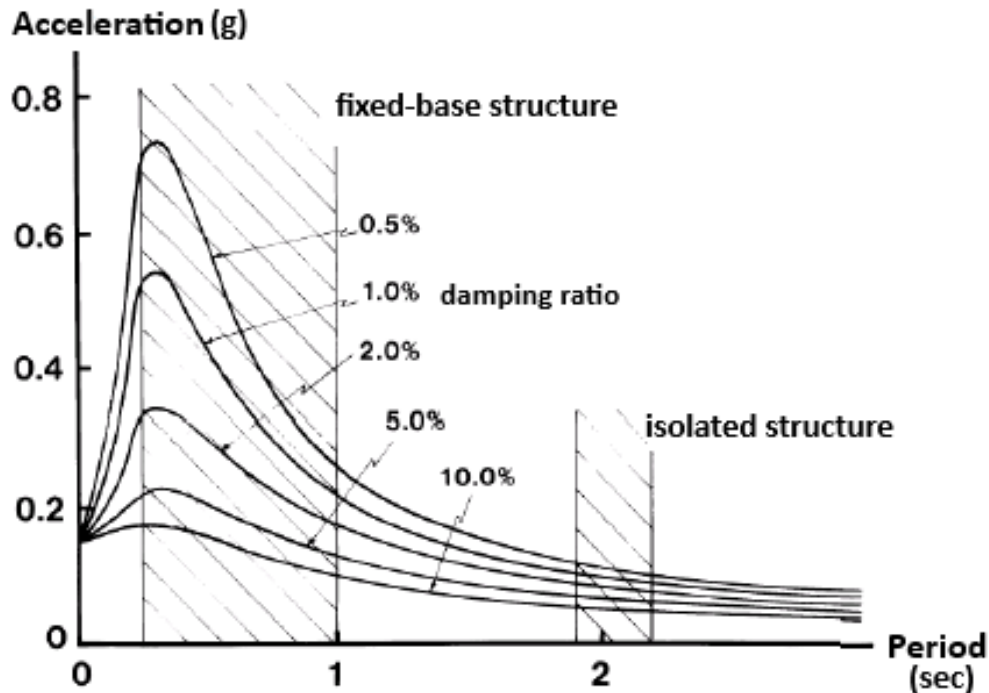
Figure 3. Changing the acceleration and damping values by increasing the period in structures

2. Types of seismic isolation

Classification can be made by considering the shapes, places of use, sizes, materials used in their production and working mechanisms of the insulators. Among these titles, French electric institution systems, EERC combined systems and TASS systems can also be analyzed as rubber-slippery systems. However, in this study, it has been grouped on the basis of slip, taking into account the working principles. Seismic isolators can generally be grouped under three headings [10]. These;

1) Elastomeric base isolation tools,
    1. Low damping natural and artificial rubber insulators
    2. Lead core rubber insulators
    3. High damping rubber insulators
2) Insulation tools designed on slip
    1. Friction pendulum systems
    2. Flexible-friction base insulation systems
    3. French Electric Institution systems (Neoprene insulators with steel plate layer)
    4. EERC unified systems
    5. TASS systems
3) Spring type systems
    1. The GERB systems

2.1. Elastomeric base isolation tools

It is the most commonly used seismic isolation type among seismic isolation systems. It is produced by bonding a steel plate with a thickness of 2-3 mm and a rubber of 8-20 mm with the effect of high temperature and pressure. It was applied for the first time in 1969, but since steel plates were not used in the application, the rubber part

swelled laterally and the desired rigidity could not be achieved. During an earthquake, the structure can move upwards while making lateral displacement. The steel plates used in the production of these insulators increase the vertical rigidity of the structure. It also acts as a preventative for lateral buckling. The lateral load damping acting on the structure is related to the lateral displacement capability of the structure. This feature can be provided with an elastomeric insulator. The insulator is mounted to the structure with the steel cap parts on the top and bottom. Due to its material properties, it requires minimum maintenance. They have a long service life, but their production costs are high. Ensuring continuous production will reduce its high cost. As a material, it does not creep and is long-lasting. It does not lose its elastic properties at temperatures between -17 and 82 ℃. Production and modeling stages are easy [11, 12].
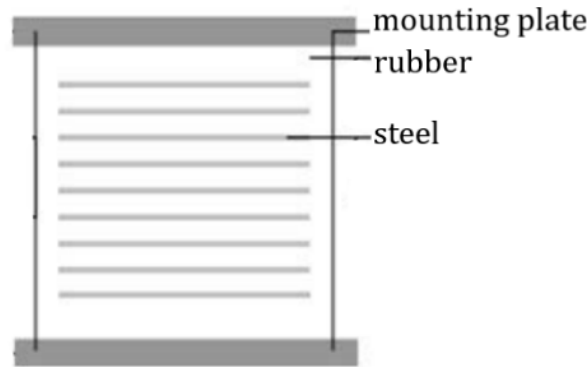
Figure 4. Elastomer insulator cross section

2.1.1. Low damping natural and artificial rubber insulators

It is a type of insulator consisting of combining a large number of sheet metal and rubber between steel heads with the effect of pressure and heat. The horizontal rigidity depends on the thickness and number of the rubber part. The desired rigidity can be achieved by changing these values. However, since the increase in the height of the insulator may cause buckling, the maximum height value is limited to half the diameter. As a material, it does not creep and is long-lasting. It does not lose its elastic properties at temperatures between -17 and 82 ℃. Production and modeling stages are easy. It shows linear elastic behavior against shear stress. The disadvantage of this isolator type is that it needs additional damper due to its low damping. The visual and force displacement behavior of this type of insulator is presented in Figure 5 [10, 11].
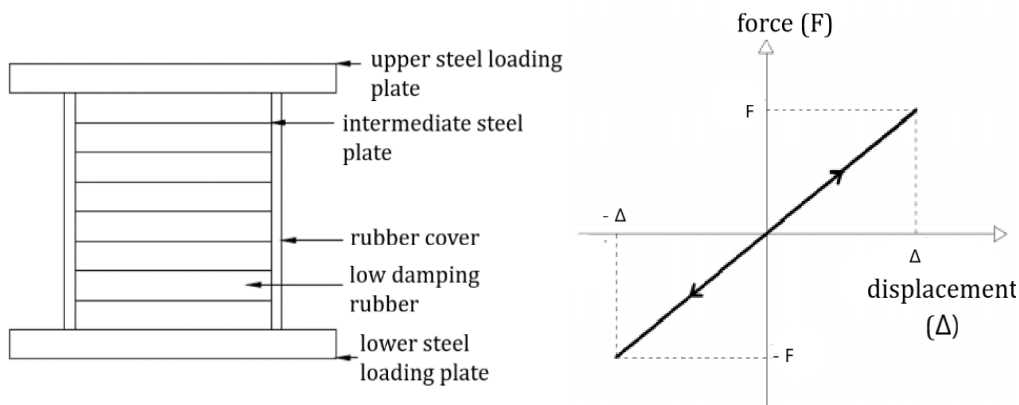
Figure 5. Cross section of low damping rubber insulator and force-displacement graph

2.1.2. Lead core rubber insulators

It is formed by placing a lead core in the center of low damping rubber insulators in order to increase the damping rate. The damping rate of this elastomer insulator type is 15-35%. After its first production in 1975, it has been widely applied in countries such as the USA and Japan. The energy absorption capacity of the lead core reduces the horizontal displacement of the insulator. The lead core used provides damping and rubber provides a stabilizing feature. Combined use of rubber and lead core; by using the stored elongation energy during the earthquake, it provides a force that returns the structure to its initial conditions after the earthquake. Lead core

rubber headstock; since it is a composite combination of lead and core, there is a behavior pattern that is characteristic of both materials. The lead core increases the rigidity of the elastomer insulator. Lead-core rubber under low load shows rigid behavior both horizontally and vertically. Layers of steel plates surround the lead core externally and force it to deform under shear stress. The yield strength of the lead core is 10 MPa. When the lead reaches its yield strength, the horizontal stiffness is significantly reduced. Damping by plastic deformation of the lead is modeled by a hysterical cycle. The inability to test the central lead core after strain can be considered as the most important disadvantage of this insulator type [11-14].
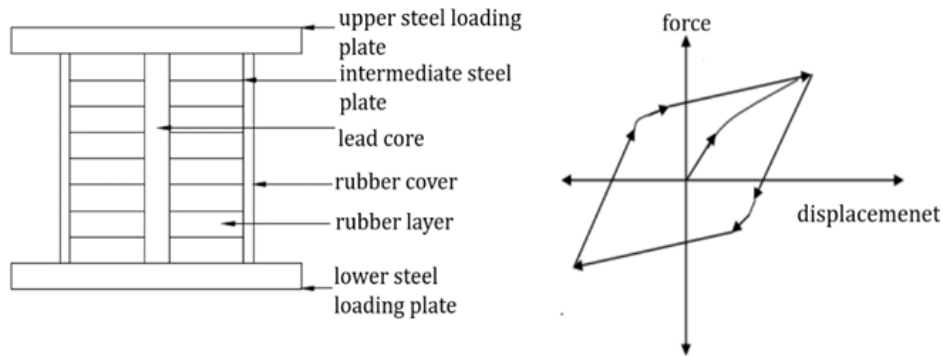
Figure 6. Cross section of lead core rubber insulator and force-displacement graph

2.1.3. High damping rubber insulators

It is an elastomer insulator type in which damping rate is increased to 8%-15% by adding special materials such as carbon and resin to low damping rubber, which has a damping rate of around 2%. The support cross-section and the bonding method of the layers are the same as for the low damping rubber insulators. High damping rubber type insulators, based on the idea of eliminating the need for additional dampers; it was first developed by MRPA, a British institution, in 1982. Highly damped rubbers exhibit nonlinear behavior at shear strains of up to 20% and are modeled with a smooth elliptical hysteresis curve [11-14].
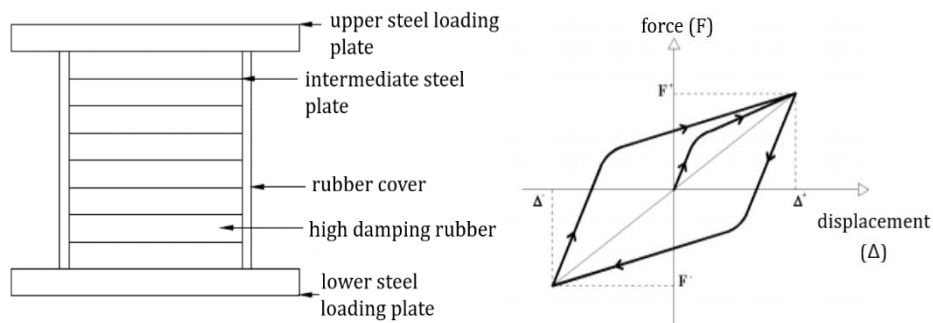
Figure 7. Cross section of high damping rubber insulator and force-displacement graph

2.2. Insulation tools designed on slip

These systems, which are based on slip as their working principle, are the oldest and simplest isolation systems. The first system based only on gliding was made by a medical doctor in 1909 in England. If the working principle is examined, there is a limitation of the shear force at the insulator interface in general. The shear force acting on the structure from the ground depends on the coefficient of the friction force, not the magnitude of the earthquake. If the materials used in the production of this type of insulator are examined, these are; It is polytetrafluoroethylene (teflon) coated on stainless steel [10].

2.2.1. Friction pendulum systems

Friction pendulum systems were first developed in 1987 for use in seismic isolation applications. If the working mechanism is examined, there is an articulated slide that moves on a spherical surface made of a stainless steel. This articulated slide absorbs the energy coming from the friction force resulting from its movement. The theory of this type of insulator is based on the Coulomb Friction Principle. Temperature, speed and cleanliness of the surface greatly affect the friction characteristics of the insulator.

Friction pendulum type insulators; they are slip-based systems that combine shear and return forces thanks to their spherical surface. The mass carried by this movement of the slider both rises and creates the return force. Here is the period of the insulator; although it is independent of mass, it depends on the radius of the spherical surface. The earthquake force acting during the earthquake is damped by the pendulum movement. The period of a simple pendulum can be calculated by the formula.

$$T = 2\pi \sqrt{\frac{R}{g}}$$

R in the formula; is the radius of curvature and g is the gravitational acceleration.

The diameter of the protective cylinder in this type of insulator; It is determined according to the largest displacement value that will occur due to the earthquake effect. Such a limitation provides safety in cases where the displacement value at the time of the earthquake used in the calculation is exceeded. In addition, this protective roller protects the inner surface from environmental pollution that affects the friction value. The force-displacement curve of friction pendulum type insulators is presented below [15, 16].
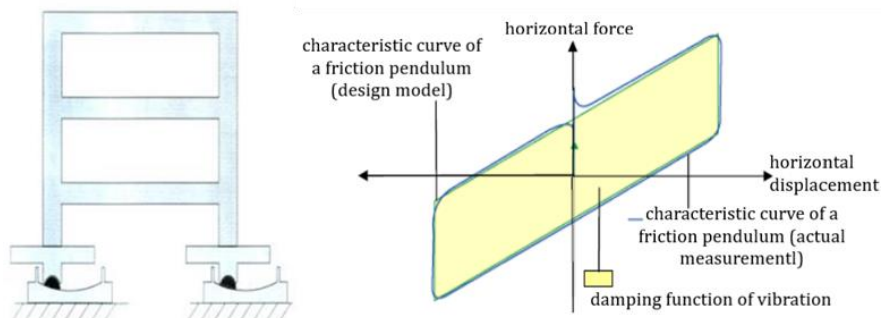
Figure 8. Cross section of friction pendulum system and force-displacement graph

2.2.2. Flexible-friction base insulation systems

It is a type of slip-based insulator with concentric and circular plates in contact with each other and a rubber core in the center. Since there is no force to return the sliding systems to the starting position, the studies have shifted to this type of insulator. Friction plates have been added to the system in order to make larger displacements to the insulator and to limit the shear stresses that will occur in the rubber core. Thanks to this layered structure, the velocity values affecting the lower and upper ends of the insulator are divided by the number of layers. Thus, the friction coefficient decreases as the speed of each layer will be lower than the total speed of the system. The rubber core in the center is used to have a reversing effect. There is a steel bar in the center of the rubber core to prevent the displacements to tag from concentrating in one spot. This type of insulators can be used in asymmetrical structures as they coincide with the centers of rigidity and mass. In addition, as long as the load acting on the system does not exceed the friction force, there will be no movement. Thus, low-impact lateral loads such as wind do not cause problems [12].
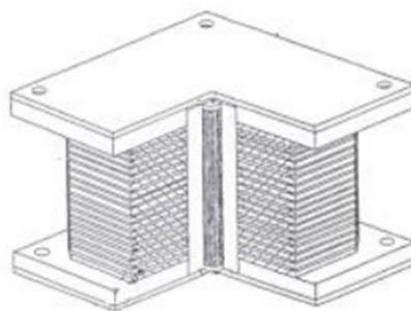
Figure 9. Flexible-friction base insulator

2.2.3. French electric institution systems (Neoprene insulators with steel plate layer)

This type of insulator, which was applied at the Koeberg Nuclear Power Plant in South Africa, was developed in the early 1970s with the support of the French Electricity Authority. Its design is achieved by placing an isolation system between two raft plates. In this system, there are steel and neoprene plates combined with a lead-bronze alloy. The sliding surface is formed between the lead-bronze alloy and the stainless-steel surface. The purpose of

the friction plates is to keep the horizontal acceleration below 0,2 g. Neoprene insulator has a very low displacement capacity (+-5 cm). When the displacement exceeds this limit, the sliding element provides the necessary movement. However, since there is no reversing mechanism in the system, permanent displacements may occur [10, 11].
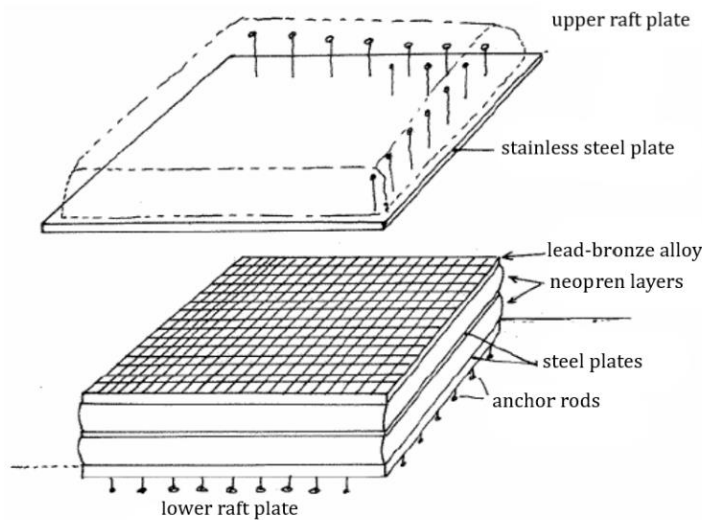

Figure 10. Cross section of neoprene insulators with steel plate layer

2.2.4. EERC unified systems

Carrying the inner columns of the building system with Teflon on the sliding elements and the outer columns with a low damping rubber support; it is an insulator type, which is a combination of sliding and elastomer bearings. The rubber part of the system ensures the re-centering of the structure after the movement, and the sliding part provides the absorption of the energy. The rubber support also controls the torsional behavior of the system. The EERC system has been used in the US at the University of Nevada Mackay School and retrofitting a hospital building [10, 11].

2.2.5. TASS systems

They are insulation systems developed by a Japanese company, in which the vertical load is carried by elements consisting of Teflon-stainless steel. The system consists of neoprene layers in addition to teflon and stainless steel. These layers do not carry vertical loads, but they provide a restoring effect to the system. The design of the system is made by taking a friction coefficient of 0.05 under 10 MPa pressure. Since the elastomer support has no vertical load carrying capacity, the system is exposed to tensile stresses. In addition, this type of system is difficult to model because the sliding surface is sensitive to low frictional velocities [17].

2.3. Spring type systems

2.3.1. The GERB systems

These systems, which are based on elastomeric and slip, are generally used to provide insulation in the horizontal direction. If there is a need for three-dimensional insulation, it is possible, but not common, to use elastomeric insulators. In such cases, it is more appropriate to use spring type systems. Developed by GERB Company in Germany for nuclear power plant turbines, this system consists of large coil springs with the ability to stretch horizontally and vertically. The vertical frequency is about 5 times the horizontal frequency. Since these springs have no damping effect, additional viscous dampers are used. With these additional dampers, approximately 30% critical damping occurs in the spring system. This type of system is suitable for structures such as nuclear reactors in nuclear power plants where the center of gravity and the center of rigidity are at the same level.
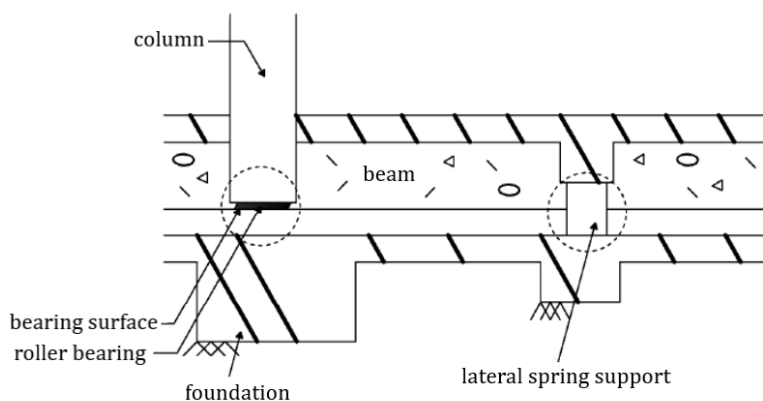
Figure 11. TASS system cross section

3. Conclusion

Minimizing the damage to the structure against earthquake effects is an important issue in the field of structural engineering. With the help of today's advanced technology, the use of insulators related to this subject has been developed and started to be applied. The use of seismic isolators, especially in special structures such as bridges and hospitals, which reduce the damage to the structure during an earthquake and which should be used during and immediately after the earthquake, is an effective solution that is becoming increasingly common.

Author contributions:

Erden Ozan Karaca: Conceptualization, Methodology, Software **Muhammed Tanyıldızı:** Data curation, Writing-Original draft preparation, Software, Validation. **Nusret Bozkurt:** Visualization, Investigation, Writing-Reviewing and Editing.

Conflicts of interest

The authors declare no conflicts of interest.

References

1. Celep, Z. (2019). Introduction to Earthquake Engineering. Istanbul: Beta Publishing and Distribution Inc.
2. Tolay, A. (2006). Cost Analysis of Seismic Isolation Systems. Istanbul: Yıldız Technical University, Graduate School of Science, Master's Thesis.
3. TBDY (2018). Turkey Building Earthquake Code. Official Newspaper.
4. Gösedag, P. B. (2002). Seismic Isolation in Structures. Istanbul: Yıldız Technical University, Graduate School of Sciences, Master's Thesis.
5. Gökhan, E. (2009). The Effects of the Use of Insulators on the Behavior of the Structural System in Reinforced Concrete Structures. Istanbul: Istanbul Technical University, Institute of Science, Master's Thesis.
6. Özpalalar, C. G. (2004). Seismic Isolation and Energy Absorbers In Earthquake Resistant Building Design. Istanbul: Istanbul Technical University, Institute of Science, Master's Thesis.
7. Erseker, B. (2017). The Effect of Earthquake Impact Angle on Maximum Insulator Displacements in Lead Core Rubber Insulators. Eskişehir: Anadolu University, Graduate School of Sciences, Master's Thesis.
8. https://www.emke.com.tr/sismik-izolasyon-nedir-sismik-izolator-utilimi-deprem-izolasyon/
9. https://insapedia.com/sismik-izolator-nedir-ne-ise-yarar-maliyeti-ve-fiyatlari/

10. Hoşbas, A. B. (2006). Modeling of Multi-Storey Reinforced Concrete Building with Seismic Isolators and Curtains. Istanbul Technical University, Institute of Science, Master's Thesis.
11. Sevim, E. (2016). The Effect of Seismic Isolators on The Dynamic Response of Buildings: Yıldız Technical University, Institute of Science, Master's Thesis.
12. Baştuğ, B. K. (2004). Using Seismic Isolators Against Earthquakes in Building Systems. Yıldız Technical University, Institute of Science, Master's Thesis.
13. Türk, H. A. (2019). The Effect of Different Seismic Isolator Systems and Floor Number to Earthquake Behavior on Multi-Storey Reinforced Concrete Structures. Konya Technical University, Institute of Science, Master's Thesis.
14. Yücesoy, A. (2005). Design of Eartquake Resistant Structure with Seismic Base Isolation. Mustafa Kemal University, Institute of Science, Master's Thesis.
15. Çamgöz, Ç. (2002). Base Isolation Systems. Istanbul Technical University, Institute of Science, Master's Thesis.
16. Murat, E. (2007). Seismic Isolation Application by Placing Elastomer Bearings on the Bases of Buildings. Istanbul Technical University, Institute of Science, Master's Thesis.
17. Toprak, T. (2012). The Effect of Using Seismic Isolation to Behavior of Structures with Torsional Irregularity under Earthquake Loads. Istanbul Technical University, Institute of Science, Master's Thesis
18. Karaca, E. O., Tanyıldızı, M., & Bozkurt, N. (2022). A study of seismic isolators used in buildings and their properties. *Advanced Engineering Days (AED)*, *2*, 59-61.

24V input 12V and 36V output buck-boost converter design

Muslime Altun*[1], **Mehmet Rida Tur [2]**, **Fevzi Çakmak[3]**

[1] Batman University, Energy Coordination Center, Batman, Türkiye, muslime.altun@batman.edu.tr
[3] Batman University, Department of Electrical & Energy Engineering, Batman, Türkiye, mrida.tur@batman.edu.tr
[3] Mardin Artuklu University, Midyat Vocational School, Mardin, Türkiye, fcakmak72@hotmail.com

Abstract
In this modern era of electronic technologies, all the appliances require a separate power supply. To overcome this drawback, the concept of a single converter with multiple power supply has been proposed. Furthermore, the proposed research work clarifies about multipurpose charger, which alters and uses a boost topology to supply different outputs as required for different applications. Proposed method consists of multiple PWM duty cycles to produce multiple regulated power supply voltages, and so it is also referred as multi power boost converter. It uses one converter for obtaining various outputs. For example, mobile, laptop, electric vehicle, or any other electronic appliances can be charged using multi power boost converter.

1. Introduction

Nowadays, most of DC power supply uses are needed in electronic devices. This utilization is required in order to be able to convert DC voltages from certain voltage to desired voltage. Buck-boost converter is a type of switching converter that is able to produce voltage levels greater or smaller than the input voltage. Voltage regulation is carried out by adjusting the duty cycle of Pulse Width Modulation (PWM) [1]. Buck-boost converters are widely used in alternative and renewable energy power plants, portable devices and industrial installations [2]. On the other hand, buck boost converter is capable of producing an output voltage higher/lower than the input voltage and has the ability to generate both steps up and steps down output voltage [3]. Generally a buck converter operates in two conduction mode namely continuous and discontinuous conduction mode whereas, a buck boost converter can be operated either in buck converter mode or boost converter mode [6]. The solutions of buck boost converter usually have lower efficiency and a larger footprint than buck converter solutions [4]. Inductor's reluctance to allow rapid change in current is used to best understand the operation of a buck boost converter [8].

In an electronic circuit, buck converters are commonly used to get the required output voltage from a higher voltage source [9]. Sometimes, may be required negative voltage from a positive input voltage source. The audio amplifiers, line drivers and receivers, or instrumentation amplifiers can include by these applications [7].

2. Material and Method

2.1. Buck-Boost Transducer Design, Modeling and Control

Switched power supplies are widely used today, especially in electric vehicles, renewable energy systems, computers, televisions, mobile phones and many electrical household appliances. The advantage of switch-mode power supplies over other conventional power supplies is that they are quite light, smaller and therefore take up less space.

Dc-dc converters are structures that are used to transform the unregulated or the regulated voltage at the output of a rectifier, battery or solar cell. Buck-boost converter can generally be in two different structures as isolated and non-isolated. However, non-insulated structure is more widely used. The output voltage value of the buck-boost converter can be greater or less than the input voltage value depending on the value of the duty period. In addition, the polarity of the output voltage is opposite to the polarity of the input voltage [5].

2.2. Buck-Boost Converter

The buck–boost converter is a type of DC-to-DC converter that has an output voltage magnitude that is either greater than or less than the input voltage magnitude. It is equivalent to a flyback converter using a single inductor instead of a transformer [4]. Two different topologies are called buck–boost converter. Both of them can produce a range of output voltages, ranging from much larger (in absolute magnitude) than the input voltage, down to almost zero.

In the inverting topology, the output voltage is of the opposite polarity than the input. This is a switched-mode power supply with a similar circuit topology to the boost converter and the buck converter. The output voltage is adjustable based on the duty cycle of the switching transistor. One possible drawback of this converter is that the switch does not have a terminal at ground; this complicates the driving circuitry. However, this drawback is of no consequence if the power supply is isolated from the load circuit (if, for example, the supply is a battery) because the supply and diode polarity can simply be reversed. When they can be reversed, the switch can be on either the ground side or the supply side.

When a buck (step-down) converter is combined with a boost (step-up) converter, the output voltage is typically of the same polarity of the input, and can be lower or higher than the input. Such a non-inverting buck-boost converter may use a single inductor which is used for both the buck inductor mode and the boost inductor mode, using switches instead of diodes [5], sometimes called a "four-switch buck-boost converter", it may use multiple inductors but only a single switch as in the Sepic and Cuk topologies.

The circuit diagram of the buck-boost converter is shown in Figure 1.
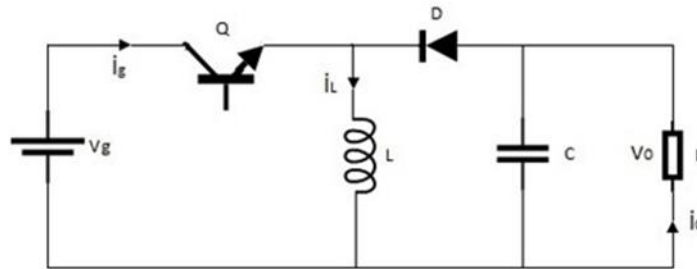
Figure 1. Buck-boost converter circuit

To analyze the buck-boost circuit, it is necessary to consider two cases where switch Q is on (Qon) and switch Q is on cut (Qoff).

If the duty period of the switch is d;

$$d = \frac{t_{on}}{t_{on} - t_{off}} - \frac{t_{on}}{T_s}$$

(1)

Here t_{on} and t_{off} are the on and off times of the switch, respectively. T_s is the switching period.
The output voltage of the converter under ideal conditions changes to;

$$V_o = \frac{d}{1-d} * V_g$$

(2)

Here, the duty period d varies in the range of 0-1. Different output voltage values can be obtained for different d values. Output voltage; If d<0.5 it becomes buck (reducer), if d>0.5 it becomes boost. The current is also intermittent, as the output of the Buck-Boost converter is a bit too fluctuating.

Like the buck and boost converters, the operation of the buck-boost is best understood in terms of the inductor's "reluctance" to allow rapid change in current. From the initial state in which nothing is charged and the switch is open, the current through the inductor is zero. When the switch is first closed, the blocking diode prevents current from flowing into the right hand side of the circuit, so it must all flow through the inductor. However, since the inductor doesn't allow rapid current change, it will initially keep the current low by dropping most of the voltage provided by the source.

Over time, the inductor will allow the current too slowly increase by decreasing its own resistance. In an ideal circuit the voltage drop across the inductor would remain constant. When the inherent resistance of wires and

the switch is taken into account then the voltage drop across the inductor will also decrease as the current increases. Also during this time, the inductor will store energy in the form of a magnetic field.
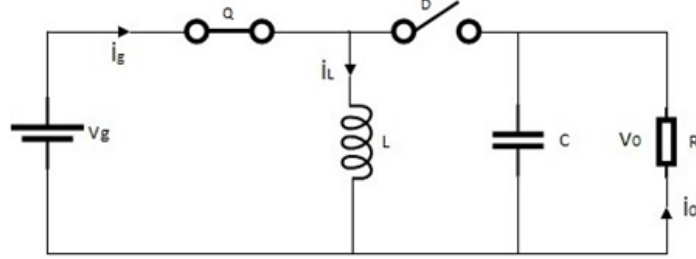

Figure 2. On state of the Q switch in transmission the buck-boost converter circuit

While the switch is transmitting (Qon), the situation in Figure 2 will occur. In this case, switch Q is on, and diode D is off because it is subject to reverse voltage. The input source current flows incrementally through the Q switch and the inductance.

In this case;

$$\frac{di_L}{d_t} = \frac{V_g}{L} \tag{3}$$

$$\frac{dV_C}{d_t} = -\frac{V_o}{RC} \tag{4}$$

When the switch is in cut (Qoff), the situation in Figure 3 will occur. In this case, the Q switch is in cut. The current flowing through the inductance flows through C, D and the load. The energy stored in the inductance is transferred to the load in this way.
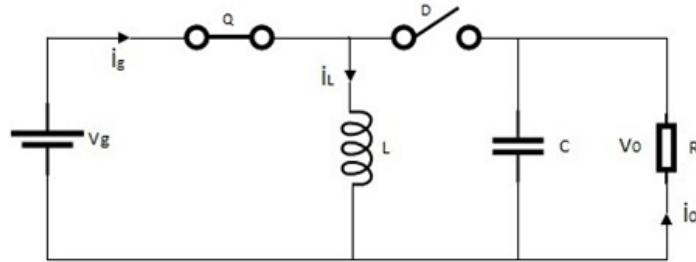
Figure 3. On state of the Q switch in cut the buck-boost converter circuit

In this case;

$$\frac{di_L}{d_t} = \frac{V_C}{L} \tag{5}$$

$$\frac{dV_C}{d_t} = -\frac{I_L}{C} - \frac{V_o}{RC} \tag{6}$$

If the equations (2-5) are combined by considering the duty period, the following equations can be obtained.

$$\frac{di_L}{d_t} = \frac{V_g}{L} \cdot d + \frac{V_C}{L} \cdot (1-d) \tag{7}$$

$$\frac{dV_C}{d_t} = -(1-d)\frac{I_L}{C} - \frac{V_C}{RC} \tag{8}$$

2.3. Proteus Model of Buck-Boost Converter

In this paper, a boost–buck-type dc–dc converter is proposed as the first stage with regulated output inductor current, and a full-bridge unfolding circuit with 50- or 60-Hz line frequency is applied to the dc–ac sage, which will unfold the rectified sinusoid current regulated by the dc–ac stage into a pure sinusoidal current, as shown in Figure 2. Since the circuit runs either in boost or buck mode, its first stage can be very efficient if the low conduction voltage drop power MOSFET and ultrafast reverse recovery diode are used. for the second stage, because the unfolding circuit only operates at the line frequency and switches at zero voltage and current, the switching loss can be omitted. The only loss is due to the conduction voltage drop, which can be minimized with the use of low on-drop power devices, such as thyristor or slow-speed insulated gate bipolar transistor (IGBT). in this version, IGBT is used in the unfolding circuit because it can be easily turned ON and OFF with gating control. Since only the boost dc–dc converter or buck dc–dc converter operates with high-frequency switching all the time in the proposed system, the efficiency is improved. Also, because there is only one high-frequency power processing stage in this complete PCS, the reliability can be greatly enhanced [11]. Finally, after analyzing its model, as shown in Figure 3, an interleaved-boost-cascaded-with-buck converter is proposed to increase the resonant pole frequency by the use of a smaller boost inductor value, which improves both control and stability.

Equations in equality (7) and (8) are modeled as in Figure 4 using the Proteus program.
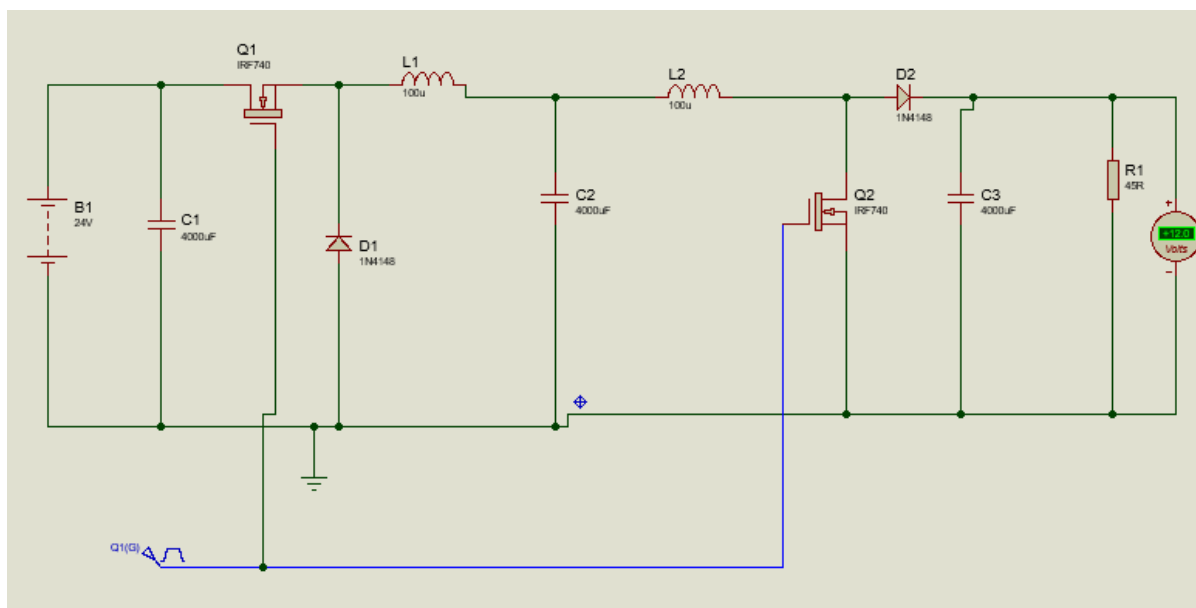
Figure 4. Proteus Model of buck-boost converter

In Figure 4, if the desired output voltage is entered into the model as Vo value, the duty period that will provide this output is calculated and applied as an input to the model.

The model in Figure 4 was operated for different reference output voltage (Vo) values by taking Vg=24 V, C=100 µF, L=4000 µH, R=45 ohm and switching frequency fs=75 kHz, and the following results were obtained. The created model calculates the duty period value of the converter according to the entered reference voltage.

The output voltage of the proposed DC-DC buck boost converter is controlled by altering its MOSFET switch and it is in a closed loop. Generally, a switching logic is used to operate this type of converter. Hence, switching status on-off is a built-in subsystem of this system. For industrial applications of this type of circuit PI controllers are the mostly used as a controller. They are simple in design but demonstrate robust performance regardless of the operating conditions [12].

The key principle that drives the boost converter is the tendency of an inductor to resist changes in current by either increasing or decreasing the energy stored in the inductor magnetic field. In a boost converter, the output voltage is always higher than the input voltage. A schematic of a boost power stage is shown in Figure-2.

- When the switch is closed (on-state), current flows through the inductor in the clockwise direction and the inductor stores some energy by generating a magnetic field. Polarity of the left side of the inductor is positive.
- When the switch is opened (off-state), current will be reduced as the impedance is higher. The magnetic field previously created will be reduced in energy to maintain the current towards the load. Thus, the polarity will be reversed (meaning the left side of the inductor will become negative). As a result, two sources will be in series causing a higher voltage to charge the capacitor through the diode D [13].

If the switch is cycled fast enough, the inductor will not discharge fully in between charging stages, and the load will always see a voltage greater than that of the input source alone when the switch is opened. Also while the switch is opened, the capacitor in parallel with the load is charged to this combined voltage. When the switch is then closed and the right hand side is shorted out from the left hand side, the capacitor is therefore able to provide the voltage and energy to the load. During this time, the blocking diode prevents the capacitor from discharging through the switch. The switch must of course be opened again fast enough to prevent the capacitor from discharging too much [14].

In order to calculate the desired reference output voltage as Vo=36.8 V, when the signal width is entered as PW=66, the duty period, output voltage and inductance current of the buck-boost converter are as seen in Figure 5, Figure 6 and Figure 7. In this case, the model calculated the duty period as d=0.454.
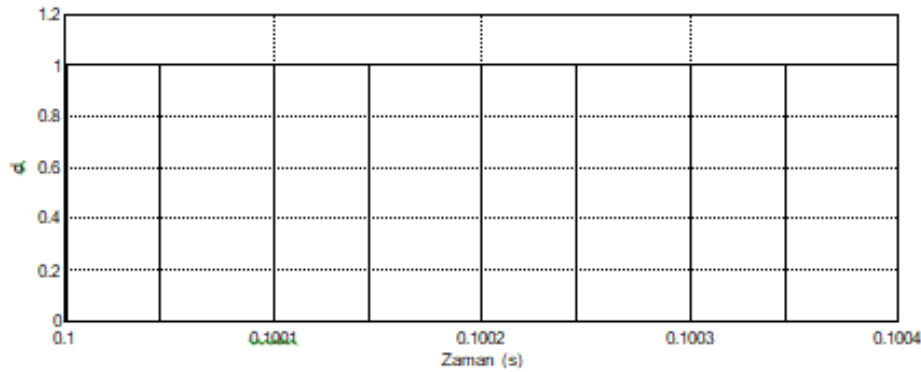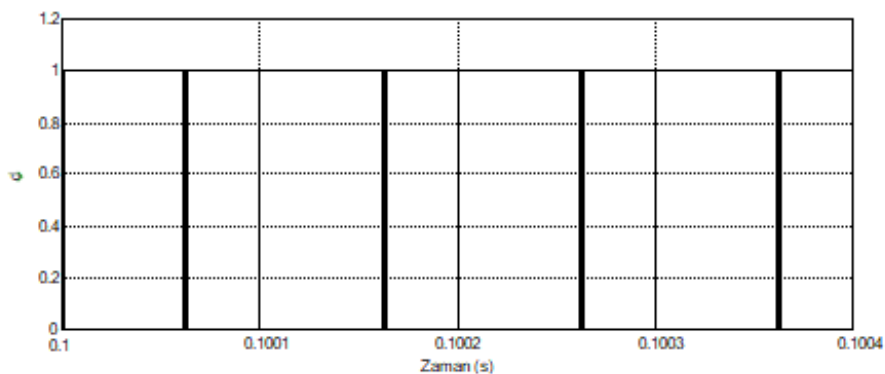

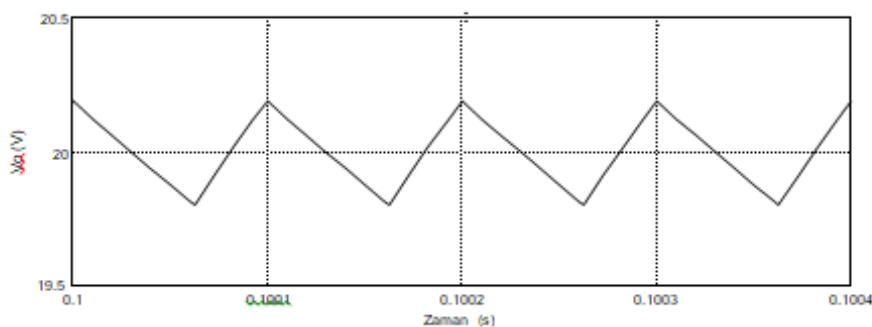**Figure 5.** Change of duty period with time for Pw=66 in buck-boost converter
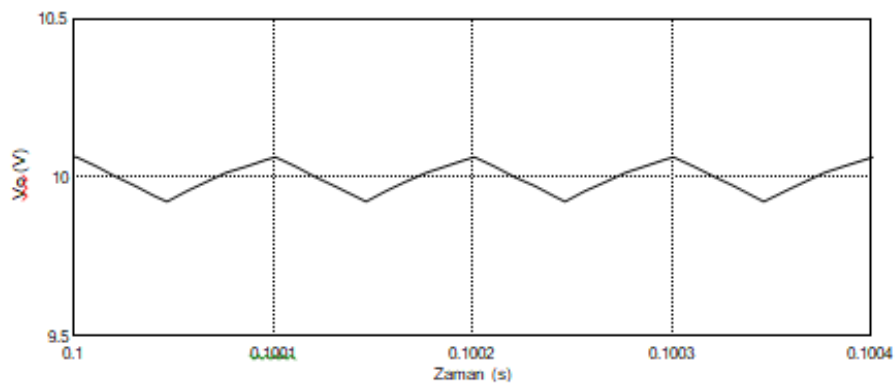
**Figure 6.** Variation of output voltage with time for Pw=66 in buck-boost converter
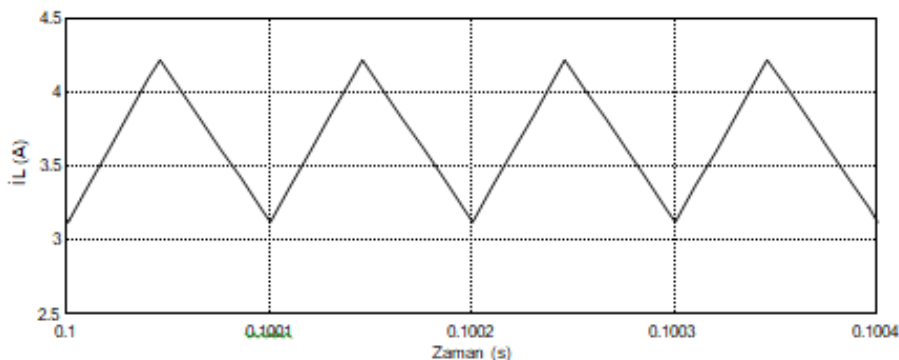
**Figure 7.** Variation of Inductance current for PW=66 in buck-boost convert

The conceptual model of the buck converter is best understood in terms of the relation between current and voltage of the inductor. Beginning with the switch open (off-state), the current in the circuit is zero. When the switch is first closed (on-state), the current will begin to increase, and the inductor will produce an opposing voltage across its terminals in response to the changing current. This voltage drop counteracts the voltage of the source and therefore reduces the net voltage across the load. Over time, the rate of change of current decreases, and the voltage across the inductor also then decreases, increasing the voltage at the load. During this time, the inductor stores energy in the form of a magnetic field.
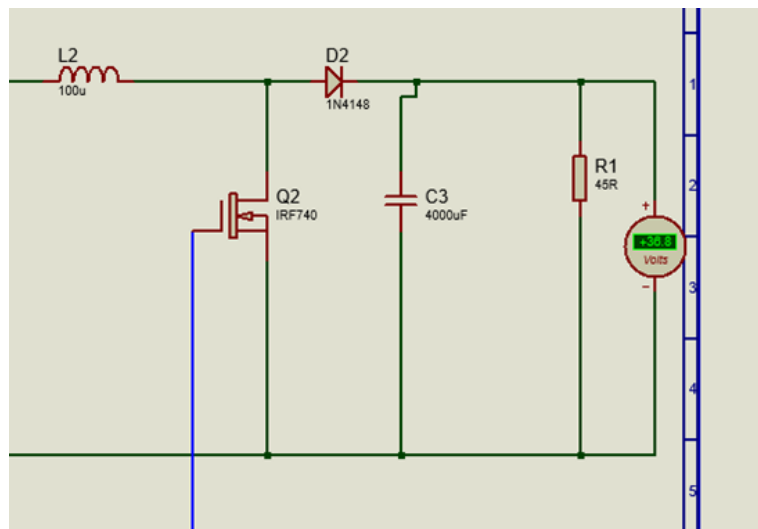
Figure 8. Output voltage value for PW=66 of the buck-boost converter

If the switch is opened while the current is still changing, then there will always be a voltage drop across the inductor, so the net voltage at the load will always be less than the input voltage source. When the switch is opened again (off-state), the voltage source will be removed from the circuit, and the current will decrease. The decreasing current will produce a voltage drop across the inductor (opposite to the drop at on-state), and now the inductor becomes a current source. The stored energy in the inductor's magnetic field supports the current flow through the load.

The "increase" in average current makes up for the reduction in voltage, and ideally preserves the power provided to the load. During the off-state, the inductor is discharging its stored energy into the rest of the circuit. If the switch is closed again before the inductor fully discharges (on-state), the voltage at the load will always be greater than zero.

When the signal width is entered as PW=37 to calculate the desired reference output voltage as Vo=12 V, the duty period, output voltage and inductance current of the buck-boost converter are as seen in Figure 9, Figure 10 and Figure 11. In this case, the model calculated the duty period as d=0.625.

Figure 9. Change of duty period with time for Pw=37 in buck-boost converter

Figure 10. Variation of output voltage with time for Pw=37 in buck-boost converter
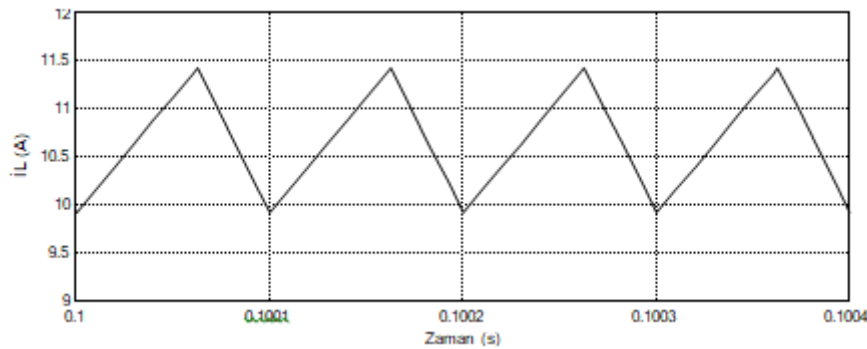
Figure 11. Variation of Inductance current for PW=37 in buck-boost convert
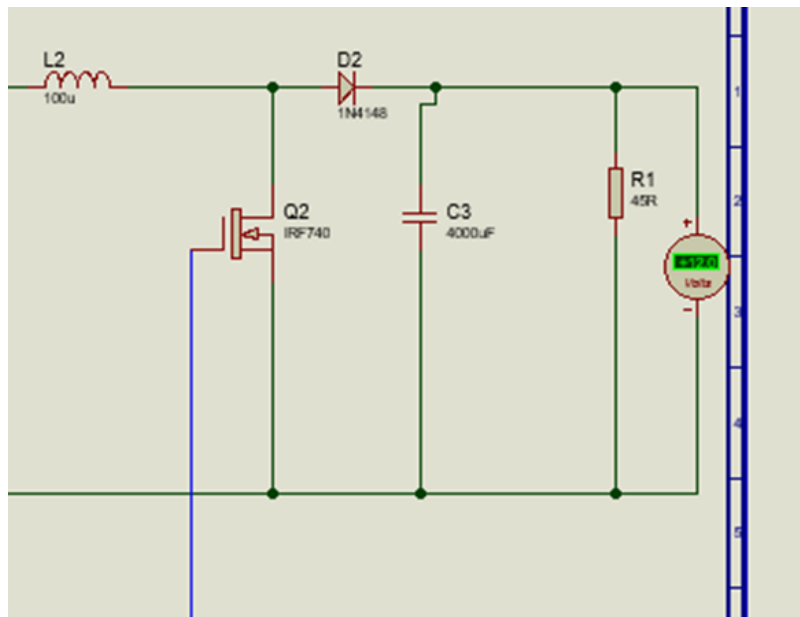
Figure 12. Output voltage value for PW=37 of the buck-boost converter

A buck boost converter can be used for the purpose of both of step up and step down output voltage. In this operation, buck boost converter provides step down output voltage and the total circuit has drawn by using the same element of conventional DC-DC buck converter. It can be concluded from the results of DC-DC buck boost converter output simulations that DC-DC buck converter performs better than the proposed DC-DC buck boost converter with the variation of frequency. An exact opposite result is found from the simulation with the variation of load where the proposed DC-DC buck boost converters performance is higher than the DC-DC buck converter. The voltage gain of experimental DC- DC buck boost converter shown that, it always provides negative output voltage with high voltage gain.

The proposed DC-DC buck boost converter will be suitable to use in audio and instrumentation amplifier, line drivers and receivers.

3. Conclusion

In this study, the design, modeling and control of da-da Buck-Boost transducer are examined. The converter system model and the applied control strategy are simulated in Simulink. The Simulink model is given in Figure-4. Different output voltages are generated against the fixed input voltage corresponding to various corresponding PWM values. It is seen in Figure 12 that the output voltage is reduced at low signal width modulation values and the buck converter circuit is effective. Likewise, when high value signal width modulation is applied, it is observed that the output voltage increases, as in Figure 8. The booster type converter circuit is active in the circuit. The Proteus model of the controlled da-da Buck-Boost converter, which provides the desired output voltage according to different reference voltages, has been realized and the results regarding this situation are presented in detail.

References

1. Ardhenta, L., Ansyari, M. R., Subroto, R. K. & Hasanah, R. N. (2020). DC Voltage Regulator using Buck-Boost Converter Based PID-Fuzzy Control. Electrical Power, Electronics, Communications, Controls and Informatics Seminar (EECCIS), 117-121, Malang, Indonesia.
2. Gayathri, A., Manimegalai, V., Anusha, A., Brindha, S., Harini S. & Harini, T. (2021). Switchingbased Single Input Multi Power Boost Converter. 5th International Conference on Computing Methodologies and Communication (ICCMC), 700-706, Erode, India.
3. Sabati, A., Bayindir, R., Padmanaban, S., Hossain, E. & Tur, M. R. (2019). Small Signal Stability with the Householder Method in Power Systems. Advanced Signal Processing Techniques Applied to Power Systems Control and Analysis, Revised: 27 August 2019, Istanbul, Turkey. 1.
4. Garcia, M. J. P., Gutierrez, G., Normey-Rico, J. E. & Prada, C. (2009). Integrated Design & Control of a Buck Boost Converter. Revista Controle & Automaçao, 20(3).
5. Rashid, M. H., Subhajit, S., Tanya, T. & Vijayakumar, D. (2013). Design and simulation of speed controller using ac-dc buck boost converter for dc motor drive with soft starter. 978-1-4673-6150-7/ 13/$31.00, IEEE.
6. Çalişkan, A., Ünal, S., Orhan, A. (2017). Buck-Boost Transducer Design, Modeling and Control. Arrived/Received: 24.05.2017.
7. Güldemir, H. (2011). Modeling and Sliding Mode Control of Dc-Dc Buck-Boost Converter. 6. International Advanced Technologies Symposium (IATS'11), 475-480. Elazığ, Turkey.
8. Buso, S. (1999) Design of Robust Voltage Controller for a Buck-Boost Converter Using μ-Synthesis. IEEE Transactions on Control Systems Technology. 7(2): 222–229.
9. Rashid, M. H. (2014). Power Electronics Devices, Circuits and Applications. Pearson Education.
10. Chen, J. & Bao. Y. J. (2013). Characteristics analysis and comparison of buck boost circuit and Cuk circuit. Power Electronics Systems and Applications (PESA). 5th International Conference on. IEEE.
11. Zhao, Z., Xu, M., Chen, Q., Lai, J. –S. & Cho, Y. (2012). Derivation, Analysis, and Implementation of a Boost–Buck Converter-Based High-Efficiency PV Inverter. EEE Transactions on Power Electronics, vol. 27, no. 3, pp. 1304-1313. doi: 10.1109/TPEL.2011.2163805.
12. Soheli, S. N., Sarowar, G., Hoque M. A., & Hasan, M. S. (2018). Design and Analysis of a DC -DC Buck Boost Converter to Achieve High Efficiency and Low Voltage Gain by using Buck Boost Topology into Buck Topology. International Conference on Advancement in Electrical and Electronic Engineering (ICAEEE). pp. 1-4, doi: 10.1109/ICAEEE.2018.8643001.
13. Mondol, M. H., Tur, M. R., Biswas, S. P., Hosain, K., Shuvo, & S., Hossain, E. (2020). Compact three phase multilevel inverter for low and medium power photovoltaic systems. IEEE Access, vol. 8, pp. 60824-60837
14. Tur, M. R. & Bayindir, R. (2019). A review of active power and frequency control in smart grid. 2019 1st Global Power, Energy and Communication Conference (GPECOM). pp. 483-488
15. Altun, M., Tür, M. R., & Çakmak, F. (2022). 24V Input 12V AND 36V Output Buck-Boost Converter Design. *Advanced Engineering Days (AED)*, *2*, 90-92.

Investigation of Turkey's climate periods in terms of precipitation and temperature changes

Taha Demirgül *1 , **Cavit Berkay Yılmaz** 1 , **Büşra Nur Zıpır** 1 , **Fatma Sena Kart** 1 ,
Muhammet Fatih Pehriz 1 , **Vahdettin Demir** 1 , **Mehmet Faik Sevimli** 1

1KTO Karatay University, Civil Engineering Department, Konya, Türkiye
demirgultaha@gmail.com; cavitberkayyilmaz@gmail.com; busranurzpr@gmail.com; senahorzum987@gmail.com;
m.f.pehriz@gmail.com; vahdettin.demir@karatay.edu.tr; mehmet.faik.sevimli@karatay.edu.tr

Abstract
In the current century, the climate crisis and the search for a solution take an essential place on the agenda of the whole world. Depending on the temperature and precipitation factors, natural disasters such as drought and flood negatively affect the living ecosystem and the economy. In this study, precipitation and temperature changes between the old climate period (1981-2010) and the new climate period (1991-2020) of Turkey were examined on the basis of 81 provinces and 25 water basins, and the climate periods of the country were compared. The precipitation and temperature data used in the study are long-term average data obtained from monthly average data. In addition, the variation of temperature and precipitation data according to the location, and separate interpolation maps were created for the old and new periods. When the old (574 mm) and new (573,4 mm) precipitation normals are examined throughout the country, a decrease of 0.6 mm (0.1%) has been detected.

1. Introduction

In the 21st century, the whole world has accepted the reality of the climate crisis and the search for effective solutions has increased. However, industrialization and the human population, which started in the 18th century and increased exponentially every century, accelerated the climate change process by causing mistakes that are very difficult to reverse on a global scale. In this process, despite the warnings of scientists, politicians especially in developed countries ignored these warnings and continued to industrialize rapidly, and by releasing a terrible amount of greenhouse gas into the atmosphere, they caused the deterioration of climate balance, especially temperature and precipitation [1].

Time-dependent changes in temperature and precipitation parameters cause irreversible deterioration in the hydrological balance with events such as drought and flood. Changes in air temperature, melting of glaciers in the poles and inland areas, rising sea levels, and increasing the frequency and intensity of floods, droughts and precipitation are the most important of these indicators [2]. These effects negatively affect the endemic plant and animal diversity and basic production areas (agriculture and livestock) of our country, and therefore the nature and economy, with the irregularities in precipitation and temperature parameters in our country, which experiences many climates at the same time. In this context, it is of great importance to examine the management policies of limited water resources to be implemented in the future and to conduct future analyzes on these parameters.

Drought, which is a natural climatic event that can occur at any time and place, can be defined as water scarcity caused by the decreasing trend of the moisture content of a region. Drought usually occurs slowly and covers a long period. Animals and plants in arid climates are adversely affected by the lack of moisture and the high variability of precipitation. Drought is one of the hardest disasters to detect [3]. A flood, which is the opposite of this situation, is when a stream overflows from its bed for different reasons and damages the surrounding lands, settlements, infrastructure facilities and living things [4].

There are many studies examining precipitation and temperature parameters in our country. When the relevant literature is examined, Partal (2003) analyzed the precipitation data in 96 stations in Turkey, which he examined with Mann-Kendall and Sen's T-test, and found negative trend findings in the Central and Eastern Black Sea Regions in the winter season [5]. Büyükyıldız (2004) conducted a study on precipitation data of 25 stations belonging to the Sakarya Basin, Sen's T-test, Spearman Rho test, Mann-Kendall test, Seasonal Mann-Kendall, Sen's Trend Slope Method, Van Belle and Hughes (using the trend) Homogeneity test and Mann-Kendall Rank Correlation tests, he detected 44 significant trend presences in the 95% confidence interval and reported that this trend presence was positive with 20% and negative with 80% [2]. Özfidaner (2007), as a result of the study he carried out on the monthly and annual precipitation data of 32 stations in Turkey using T-test, Mann-Kendall Rank Correlation test and Regional Mann-Kendall Rank Correlation tests, showed that in the winter season, the negative direction, autumn, spring and in the summer seasons, positive trend findings were found [6]. Ölgen (2010) reported that annual precipitation variability in Turkey decreases regularly from south to north, and that precipitation in large parts of the country, especially in the south and southeast regions, causes significant deviations in summer due to tropical air currents. However, in the north of the Black Sea Region, he concluded that the precipitation caused by the northern air currents reduced the precipitation variability in the region [7]. Demir (2018) examined the precipitation data of 19 stations in the Black Sea region by applying the Run test, Mann-Kendall test, Linear Trend test and Şen Trend tests and determined that there was a positive trend in the East and Central Black Sea regions and a negative trend in the West Black Sea region [8]. Yılmaz (2021), examining the 57-year temperature and precipitation data of the Eastern Black Sea region, determined a positive trend as a result of his study [9].

In the literature, there are also many studies on temperature parameters. Türkeş (2000) reported that the warming of the world's surface temperatures, which started in the 1950s, increased every year and broke global temperature records. After the cold year of 1992 in Turkey, temperatures increased to a record level in 1998, and this year was the warmest year between 1850 and 2000, both in the global average and in the temperature averages of the northern and southern hemispheres [10]. Öztürk (2002) reported that according to the scenarios put forward by the United Nations Intergovernmental Panel on Climate Change (IPCC), an average increase of 1 to 3.5 degrees in global temperature is foreseen until 2100. From this, it follows that even under the most optimistic conditions, there will be an increase in temperature of about 0.1 degrees every 10 years. As a result of this; he stated that there will be very different consequences that will result from the rise in sea level, change in temperature and precipitation regimes and reach the dimensions of the disaster. Again, according to Öztürk (2002), semi-arid and arid regions (South East and Central Anatolia regions) and semi-humid (Aegean and Mediterranean regions) regions will be more affected by the increase in temperature [11]. Bahadır (2011) in his study examining the effects of global climate changes in Turkey, stated that there was a decreasing trend in annual and seasonal average temperatures in our country from 1975 to 1992, and an increase in average temperatures began to be observed after 1992 [12]. Dabanlı (2017) investigated the impact of climate change on precipitation and temperatures using SRES A2 and B2 scenarios of Max-Plank Meteorology Institute (EH40PYC) and Hadley Center (HadCM3) models. As a result of the study, it was determined that the land and sea temperatures increased in parallel with each other. Looking at the temperature records in the northern hemisphere, it was seen that the 1990s were the hottest years of the last 1000 years [13]. According to the Climate Change and Agriculture Evaluation Report, there has been a rapid increase in the accumulation of greenhouse gases released into the atmosphere as a result of activities that do not comply with sustainability principles, and this situation has strengthened the natural greenhouse effect and caused an increase in the average surface temperatures of the earth, triggering global warming. As a result of global warming, climate change has manifested itself with varying effects in different areas [14]. According to the climate change model studies conducted according to the Turkey Drought Assessment Report, temperatures are expected to increase by 0.5 to 3.0 °C until 2050 and by 0.5 to 4.0 °C until 2100, according to the optimistic scenario. According to the pessimistic scenario, temperatures are expected to increase by 0.9 to 3.5°C by 2050 and by 0.9 to 6.3°C by 2100 [15]. The basins most sensitive to temperature increase are those in the Eastern Mediterranean and Southeastern Anatolia Regions. In the Climate Assessment (2021), it has been reported that the average temperature of Turkey in 2021 (14.9°C) is 1.4°C higher than the average temperature (13.5°C) between 1981 and 2010 [16]. According to the IPCC 3rd Assessment Report, it is estimated that the annual average temperatures of Turkey will increase by 1 to 3 °C until 2050. Every region in our country will be affected by climate change in different ways) [17].

Scopus is one of the two most comprehensive databases in the world. Vosviewer, on the other hand, is a program that visualizes data obtained from databases such as scopus and web of science with the network

analysis method [18]. For the literature review, the results obtained in the search with the keywords 'precipitation and temperature and change and turkey' in scopus were divided into author (Figure 1a), country (Figure 1b) and keyword (Figure 1c) categories with vosviewer analysis was made.
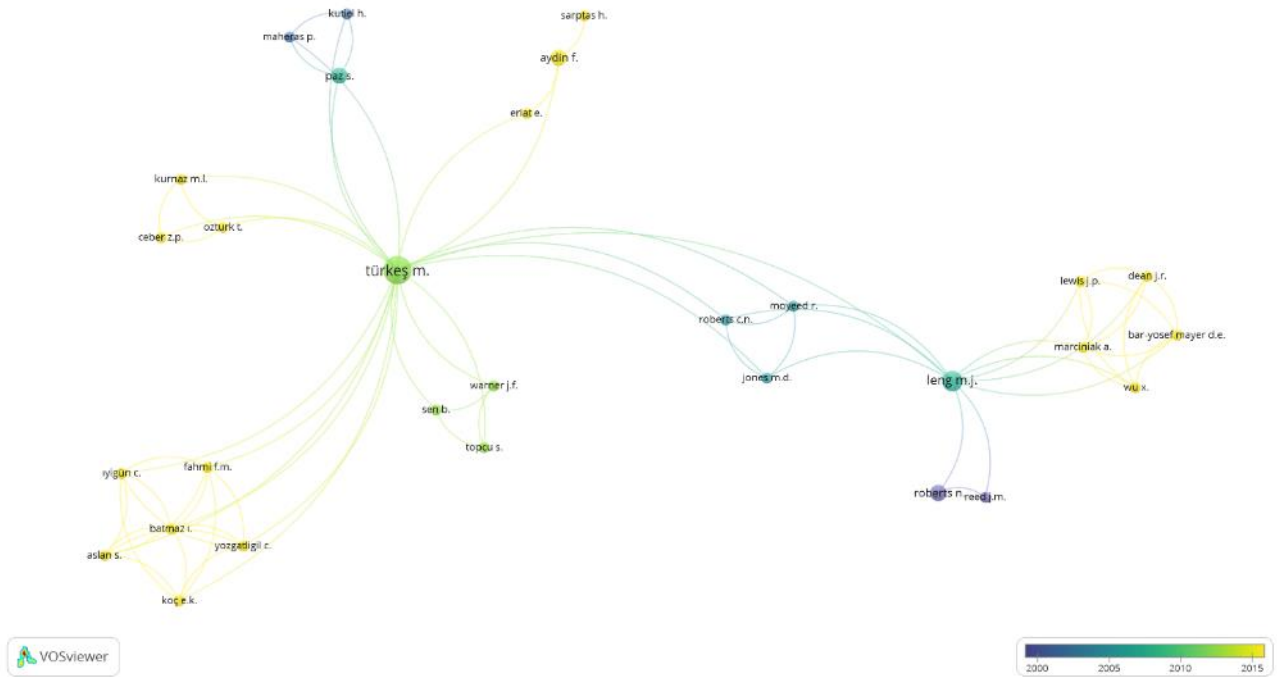

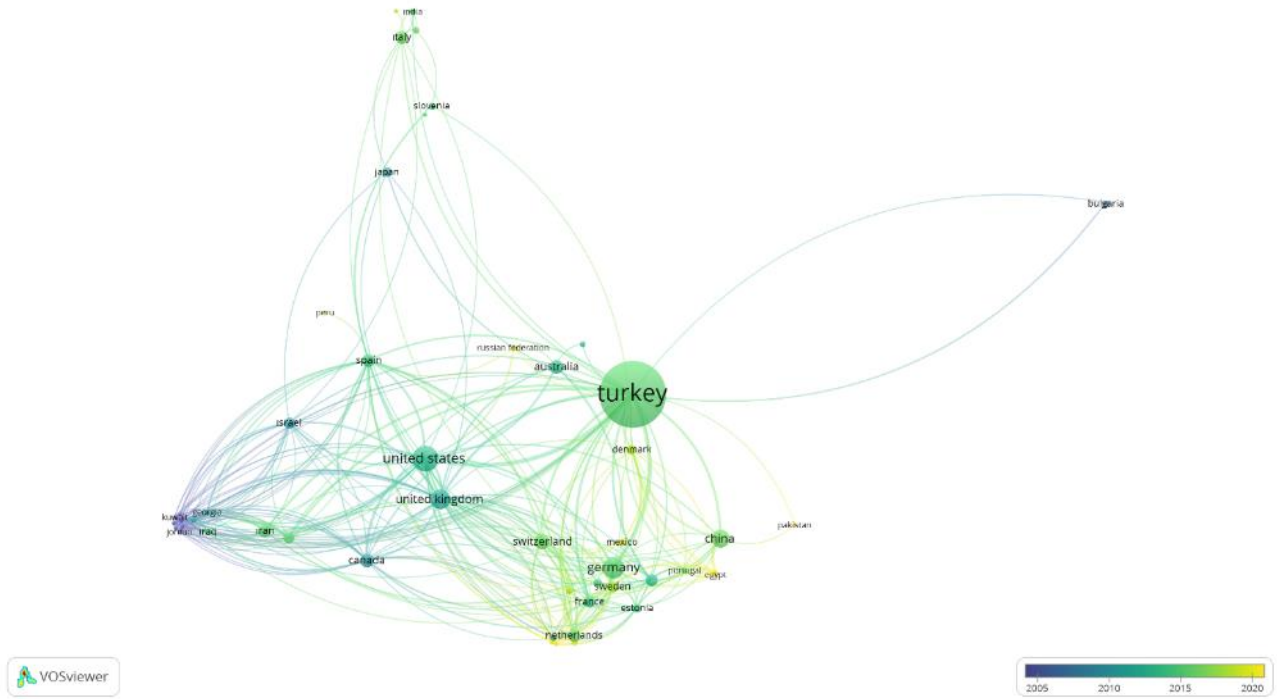**Figure 1a** Network map of the authors according to the results from the Scopus Database

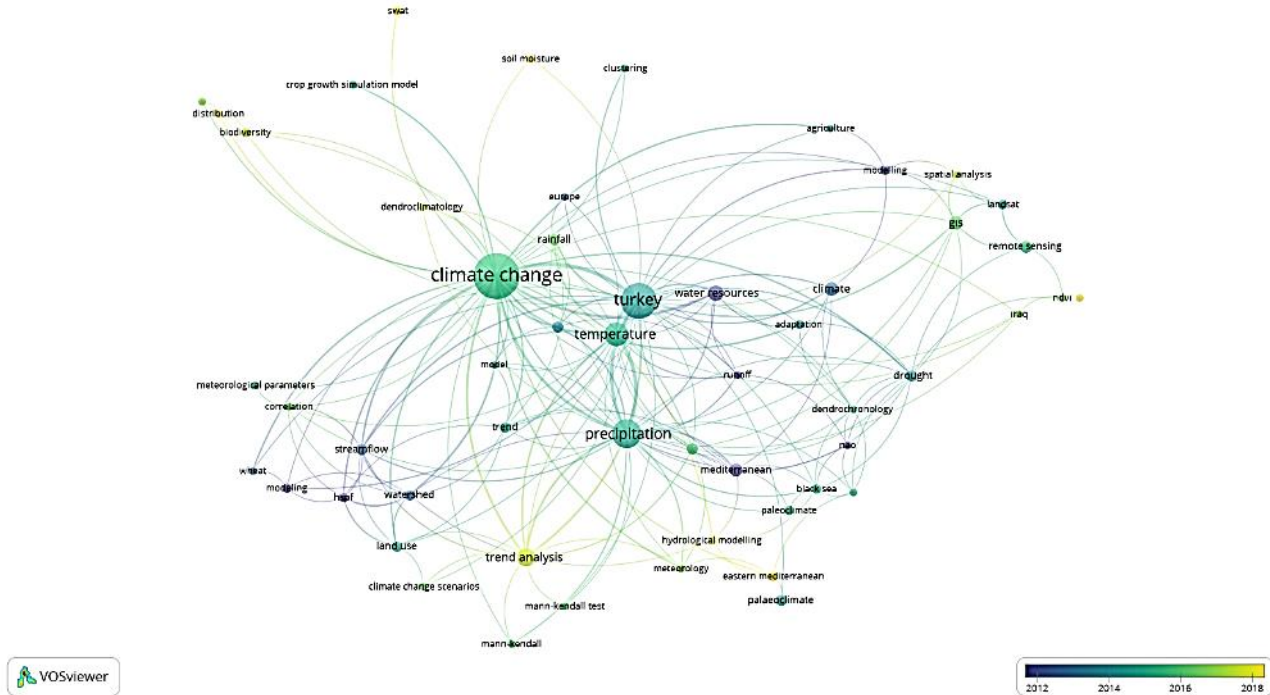**Figure 1b** Network map of countries according to the results obtained from the Scopus database

Figure 1c Network map of the keywords used according to the results obtained from the Scopus database

As can be seen in Figure 1a, the authors working in the field of precipitation and temperature change in turkey and the years of study started to increase after 2010 and intensified in recent years.

In Figure 1b, it is seen that the country working the most on this issue is Turkey, and these studies have increased after 2015. It is seen that the countries that have been working on these issues in recent years are Egypt, Pakistan and the Russian federation.

As can be seen in Figure 1c, it was seen that the most common and written keywords were Turkey, climate change, precipitation and temperature.

In this study, the monthly average temperature and precipitation data of the old normal (1981-2010) and the new normal (1991-2020) of Turkey, the changes in the province, water basins and Turkey-wide were visualized by using IDW interpolation method and the results were interpreted.

2. Material and Method

2.1. Study Area

Turkey (26°-45° E, 36°-42° N) is a country surrounded by seas on three sides [19]. Turkey is located both in the temperate and subtropical zones due to its location. While the coasts of Turkey are suitable for a temperate zone climate due to the effect of the seas, continental climate characteristics are observed since the sea effects are not observed in the inner parts of the country. Therefore, different climates are seen in Turkey: Mediterranean climate, Marmara (transitional climate) climate, Continental climate and the Black Sea climate. Considering today's climatic conditions, the effects of global climate change in Turkey are manifested as a decrease in water resources, drought, heatwaves, an increase in floods and a reduction in agricultural productivity [20]. In middle belt countries like Turkey, there are two different periods during the year: rainy winter and dry summer periods. Turkey receives 35% of its annual total precipitation during the winter months. This is followed by the spring and autumn seasons, and this rate drops to 11% in the summer months. All of the Eastern Mediterranean and Central Anatolia and some parts of the Southeastern Anatolia Region are considered arid, and some areas are considered very arid and desert [3].

Flood, which is one of the dangerous situations seen in Turkey, is seen in the Black Sea region, which receives the most precipitation [21]. In the Marmara, Aegean and Mediterranean regions, floods occur due to the geomorphological features of these regions. In the Mediterranean region, precipitation events in the spring season cause floods [22]. The risk of flood disasters in the Eastern Anatolia, Central Anatolia and Southeastern Anatolia regions of the country is at the lowest level compared to other regions [23]. Even if precipitation is high in these regions, the geological forms of the regions prevent flooding.

Turkey is among the countries in the risk group in terms of the possible effects of global climate change. As a result of the effects of climate change, drought in some regions and floods in others is very likely. The study area has been determined as 81 provinces of Turkey, 25 water basins and the country in general.

Figure 2a The study area and locations of stations

Figure 2b The study area and locations of water basins

2.2. Material

Long-term monthly average temperature (°C) and precipitation (mm) data were obtained from the report of the General Directorate of Meteorology on "Temperature and Precipitation Normals for the period of 1991-2020" and dated 25.11.2021. The temperatures of the water basins were obtained by taking the average of the temperatures of the stations in the basin. The table containing the statistical information of the old and new normals all the provinces is given below (Table 1).

Table 1. Descriptive statistical information on old and new precipitation and temperature normal for provinces

	Precipitation (mm) (1981-2010)	Precipitation (mm) (1991-2020)	Temperature (°C) (1981-2010)	Temperature (°C) (1991-2020)
Mean	618,97	619,08	13,09	13,55
Maximum	1407,5	1602,2	19,5	20,2
Minimum	352,3	349,2	3,6	4,3
Standard Error	18.58	21.11	0,37	0,36
Standard Deviation	167.30	190.07	3,29	3,28
Kurtosis	5.08	7.78	0,40	0,43
Skewness	1.53	1.95	-0,42	-0,44

In Table 1, the average of the precipitation normals for the provinces increased from 618.97 mm to 619.08 mm. Temperature normals increased from 13.09°C to 13.55°C. The highest temperature increased from 19.5 °C to 20.2 °C, while the lowest temperature increased from 3.6 °C to 4.3 °C.

2.3. Method

2.3.1 Inverse Distance Weighting (IDW) Method

The Inverse Distance Weighting (IDW) is an interpolation method used to create data from the data that cannot be sampled by the exemplary points, wherein the creation of these data depends on the interpositional distance and formula applied by considering relations with various points [24].

$$f(x, y) = \sum_{i=1}^{n} w_i f_i \tag{1}$$

$$w_i = \frac{h_i^{-p}}{\sum_{j=1}^{n} h_i^{-p}} \tag{2}$$

Here;
f_i; represents the known height value,
w_i; represents the weights and the sum of their values must Equation 1,
p; is taken as a power parameter and denoted by exponent,
h_i; represents the spatial distance between the sample points and the interpolation points [25-26].

3. Application

Determination of precipitation and temperature normals and analysis of changes are of great importance for Turkey, which is very sensitive to drought and flood hazard [27]. These analyzes play a key role in the studies to be carried out in terms of water management. In this study, the data of precipitation and temperature normals of 81 provinces were visualized using the IDW interpolation method.

IDW interpolation maps of old and new precipitation normals are shown in Figures 3, 4, 7, 8 and temperature normal are shown in Figures 5, 6, 9, 10.

When Fig. 3 and Fig. 4 are examined, it is seen that the highest precipitation normal and the highest increase were in Rize with a difference of 194.7 mm and a percentage of 13.83% new normal- old normal/old normal for example ((1602.2mm-1407.5mm)/1407.5mm). On a provincial basis, the highest decrease was seen in Erzurum with a difference of 75.3 mm and a percentage of 12.84%. Since the precipitation heights in the central part of the country are well below 573.4 mm, which is considered the precipitation normal, these regions are under the threat of drought. Rize station, on the other hand, continues to be the riskiest station that can be flooded by exceeding the old precipitation height.

When Figure 5 and Figure 6 are examined, it is seen that there is an increase in temperature in all provinces except Bitlis. The highest increase on a provincial basis was seen in Ardahan with a difference of 0.7 °C and an increase of 19.44% ((4.3°C-3,6°C)/3.6°C). The only province with a temperature decrease was Bitlis with a difference of 0.2 °C and a decrease of 2.08%. The desert climate coming from Syria is effective in the stations adjacent to Syria. In the stations on the Mediterranean coast, the temperatures are above the country average

due to the Mediterranean climate. Northeast stations, on the other hand, are the stations where the lowest temperatures of the country are seen due to both terrestrial and high altitudes.
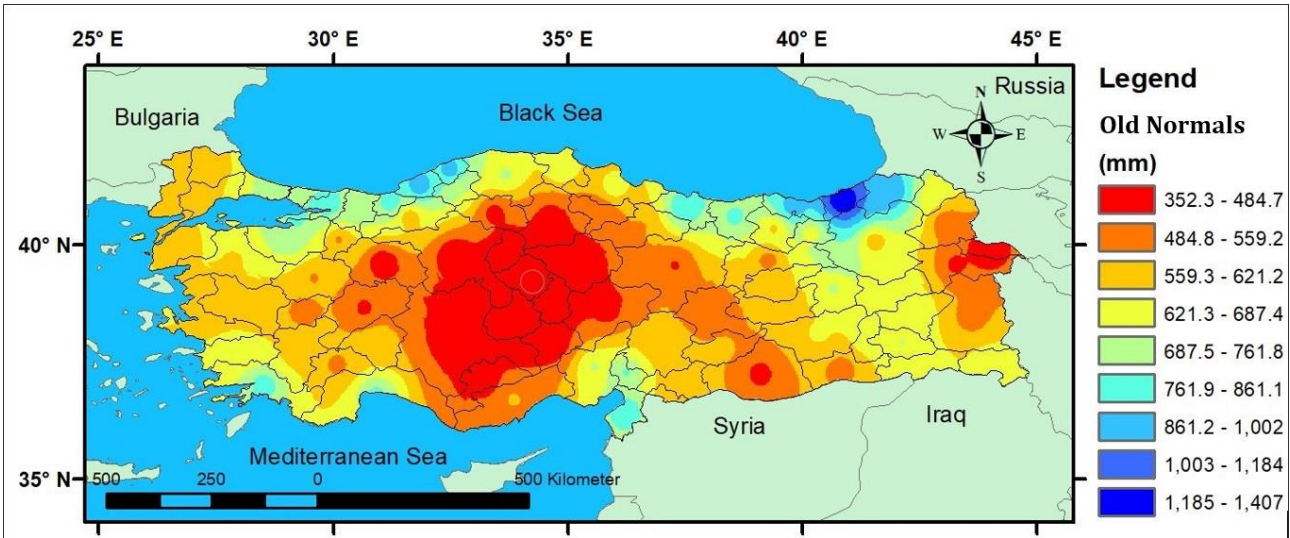

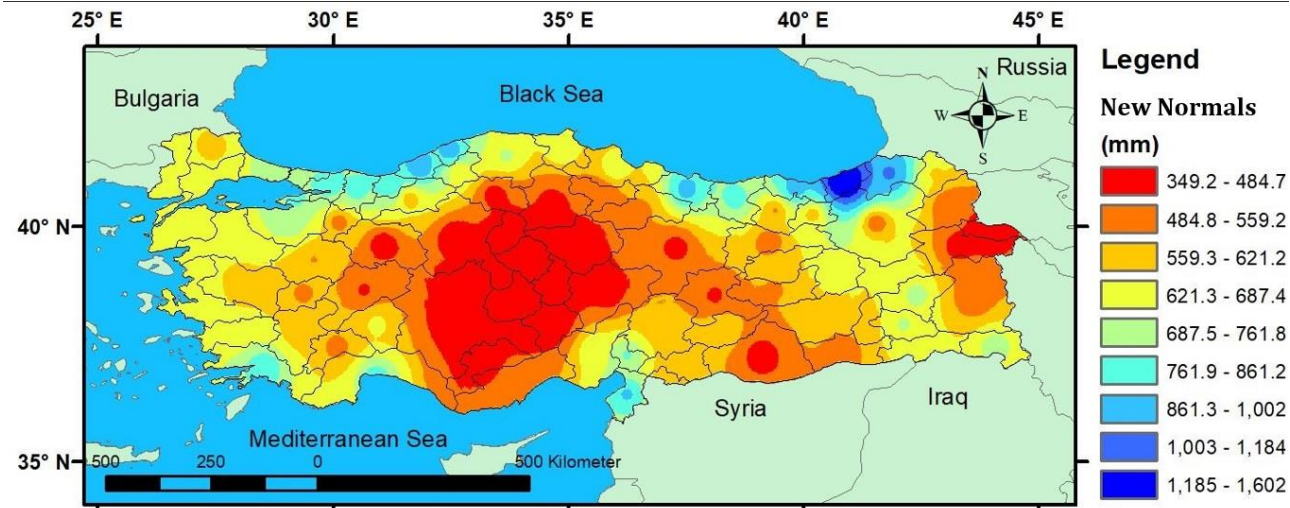**Figure 3.** Old Precipitation Normals (1981-2010)
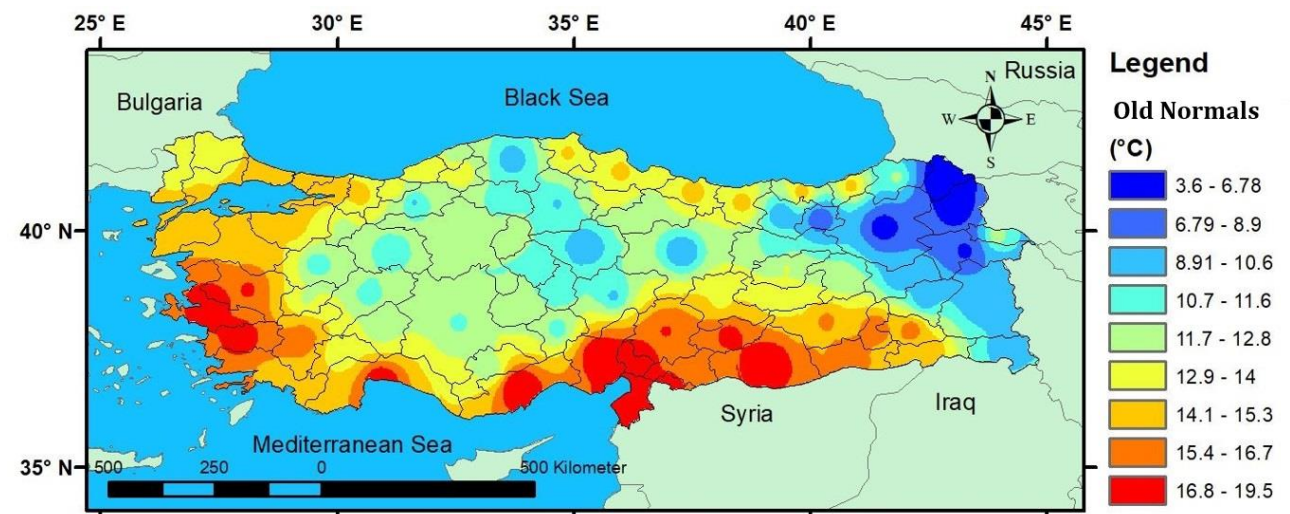

Figure 4. New Precipitation Normals (1991-2020)
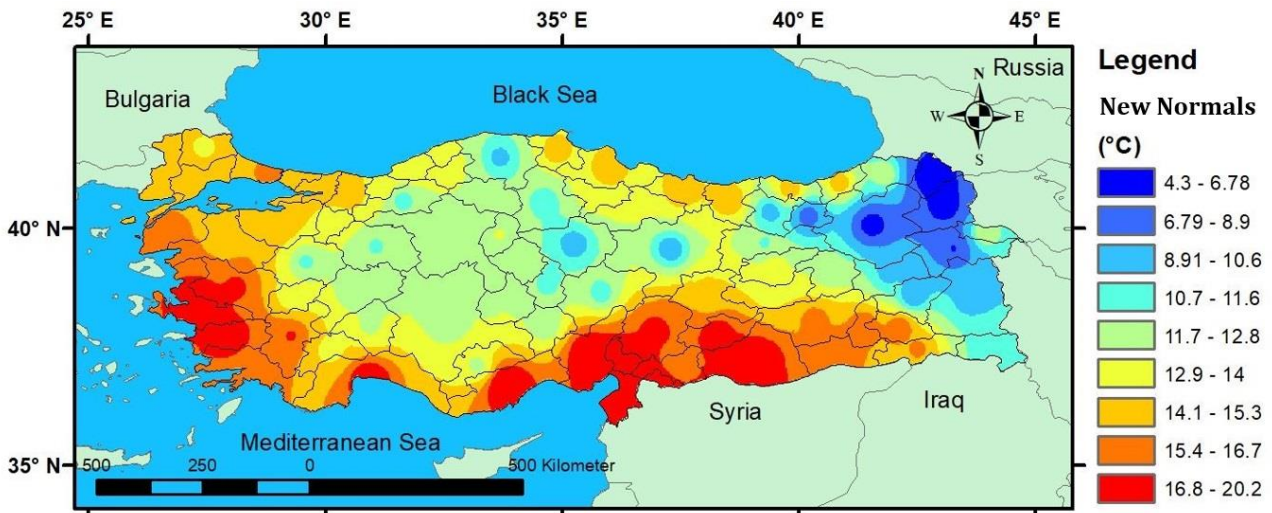

Figure 5. Old Temperature Normals (1981-2010)
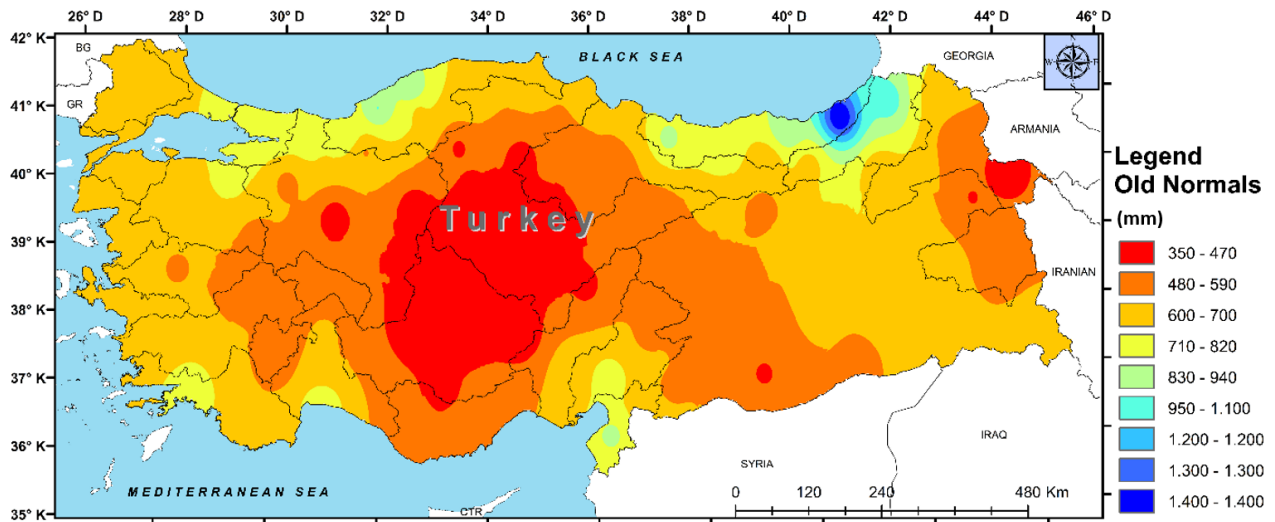
Figure 6. New Temperature Normals (1991-2020)
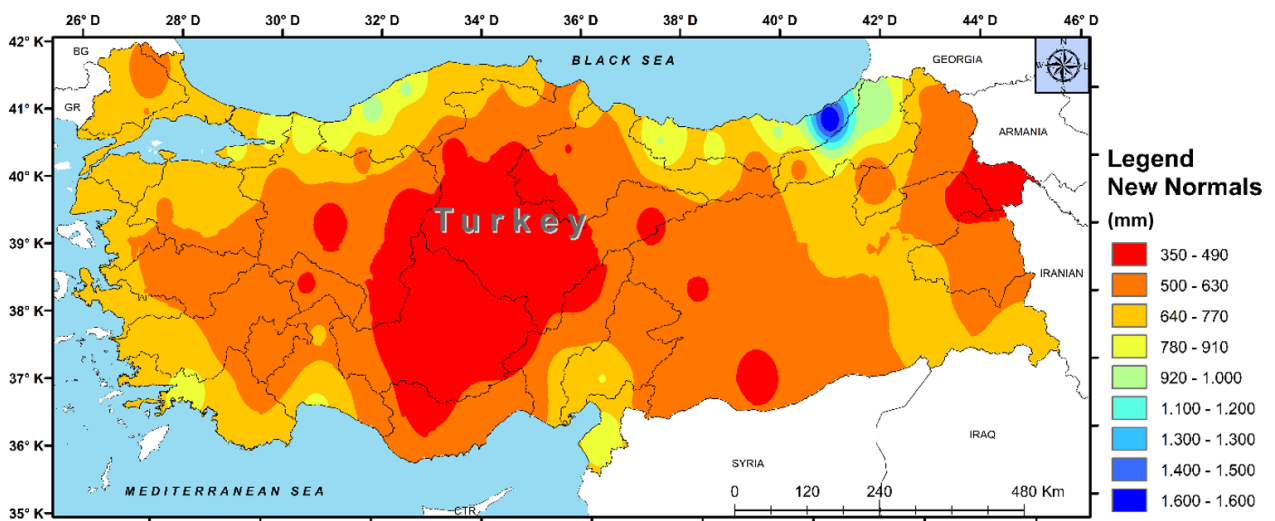

Figure 7. Old Precipitation Normals (1981-2010)

Figure 8. New Precipitation Normals (1991-2020)

Looking at Figure 7 and Figure 8 it has been determined that the water basin with the highest precipitation increase compared to the old normal is the Eastern Black Sea Basin with a difference of 52.1 mm and 5.50% ((999.9 mm-947.8 mm)/947.8 mm). It has been determined that the water basin with the highest decrease in

precipitation is the Çoruh Basin with a difference of 54.6 mm (709.2 mm-763.8 mm). In terms of percentage, it was determined that there was a decrease of 8.12% ((479.7 mm-522.1 mm)/522.1 mm) in the Van Lake Basin. It has been understood that the only water basin whose precipitation height never changes compared to the old normal is the Sakarya Basin with 472.8 mm.
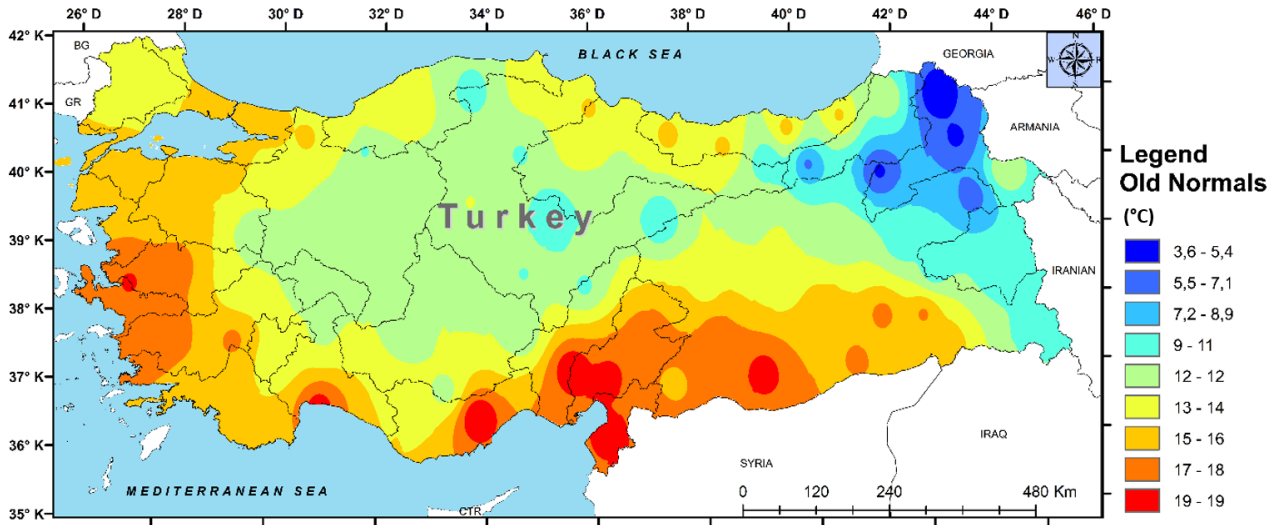
Figure 9. Old (1981-2010) Temperature Normals
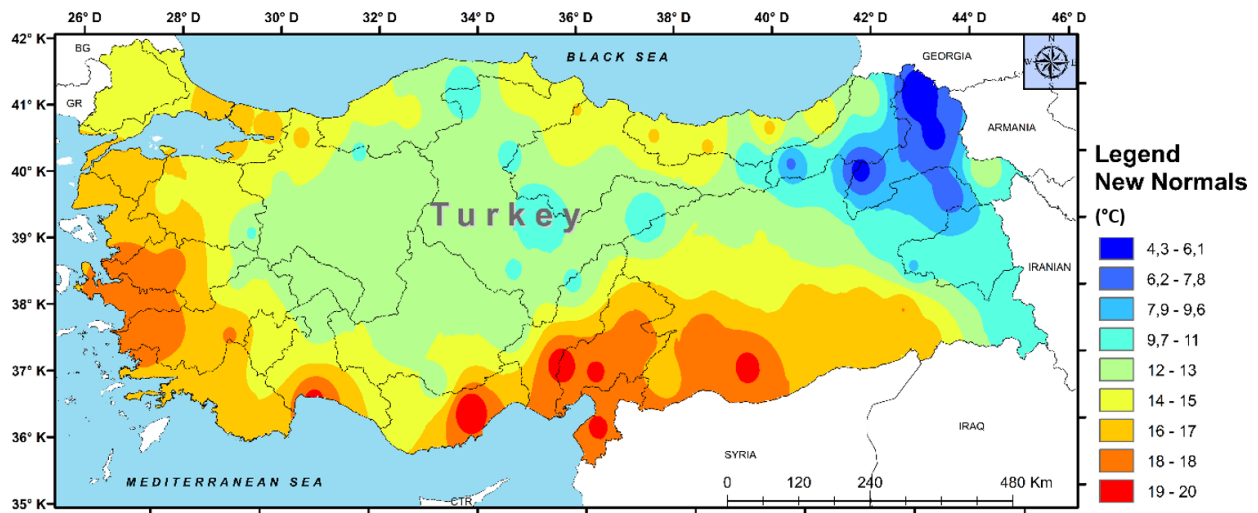
Figure 10. New (1991-2020) Temperature Normals

As can be seen in Figure 9 and Figure 10 it was determined that there was an increase in temperature in all water basins. The highest increase compared to the old normal was detected in the Eastern Mediterranean Basin with a difference of 0.7 °C (20.2 °C -19.5 °C). When the results were analyzed according to the percentage change, it was determined that there was an increase of 7.34% ((6.95 °C-6.48 °C)/6.48 °C) in the Aras Basin.

4. Conclusion and Discussion

The changes in precipitation and temperature of Turkey between the new climatic period (1991-2020) and the old climatic period (1981-2010) were analyzed by mapping with the IDW interpolation method. As a result of the examination, it was determined that the precipitation normal throughout the country decreased (from 574 mm to 573.4 mm) by 0.6 mm (0.1%).

It was observed that annual temperature normals tend to increase (from 13.09°C to 13.55°C) by 0.46°C equal (3.51%) change in all regions of our country.

Considering the average rainfall height of 25 water basins, an increase of 1.19 mm (0.2%) was detected compared to the old normal. However, the fact that the temperature increase has increased by 0.44 °C (3.19%) to the old normal and the precipitation height has not increased sufficiently indicates that it is necessary to be prepared for the fact that there may be a serious drought danger in the next climatic period. Although it is seen that the precipitation heights throughout the country are higher than 573.4 mm, which is accepted as the precipitation normal, there is a serious drought threat, especially in the interior of the country, which is

landlocked and has a continental climate. It is seen that the precipitation heights of the Kızılırmak (460.3 mm-449.4 mm), Sakarya (472.8 mm- 472.8 mm) and Akarçay (478 mm- 480.6 mm) Basins, especially in the Konya Kapali (404.8 mm-394.8 mm), are far below the precipitation normal. In light of all these data, decision-makers should make the necessary arrangements.

In the literature, it is stated that a 30-year period is sufficient to comment on the climate situation by examining the precipitation and temperature parameters of a region [28]. However, examining longer periods allows us to make clearer comments.

In this study, Turkey's climate interpretation was made by examining 30 years of precipitation and temperature data of the General Directorate of Meteorology for Turkey.

Acknowledgement

Funding

Author contributions

Taha Demirgül: Conceptualization, Methodology, **Cavit Berkay Yılmaz** Software **Büşra Nur Zıpır:** Data curation, **Fatma Sena Kart:** Writing-Original draft preparation, **Muhammet Fatih Pehriz:** Software, Validation. **Vahdettin Demir:** Visualization, Investigation, **Mehmet Faik Sevimli:** Writing-Reviewing and Editing.

Conflicts of interest

The authors declare no conflicts of interest.

References

1. Şanli, B., Bayrakdar, S., İncekara, B. (2017). Effects of the Global Climate Change and International Initiatives Aimed at Preventing Such Effects. Suleyman Demirel University The Journal of Faculty of Economics and Administrative Sciences, 22 (1), 201–12.
2. Büyükyıldız, M. (2004). Sakarya Havzası yağışlarının trend analizi ve stokastik modellenmesi [Doctoral thesis]. [Konya]: Selcuk University Institute of Science.
3. Kapluhan, E. (2013). Drought and Drought ın Turkey Effect of Agriculture. Marmara Coğrafya Dergisi, 27, 487–510.
4. Dernek, E. (2012). Taşkın Yapıları Tasarımı ve Kayı Deresi Örneği [Master's thesis]. [Tekirdağ]: Namık Kemal University Institute of Science.
5. Partal, T. (2003). Türkiye Yağış Verilerinin Trend Analizi [Unpublished master's thesis]. [İstanbul]: ITU Institute of science.
6. Özfidaner, M. (2007). Türkiye Yağış Verilerinin Trend Analizi ve Nehir Akımları Üzerine Etkisi [master's thesis]. [Adana]: Çukurova University Institute of science.
7. Ölgen, M. K. (2010). Spatial Distribution of Annual and Seasonal Rainfall Variability over Turkey. Aegean Geographical Journal, 19 (1), 85–95.
8. Demir, V. (2018). Karadeniz Bölgesi Yağışların Trend Analizi [master's thesis]. [Samsun]: Ondokuz Mayıs University Institute of Science.
9. Yılmaz, C.B., Demir, V., & Sevimli, M. F. (2021). Doğu Karadeniz Bölgesi Meteorolojik Parametrelerinin Trend Analizi. European Journal of Science and Technology, 15 (24), 489–96.
10. Türkeş, M., Sümer, U. M., & Çetiner, G. (2000). Küresel iklim değişikliği ve olası etkileri. In: Çevre Bakanlığı, Birleşmiş Milletler İklim Değişikliği Çerçeve Sözleşmesi Seminer Notları, 7–24.

11. Öztürk, K. (2002). Etkileri Global Climatic Changes and Their Probable Effect upon Turkey Kemal ÖZTÜRK. Gazi Eğitim Fakültesi Dergisi, 22(1), 47–65.

12. Bahadir, M. (2011). Türkiye'de İklim Değişikliğinin İklim Bölgelerine Yansımasında Kuzey-Güney Yönlü Sıcaklık ve Yağış Değişim Öngörüleri. Akademik Bakış Dergisi 26.

13. Dabanlı, İ. (2017). Türkiye'de İklim Değişikliğinin Yağış-Sıcaklığa Etkisi Ve Kuraklık Analizi: Akarçay Örneği [doctoral thesis]. [İstanbul]: İTU İnstitute of Science.

14. TC Tarım ve Orman Bakalnlığı. İklim değişikliği ve tarim değerlendirme raporu. (2021)

15. MGM, DSİ, SYGM. (2014). Türkiye kuraklik değerlendirme raporu iklim değişikliği ihtisas heyeti Meteoroloji Genel Müdürlüğü Devlet Su Işleri Genel Müdürlüğü Su Yönetimi Genel Müdürlüğü.

16. MGM. 2021 Yılı İklim Değerlendirmesi Ocak 2022 Ankara.

17. Arslan ER. IPPC 3 Report

18. Çelik, M. A. (2000). Bibliometric network analysis on new tendencies, techniques and terms used in drought research. International Journal of Geography and Geography Education (IGGE), 42.

19. Berberoğlu, S., Çilek, A., Dönmez, C., Erdoğan, M. A., Ersoy, M., Akin, A., et al. (2014). İklim Değişikliğinin Türkiye'de Çevresel Risk Dağılıman Etkisinin Konumsal Modeller Yardımıyla Tahmini. 5. Uzaktan Algilama-CBS Sempozyumu (UZAL-CBS 2014), 14-17 Ekim 2014, İstanbu. 2014. p. 14–7.

20. Turan, E. S. (2018). Turkey's Drought Status Associated with Climate Change. Journal of Natural Hazards and Environment, 4(1), 63–69.

21. Şenol, C. (2019). The situation of the spatial change in the lower part of the Melet River Basin is affected by potential flooding. International Journal of Geography and Geography Education (IGGE), 40, 439–453.

22. Saf, B. (2011). Batı Akdeniz Bölgesi Taşkın Tahminlerinde Homojenlik İrdelemesi. İMO Teknik Dergisi.

23. Türkoğlu, N. (2009). Analysis of Floods Occured on October 31-November 1, 2006 in Southeast Anatolia Region. e-Journal of New World Sciences Academy, 4(4).

24. Taylan, E. D., & Damçayiri, D. (2016). Isparta Bölgesi Yağış Değerlerinin IDW ve Kriging Enterpolasyon Yöntemleri ile Tahmini. İMO Teknik Dergisi.

25. Krige, D G. (1951). A Statistical approach to some basic mine valuation problems on the Witwatersrand. Chemical Journal of the Metallurgical & Mining Society of South Africa, 52, 119–139.

26. Shepard, D. A two-dimensional interpolation for irregularly-spaced data function.

27. Cebeci İ, Demirkıran O, Doğan O, Karagöz Sezer K, Öztürk Ö, Elbaşı F. Türkiye'nin İller Bazında Kuraklık Değerlendirmesi. Toprak Su Dergisi. 2019 Dec 16;169–76.

28. Bayazit M. (1981) Statistical Methods in Hydrology. Istanbul Technical University Press

29. Demirgül, T., Yılmaz, C. B., Zıpır, B. N., Horzum, F. S., Pehriz, M. F., Demir, V., & Sevimli, M. F. (2022). Investigation of precipitation and temperature changes in Turkey in the last climate period. *Advanced Engineering Days (AED)*, *2*, 69-71.

Effect of energy storage on power system stability

Ayşe Acar*1 , **Asım Kaygusuz 1**

1Inonu University, Electrical Electronics Engineering, Malatya, Türkiye, ayseyold@gmail.com; asim.kaygusuz@inonu.edu.tr

Abstract
Nowadays, the difference between the amount of energy produced and the amount of energy consumed is increasing. However, the resources of traditional energy production methods are gradually decreasing and cause environmental pollution. Limited resources lead us to renewable energy sources. On the other hand, production with renewable energy sources brings with it the changing global climate problem. The efficient, functional and continuous use of this energy is as important as the production of energy. However, systems based on renewable energy sources such as solar and wind cannot respond quickly and reliably to fluctuating demand as they have different generation profiles seasonally and during the day. This indicates that energy storage is an important issue. It is academically important to analyze the changes in the stability of power systems by integrating storage systems into power systems. In this study, it is aimed to minimize the production-consumption imbalance by integrating energy storage systems into smart grids and the response of system stability is analyzed. In practice, development studies were carried out on the basis of the MATLAB contents applied by Hadi Saadat. For this analysis, hypothetical generation and consumption systems have been created using the IEEE 14 bus power system.

1. Introduction

Energy, which is the key in our daily life, is very important socially and economically for all the countries of the world. The word energy brings to our memory primarily electrical energy, which is the cornerstone of our lives. Energy can be used in different forms in many parts of our lives, thanks to the various sources used during its production. The amount of energy we use in many areas of our lives such as energy lighting, heating, industry, communication and transportation is increasing and will continue to increase due to the increase in the world population and the continuous development of technology.

In parallel with this increase in demand, production also increases. Today, in order to respond to this increase, continuous and efficient energy is demanded in production areas. However, the depleted fossil fuel resource and the energy crises that may occur as a result, environmental pollution and global climate change lead us to the use of RES (Renewable Energy Resources). It is aimed to provide energy efficiency with the production made with RES. The place of renewable energy generation systems, whose source is sun and wind, is growing day by day in the global energy circle, as they do not harm the environment and do not run out of resources.

However, the fact that the seasonally fluctuating and intermittent power outputs of systems based on RES such as solar and wind during the day and the traditional grid infrastructure used today are not suitable for power systems based on RES leads us to find a solution to this problem. With the development of smart grid

infrastructures, it is aimed that the use of ESS (Energy Storage Systems) will become widespread in order to ensure energy efficiency and continuity. Energy storage systems store the increased electricity at a certain time and give it back to the grid when needed.

Energy storage in smart grids [1];
• Having options to supply power for short or long periods,
• Can be used together with YEK,
• Intermediate gain,
• Increasing the quality of power,
• Additional benefits; rotating reserve, voltage regulation, frequency response,
• Load flow, correction of fluctuations in the load curve, correction of peak points,
• Flexible time use and safety.

It has many advantages such as. In addition, energy storage systems provide stability in frequency and voltage by reducing the difference between energy demand and generation capacity. Energy storage technologies (EDT) provide more stable power for large-scale manufacturers. Since this feature will solve the problems that may arise in the system on the basis of power, the use of energy storage systems instead of increasing the production systems in parallel with the increasing demand will protect it from material damages such as plant installation and operating costs. The widespread use of energy storage systems during the distribution of energy increases the efficiency by making the operation of the networks more efficient. There are several methods of storing excess energy demanded. As RES integration in conventional power systems becomes widespread, our need for energy storage methods for uninterrupted, efficient and safe power use will play a key role. It will also benefit financially as there will be no need to build new power plants [1].

Considering the increasing population, industrial growth and technological developments, we see that most of the investments and government incentives are aimed at meeting our increasing energy demand. All this shows that our efforts to obtain the uninterrupted energy we need for our social development and welfare through continuous and nature-friendly methods will increase gradually. With the widespread use of RES, it is predicted that the use of ESS will become widespread for our continuous and uninterrupted energy needs. This has made it an important issue to investigate the technical, cost, compatibility of the ESS with the power system infrastructure, and the effect on the stability of the system after they are integrated into the system.

2. Material and Method

Studies on the interaction of power systems based on renewable energy, which are increasing rapidly today, on system stability are academically important. In addition, the uncertain production situation of renewable energy and the need for an energy storage system in order to minimize the imbalance in the consumption-production band. When these issues are considered in their entirety, it is very important to transfer the production-consumption imbalances to the test systems correctly. In this direction, representative test systems with a certain scale have been created to investigate the effect of energy storage systems on system stability in cases where energy storage systems are integrated into existing power systems and renewable energy-based power systems. In this context,

IEEE's 14 bus test system, which is frequently used in the literature, was preferred and analyzes were made through the MATLAB program. The codes written by Hadi Saadat, which are accepted as the basis for stability analysis, were developed and analyzes were carried out. Newton-Raphson renewal method was used for stability analysis. While creating the scenarios, the energy storage system, solar generation unit and wind generation unit were integrated into the system, taking into account the load flow densities of the system. By creating possible fault scenarios in the system, the rotor angle, voltage and frequency stability of the system against these faults are analyzed. In terms of high efficiency, the charging and discharging time of the battery was chosen as 3 hours [2]. In determining the charging and discharging times of the energy storage system, the consumption profiles in the Production Capacity Projection report of the Turkish Energy Market Regulatory Authority covering the dates 2021-2025 are taken as a basis. Analyzes were performed with increasing iterations at intervals of 0.05.

2.1. Introducing the scenarios used in stability analysis

• **Current State**

The basic information about the current status of the 14-bus system is as follows14 bus power system: It consists of 15 transmission lines, 3 transformers, 5 machines and 11 loads [3]. The system is shown in Figure 1.
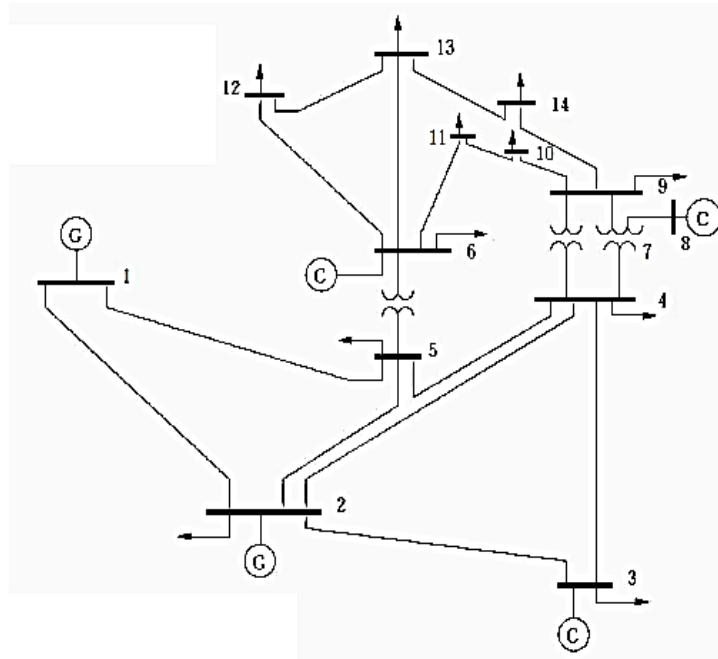
Figure 1. IEEE 14 bus system [4]

- **Scenario 1**

Considering the load densities of the buss, the busiest bus is the 2nd bus with a density value of 73%. Therefore, the energy storage system is integrated into the 2nd bus and faults are created close to the 2nd bus.
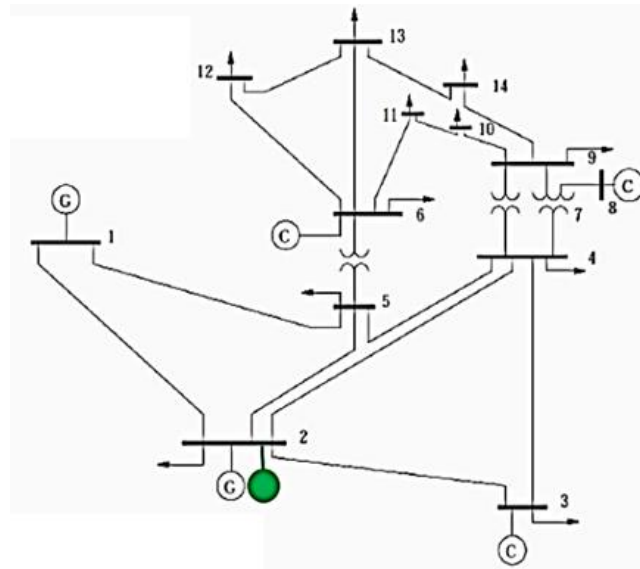

Figure 2. IEEE 14 bus system with added storage system (green circle)

The stability of the system in its current state is analyzed and the stability in the state after the energy storage system is added to the 2nd bus. The system is shown in Figure 2.

- **Scenario 2**

Considering the load density in the system, a solar generation unit was added to the 5th bus, and in the same case, an energy storage system was added to the 5th bus and the stability was analyzed. The system is shown in Figure 3.
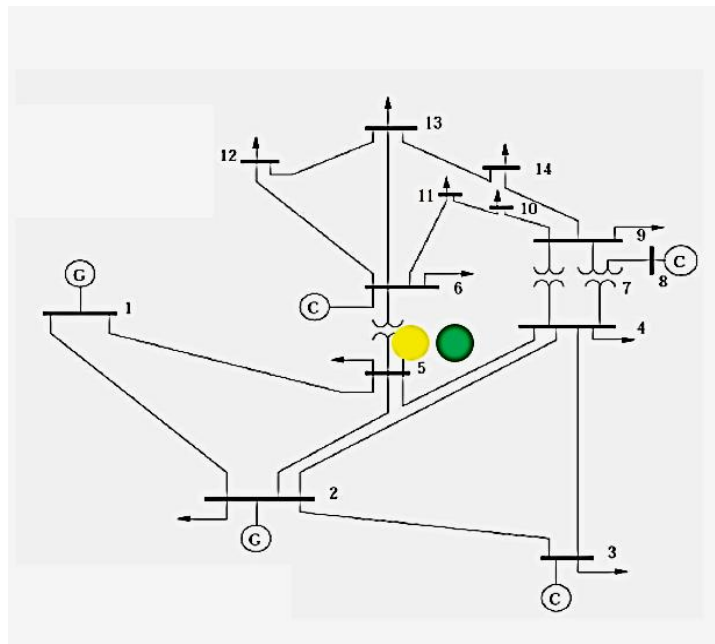
Figure 3. IEEE 14 bus system with added storage and solar system (yellow circle)

- **Scenario 3**

Considering the load density in the system, the current situation was accepted by adding a wind generation unit to the 5th bus, and in the same case, the stability was analyzed by adding an energy storage system to the 5th bus. The system is shown in Figure 4.
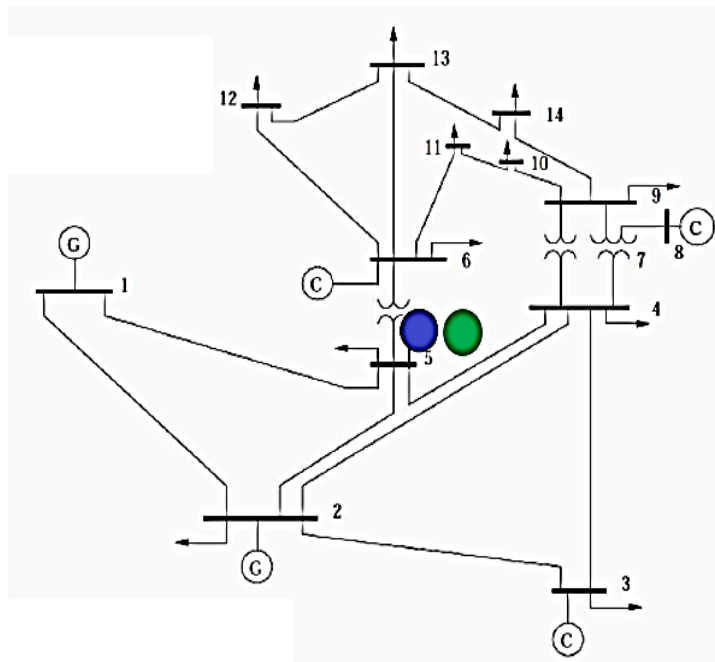
Figure 4. IEEE 14 bus system with added storage and wind system (blue circle)

- **Scenario 4**

By adding a wind generation unit to the 5th and 2nd buss and a solar generation unit to the 4th bus, it has been accepted as the current situation. In the current situation, stability has been analyzed by adding an energy storage system to the 4th bus. The test system is shown in Figure 5.
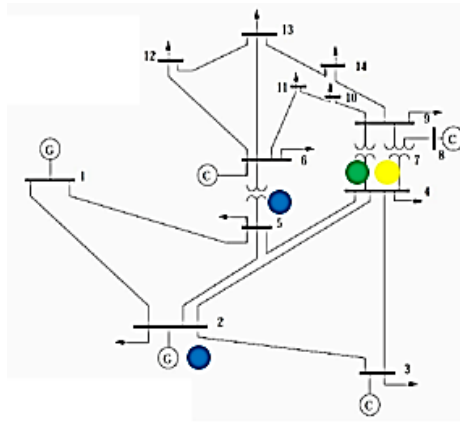
Figure 5. IEEE 14 bus system with added storage system (green circle), solar generation unit (yellow circle), wind generation unit (blue circle)

3. Results

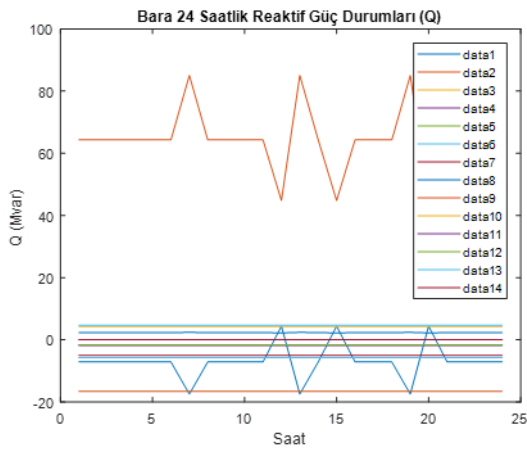• The results of the analyzes for scenario 1 are shown in Figure 6a, 6b.
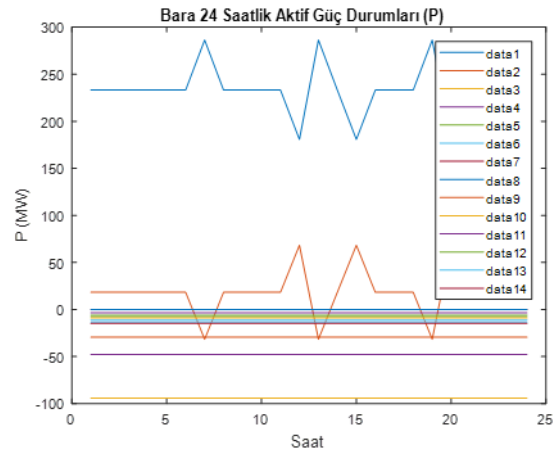

Figure 6 a) Reactive power state

Figure 6 b) Active power state

In Figure 6a, it is seen that the most affected buses are the 2nd Bus (indicated in orange) and the 1st Bus (indicated in blue). In Figure 6b, the most affected buses are the 1st bus (shown in blue), the 2nd bus (shown in orange).

• Analysis results for scenario 2 are shown in Figure 7a, 7b.

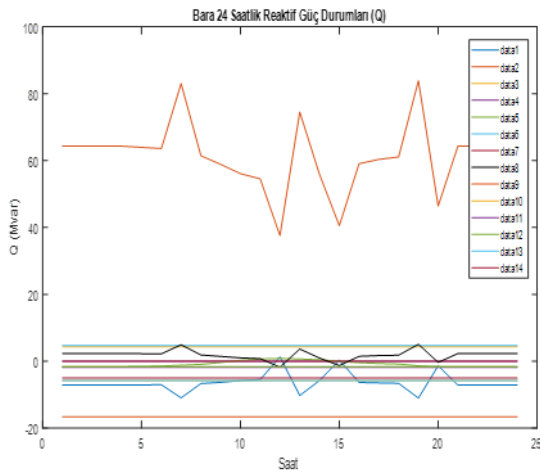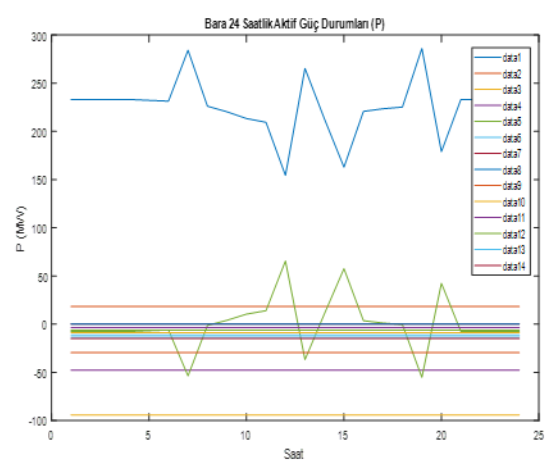**Figure 7 a)** Reactive power state

Figure 7 b) Active power state

In Figure 7a, it is seen that the most affected buses are the 2nd Bus (indicated in orange) and the 1st Bus (indicated in blue). In Figure 7b, the most affected buses are the 1st bus (shown in blue), the 5th bus (shown in green).

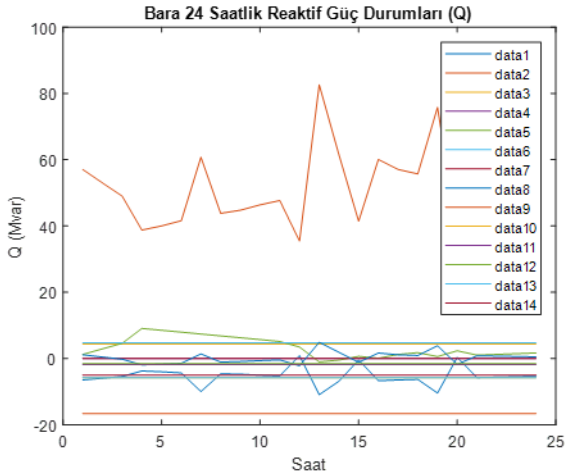• The results of the analyzes for scenario 3 are shown in Figure 8a, 8b.
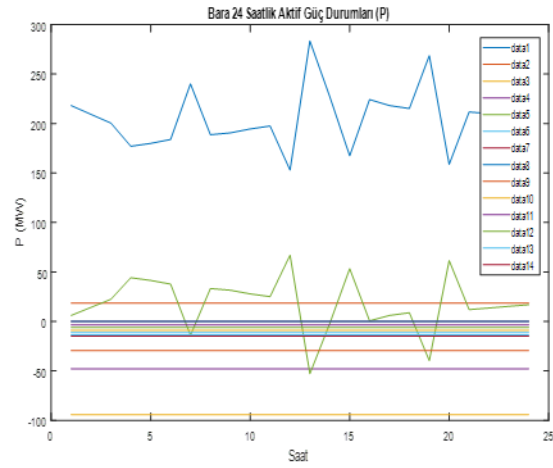

Figure 8 a) Reactive power state

Figure 8 b) Active power state

In Figure 8a, it is seen that the most affected bus is the 2nd Bus (indicated in orange) and the 5th Bus (indicated in green), respectively. In Figure 8b, the most affected buses are the 1st bus (shown in blue), the 5th bus (shown in green).

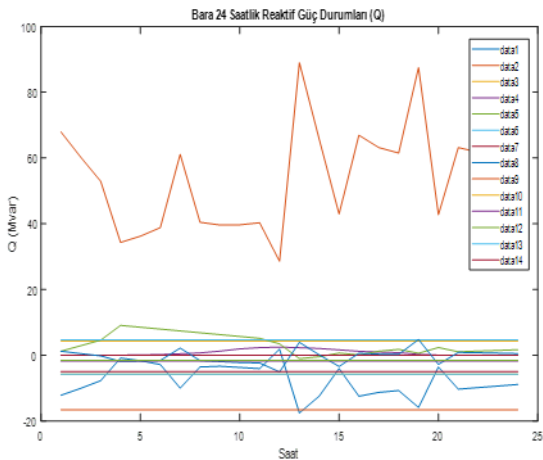• The results of the analyzes for scenario 4 are shown in Figure 9a, 9b.

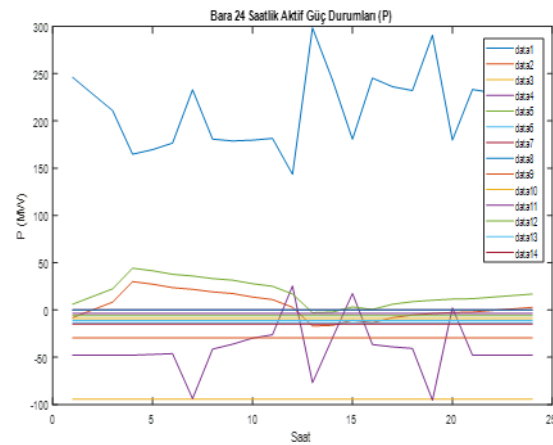**Figure 9 a)** Reactive power state

Figure 9 b) Active power state

In Figure 9a, it is seen that the most affected buss are Bus 2 (shown in orange) and Bus 1 (shown in blue), respectively. In Figure 9b, the most affected buses are the 1st bus (shown in blue), the 4th bus (shown in purple).

Analyzes were made by taking into account the hourly consumption-production values of Turkey. The stability of the system was examined with 0.05 second iteration. Since there is production at 07.00, 13.00 and 19.00, the energy storage system behaves like a load, that is, it is charging. Since consumption is high at 12:00, 15:00 and 20:00, the energy storage system acts as a generator. In other words, it provides extra power to the system.

When the data in Table 1 is examined, the energy storage system alone does not show a different result in case of failure in Scenario 1. However, when the energy storage system is used together with solar and wind generation units (Scenario 2, 3, 4), it has been observed that the stability of the system is longer when the storage system energizes the system.

Table 1. System instability times

Hour/Scenario	Scenario 1	Scenario 2	Scenario 3	Scenario4	Current state
07.00	0.10	0.10	0.10	0.10	0.15
12.00	0.10	0.15	0.15	0.15	0.15
13.00	0.10	0.10	0.10	0.05	0.15
15.00	0.10	0.15	0.15	0.15	0.15
19.00	0.10	0.10	0.10	0.10	0.15
20.00	0.10	0.15	0.15	0.15	0.15

4. Discussion

In this study, it is aimed to see the changes in system stability with the integration of energy storage systems in power systems based on renewable energy sources. Since the energy obtained from smart grid integration renewable resources changes seasonally, annually, daily or even hourly, the importance of energy storage systems emerges to ensure the continuity of this energy.

Renewable energy sources have a great place in regulating the supply-demand imbalance of energy. Considering that the energy obtained from smart grid integration renewable resources changes seasonally, annually, daily or even hourly, the importance of energy storage systems emerges. However, it is of great importance to investigate the positive or negative consequences of energy storage systems when used together with existing power systems, smart grids, power systems based on renewable energy, academically and considering the future of our country in terms of energy production.

5. Conclusion

According to the results of the analysis, it is seen that the energy storage system has a positive effect on the stability of the system in case of a possible failure, while providing energy to the system, that is, in case of discharge. It has been observed that while storing energy from the system, that is, in the charging state, it behaves like a load and does not have a serious deterioration effect on the stability of the system.

It is predicted that the use of IEEE's 9, 30 and 39 bus power systems as a test system will also have positive effects on the literature.

In this study, the fact that test systems give different stability responses in different time periods during the day causes us to think that they will give different stability responses in real networks. For this purpose, smart technologies are included in the integration of distributed generation units and variable consumption units together with the energy storage system, and efforts to ensure the most suitable conditions continue without slowing down.

Author contributions

Ayşe Acar: Conceptualization, Methodology, Software, Visualization, **Asım Kaygusuz:** Data curation, Writing-Original draft preparation, Software, Validation, Writing-Reviewing and Editing.

Conflicts of interest

The authors declare no conflicts of interest.

References

1. Özdemir, E., Aktaş, A., Erhan K. & Özdemir, Ş., (2017). Opportunities and challenges for energy storage applications in smart grids, Journal of Gazi University Faculty of Engineering and Architecture, 32(2), 499-506. http://doi.org/10.17341/gazimmfd.322175.

2. Yilmaz, R. Ş., Baykal, S., Terciyanli, A., Aydin, R. and Cam, E., (2021). Optimal Energy Storage and Geostipal Analysis Study for Hybrid Microgrids, Al-Jazari Journal of Science and Engineering, volume 8, issue 2, page 859-872. http://doi.org/10.31202/ecjse.884181.

3. Kaygusuz, A., (2020). Investigation of the effects of distributed-uncertain production and consumption conditions on the stability of power systems. 88, Url: https://app.trdizin.gov.tr/proje/TWpFNE1qQXc/dagitik-belirsiz-uretim-ve-tuketim-kosullarinin-guc-sistemlerinin-kararliligi-uzerindeki-etkilerinin-incelenmesi

4. Tuttokmağı, Ö., (2019). Investigation of Smart Grids in Terms of System Stability, Master Thesis, İnönü University Institute of Science and Technology, Malatya.

5. Acar, A., & Kaygusuz, A. (2022). Effect of energy storage on power system stability. *Advanced Engineering Days (AED)*, *2*, 83-85.